Automated Lattice Perturbation Theory in the Schrödinger Functional

Implementation and Applications in HQET

D I S S E R T A T I O N

zur Erlangung des akademischen Grades

doctor rerum naturalium (Dr. rer. rat.)
im Fach Physik

eingereicht an der
Mathematisch-Naturwissenschaftlichen Fakultät I
Humboldt-Universität zu Berlin

von
Dirk Hesse

Präsident der Humboldt-Universität zu Berlin:
Prof. Dr. Jan-Hendrik Olbertz

Dekan der Mathematisch-Naturwissenschaftlichen Fakultät I:
Prof. Dr. Stefan Hecht

Gutachter:
1. PD. Dr. Rainer Sommer
2. Prof. Dr. Ullrich Wolff
3. Prof. Kari Rummukainen, PhD

eingereicht am: 10. April 2012
Tag der mündlichen Prüfung: 13. Juli 2012

Acknowledgements

First and foremost I am grateful to Rainer Sommer for providing me with a challenging and most interesting topic for my thesis. His support and expertise played an important role in the success of this work. Enthusiasm *is* contagious, and so it is easy for Rainer to encourage his students and fascinate us with this interesting field of science.

Georg von Hippel kindly helped me familiarizing myself with lattice perturbation theory and its automation and never failed to provide us with interesting facts and anecdotes way beyond that. He and Shinji Takeda provided me with their excellent computer codes, which served as a starting point for my own implementation. I benefited from the fruitful and always interesting discussions with them.

Ulrich Wolff and Hubert Simma greatly helped me with valuable advice in many matters ranging form quantum field theory to computer science.

It was Patrick Fritzsch wo performed the Monte Carlo simulations used in section 4.3, and went out of his way to make sure everything was completed before the APE machines in Zeuthen were finally switched off. The data I could use for the check in section 4.2 comes from earlier investigations of Martin Kurth and was kindly made available to me.

I want to thank the authors of Blossier et al. [2010b], especially Nicolas Garron, for providing me with the non-perturbative data for figure 5.10 just before a big conference, even though being under time pressure himself.

I had many interesting, enlightening, and often also very amusing discussions with my fellow PhD students and staff members at DESY Zeuthen, in particular with Petra Kovacikova, Francesco Virotta, and Valery Yundin. Furthermore, I could benefit from Valery's knowledge on the more esoteric sides of C++.

Abstract

The author developed the `pastor` software package for automated lattice perturbation theory calculations in the Schrödinger functional scheme. The `pastor` code consists of two building blocks, dealing with the generation of Feynman rules and Feynman diagrams respectively.

Accepting a rather generic class of lattice gauge and fermion actions, passed to the code in a symbolic form as input, a low level part of `pastor` will generate Feynman rules to an arbitrary order in the bare coupling with a trivial or an Abelian background field.

The second, high level part of `pastor` is a code generator whose output relies on the vertex generator. It writes programs that evaluate Feynman diagrams for a class of Schrödinger functional observables up to one loop order automatically, the relevant $O(a)$ improvement terms are taken into account.

We will describe the algorithms used for implementation of both parts of the code in detail, and provide cross checks with perturbative and non-perturbative data to demonstrate the correctness of our code.

We demonstrate the usefulness of the `pastor` package through various applications taken from the matching process of heavy quark effective theory with quantum chromodynamics. We have e.g. completed a one loop analysis for new candidates for matching observables timely and with rather small effort, highlighting two advantages of an automated software setup. The results that were obtained so far will be useful as a guideline for further non-perturbative studies.

Zusammenfassung

Der Autor hat das `pastor`-Softwarepaket für automatisierte Gitterstörungstheorie im Schrödingerfunktional entwickelt. Das `pastor`-Paket besteht aus zwei Bausteinen, die die Erzeugung von Vertexfunktionen und Feynmandiagrammen übernehmen.

Ausgehend von recht generischen Formulierungen der Gitterwirkungen für Fermionen und Gluonen, die dem Vertexgenerator in symbolischer Form übergeben werden, erzeugt dieser Feynmanregeln zu beliebiger Ordnung in der nackten Kopplung. Dabei kann sowohl ein triviales als auch ein Abelsches Hintergrundfeld verwendet werden.

Die vom zweiten Teil von `pastor`, einem Code-Generator, erzeugten Programme greifen auf den Vertexgenerator zu und berechnen alle Terme der perturbativen Entwicklung für eine Klasse von Schrödingerfunktional-Observablen bis zur Einschleifenordnung. Verbesserungsterme der Ordnung a werden dabei berücksichtigt.

Wir werden die für die Funktionen der beiden Teile von `pastor` relevanten Algorithmen detailliert beschrieben und die Korrektheit unserer Implementierung mit einer Reihe von Vergleichen mit perturbativen und nichtperturbativen Daten belegen.

Wir werden darauf die Nützlichkeit von `pastor` Anhand einiger Beispiele aus dem Abgleich von Heavy Quark Effective Theory mit Quantenchromodynamik demonstrieren. Wir haben unter Anderem eine Einschleifenrechnung zweier Kandidaten für Observablen, die aller Voraussicht nach in Zukunft für den Abgleich verwendet werden, zügig und mit geringem Aufwand durchgeführt. Dies zeigt die Stärken eines Softwarepakets für automatisierte Störungsrechnungen. Unsere Resultate werden als nützliche Richtschnur für zukünftige nichtperturbative Berechnungen dienen.

Contents

1. Continuum Quantum Chromodynamics

1.1. Introduction

Quantum chromodynamics (QCD) is the theory of the strong force, one of the fundamental interactions in nature. It describes the phenomena associated with *quarks* and *gluons*, which make up all hadrons such as protons, neutrons, or pions. We will give a brief summary of some important aspects of QCD in this chapter. The theory exhibits two prominent features associated with high and low energies. At energies below ~ 1 GeV quarks and gluons are confined into hadrons and cannot be observed as individual particles Wilson [1974]. On the other hand, at high energies, quarks are asymptotically free and QCD becomes a weakly interacting theory Gross and Wilczek [1973]. These two regimes are the respective realms of two prominent methods used to extract physical observables. Monte Carlo methods are very commonly used in combination with the lattice version of QCD and can in principle be employed both in the high and low energy regime. However, the weak-coupling expansion is more cost efficient in terms of the necessary computer power and thus the method of choice when it is valid, namely at short distances (or equivalently high energies) where the coupling is indeed small. Furthermore, the Monte Carlo approach is only applicable in Euclidean spacetime, while the weak-coupling expansion may be used in Minkowski space as well. The latter method applied to lattice QCD, the automation thereof, and its application to heavy quark effective theory (HQET) will be the subject of this thesis. We will explain the lattice formulation of QCD in chapter 2, and the basic idea of Monte Carlo methods will be dealt with in section 2.6. We will then focus on the weak-coupling expansion of the lattice formulation of QCD in the second half of this thesis.

Together with the Salam-Weinberg model of electroweak interactions, QCD forms the standard model of particle physics (e.g. Halzen and Martin [1984]), the as of today most fundamental and complete description of the dynamics of all known subatomic particles. QCD is an important and well established part of the standard model, and thus it is worthwhile to obtain precision predictions from QCD to test its validity in its own right. Apart from that, QCD also plays a role in the analysis of weak processes because the quarks taking part in them are always confined to hadrons Buchalla et al. [1996]. Furthermore, QCD is of interest in flavor physics, where usually weak processes that involve the heavy quark flavors e.g. *charm* and *bottom* with masses of ~ 1.3 GeV and ~ 4.2 GeV (as opposed to the in comparison almost massless light flavors *up* and *down* with masses of only a few MeV Nakamura et al. [2010]) are of special interest. The lattice formulation of QCD can make a valuable contribution here Heitger [2010]. Precision predictions for many processes are not available, and hence flavor physics is an interesting field in the search for new physics beyond the standard model Lellouch

[2011].

The Schrödinger functional (section 1.9), which we will use here, is employed in various applications of lattice QCD. It is of value in investigations that involve an external energy scale, for example when dealing with renormalization, and it thus seems worthwhile to make an effort to develop a set of tools for calculations in the Schrödinger functional. We will describe the details of our implementations in chapter 3, check for correctness of our software in chapter 4 and describe some applications in chapter 5. The interested reader can find a step-by-step introduction to the usage of our software in appendix A.

1.2. Euclidean QCD

It is in most cases of advantage to formulate QCD in *Euclidean* space-time and most techniques to explicitly perform loop integrals are defined in Euclidean space time. The Euclidean theory may be obtained from the Minkowski one by replacing the physical time t by $i\tau$, where τ represents its Euclidean counterpart. In principle, all matrix elements and energy levels of the Minkowski space theory are accessible in the Euclidean formulation. Since we are ultimately interested in the lattice version of QCD, which is formulated in Euclidean space-time, we will use this formulation from the start. In the following, letters from the end of the roman alphabet e.g. $x = (x_0, x_1, x_2, x_3)$ are chosen to represent four-vectors in Euclidean space-time, x_0 being the temporal component. Letters from the middle of the Greek alphabet, e.g. μ will represent directions $0, 1, 2, 3$, and $\hat{\mu}$ is the corresponding unit vector. Roman letters k, l etc. represent the spatial directions $1, 2, 3$ and a hat (as in $\hat{k}$) again indicates that we refer to the unit vectors.

1.3. Field Content

The quark and anti-quark fields $\psi(x), \overline{\psi}(x)$ are massive spin 1/2 Dirac fields. Being in the fundamental representation of $SU(3)$, they have a color index $b = 1, 2, 3$. The Dirac index will be denoted with a Greek letter $\alpha = 1, 2, 3, 4$ and the flavor index by $f = 1, \ldots, N_f$,

$$\psi(x) = \left(\psi_f^b(x)\right)_\alpha . \tag{1.1}$$

We will frequently suppress the flavor, color and Dirac indices. In addition to their color charge, quarks and anti-quarks carry electric charge of $\pm 2/3e$ for (anti-)*up*, *charm*, and *top*, and $\mp 1/3e$ for (anti-)*down*, *strange*, and *bottom* flavored quarks. All quarks participate in weak interactions as well, which will however play no role here. The gluon field $A_\mu(x)$ is a spin one boson field in the adjoint representation of $SU(3)$ and may be decomposed into its color components according to

$$A_\mu(x) = \sum_{a=1}^{8} A_\mu^a(x)\, T_a, \tag{1.2}$$

with the generators T_a of $SU(3)$ as in (B.1). In Euclidean space-time, the position of the Lorentz index $\mu = 0, 1, 2, 3$ is not relevant, since we do not distinguish co- and contravariant vectors.

1.4. Expectation Values of Observables

Given an observable $\mathcal{O}\Big[\overline{\psi}, \psi, A\Big]$, we are interested in extracting the expectation value

$$\langle \mathcal{O} \rangle = \langle \langle \mathcal{O} \rangle_F \rangle_G, \tag{1.3}$$

where $\langle \cdot \rangle_F$ and $\langle \cdot \rangle_G$ represent the fermion and gauge average. Using path integral quantization, they are given as ensemble averages with the corresponding Euclidean actions S_G and S_F in the respective Boltzmann factors. The path integral formulation can be found in any quantum field theory textbook, we follow here Peskin and Schroeder [1995], Gattringer and Lang [2010]. The fields are not regarded as operators but since the fermion fields anti-commute they must be represented by Grassmann numbers. The expectation value $\langle \cdot \rangle_F$ with respect to the fermion field may be calculated using the generating functional $\mathcal{Z}$. It is defined as a functional of Grassmann valued source fields $\eta, \overline{\eta}$,

$$\mathcal{Z}_F[\overline{\eta}, \eta, A] = \int \mathcal{D}\Big[\overline{\psi}, \psi\Big]\, e^{-S_F[\overline{\psi}, \psi, A] + \int \mathrm{d}^4x\, \{\overline{\eta}(x)\psi(x) + \overline{\psi}(x)\eta(x)\}}. \tag{1.4}$$

If we now replace

$$\psi(x) \to \frac{\delta}{\delta \overline{\eta}(x)}, \quad \overline{\psi}(x) \to -\frac{\delta}{\delta \eta(x)} \tag{1.5}$$

in $\mathcal{O}$, the fermion average is given by

$$\langle \mathcal{O} \rangle_F = \frac{1}{\mathcal{Z}_F[A]}\, \mathcal{O}\Big[-\frac{\delta}{\delta \eta}, \frac{\delta}{\delta \overline{\eta}}, A\Big]\, \mathcal{Z}_F[\overline{\eta}, \eta, A]\Big|_{\eta = \overline{\eta} = 0}, \tag{1.6}$$

with the fermion partition function $\mathcal{Z}_F[A] = \mathcal{Z}_F[0, 0, A]$. A is considered to be an external field in (1.6). The gauge field average of any function $f[A]$ is in turn defined as

$$\langle f \rangle_G = \frac{1}{Z} \int \mathcal{D}[A] e^{-S_G[A]} \mathcal{Z}_F[A] f[A], \tag{1.7}$$

where $Z = \int \mathcal{D}[A] e^{-S_G[A]} \mathcal{Z}_F[A]$. The integration with measure $\mathcal{D}[A] = \prod_{\mu, x} \mathcal{D}A_\mu(x)$ over all gauge field configurations has to be performed with some care, as will be discussed in section 1.7.

1.5. Continuum Actions

We will first introduce the fermion action S_F and then comment on its form using $SU(3)$ gauge symmetry, wich plays a fundamental role in QCD. After that we will deal with the gluon action and some technical aspect, namely gauge-fixing that is connected with

it. Again, we will follow Peskin and Schroeder [1995].

1.5.1. Fermion Action

The fermion action S_F reads Dirac [1928]

$$S_F\left[\overline{\psi}, \psi, A\right] = \int \mathrm{d}^4x \; \overline{\psi}(x) \left[\gamma_\mu D_\mu + m_0\right] \psi(x), \quad D_\mu = \partial_\mu + g_0 A_\mu, \tag{1.8}$$

suppressing flavor, color, and Dirac indices. The Euclidean Dirac matrices γ_μ are defined in (B.7). We are using the Einstein sum convention for $\mu = 0, 1, 2, 3$ and the bare mass matrix m_0 in flavor space reads $m_0 = \mathrm{diag}(m_1, \ldots, m_{N_f})$. Often, we will consider only one flavor.

Formally, one can write the fermion partition function in (1.6) as a determinant,

$$\mathcal{Z}_F[A] = \det\left[\gamma_\mu D_\mu + m_0\right]. \tag{1.9}$$

1.5.2. Gauge Invariance

A very fundamental property of QCD is the invariance under a local $SU(3)$ *color* gauge transformation $\Omega(x)$. The quark fields transform under Ω according to

$$\psi(x) \to \Omega(x)\psi(x), \quad \overline{\psi}(x) \to \overline{\psi}(x)\Omega^{-1}(x). \tag{1.10}$$

Inspecting the definition of the derivative,

$$\partial_\mu \psi(x) = \lim_{\epsilon \to 0} \frac{1}{\epsilon} \left\{\psi(x + \epsilon\hat{\mu}) - \psi(x)\right\}, \tag{1.11}$$

one sees that a simple kinetic term $\overline{\psi}(x)\gamma_\mu \partial_\mu \psi(x)$ is not gauge-invariant, as opposed to the mass term $\overline{\psi}(x)\, m_0\, \psi(x)$. If we introduce a parallel transporter $\mathcal{U}(x, y)$, which transforms according to

$$\mathcal{U}(x, y) \to \Omega(x)\, \mathcal{U}(x, y)\, \Omega^{-1}(y), \tag{1.12}$$

and obeys $\mathcal{U}(x, x) = 1$, we can introduce the covariant derivative

$$D_\mu \psi(x) = \lim_{\epsilon \to 0} \frac{1}{\epsilon} \left\{\mathcal{U}(x, x + \epsilon\hat{\mu})\, \psi(x + \epsilon\hat{\mu}) - \psi(x)\right\}. \tag{1.13}$$

The kinetic term $\overline{\psi}(x)\gamma_\mu D_\mu \psi(x)$ is indeed gauge-invariant. The key observation is that we can write the parallel transporter $\mathcal{U}$ in terms of a field A_μ in the Lie algebra of $SU(3)$ with color decomposition (1.2), if it transforms according to

$$A_\mu(x) \to \Omega(x) A_\mu(x) \Omega^{-1}(x) + \frac{1}{g_0} \Omega(x) \partial_\mu \Omega^{-1}(x). \tag{1.14}$$

We may then use the exponential of a line integral along a curve C connecting the points x and y to define $\mathcal{U}$,

$$\mathcal{U}(x,y) = P \exp\left\{ g_0 \int_C A \cdot \mathrm{d}s \right\}. \tag{1.15}$$

The operator P enforces path ordering along C in the exponential, such that for a given parametrization x_t of C the fields $A(x_t)$ for a smaller value of t precede those with a higher value of t. If we now Taylor expand $\mathcal{U}(x, x+\epsilon\hat{\mu})$ in ϵ around $\mathcal{U}(x,x)$ and plug the result into (1.13), we obtain the exact form of the covariant derivative of (1.8),

$$D_\mu = \partial_\mu + g_0 A_\mu(x). \tag{1.16}$$

The parallel transporter is an important building block for the lattice theory.

1.5.3. Gauge Action

The gluon action S_G is defined as in Yang and Mills [1954] by

$$S_G[A] = -\frac{1}{2} \int \mathrm{d}^4x \ \mathrm{tr}\left[F_{\mu\nu}(x)\, F_{\mu\nu}(x) \right], \tag{1.17}$$

and the field strength tensor $F_{\mu\nu}$ reads

$$F_{\mu\nu}(x) = \frac{1}{g_0}\left[D_\mu(x),\, D_\nu(x) \right] = \partial_\mu A_\nu(x) - \partial_\nu A_\mu(x) + g_0 \left[A_\mu(x), A_\nu(y) \right]. \tag{1.18}$$

Elements of the gauge group act on it according to

$$F_{\mu\nu}(x) \to \Omega(x)\, F_{\mu\nu}(x)\, \Omega^{-1}(x). \tag{1.19}$$

The trace operation then makes the gauge action invariant under local gauge transformations.

1.6. Weak-Coupling Expansion

Even if we are ultimately interested in the weak-coupling expansion of the lattice theory, it is worthwhile to briefly sketch continuum perturbation theory to introduce some general concepts we will need later on. One can split the fermion and gluon action into a free and an interacting part,

$$S_G[A] = \int \mathrm{d}^4x \ \{ \mathcal{L}_G^0(x) + g_0 \mathcal{L}_G^I(x) \} \tag{1.20}$$

$$S_F[\overline{\psi}, \psi, A] = \int \mathrm{d}^4x \ \{ \mathcal{L}_F^0(x) + g_0 \mathcal{L}_F^I(x) \} \tag{1.21}$$

Explicitly, the interacting parts read

$$\begin{aligned}\mathcal{L}_G^I(x) = & -if_{abc}(\partial_\mu A_\nu^a(x))A_\mu^b A_\nu^c(x)) \\ & + \frac{1}{4}g_0(f_{abc}A_\mu^b(x)A_\nu^c(x))(f_{ade}A_\mu^d(x)A_\nu^e(x)), \end{aligned} \tag{1.22}$$

$$\mathcal{L}_F^I(x) = A_\mu^a(x)\overline{\psi}(x)\gamma_\mu T_a\psi(x), \tag{1.23}$$

with f_{abc} as in (B.3). Interaction terms like the ones in (1.22), (1.23) are collectively called vertices. Using the expansions (1.20), (1.21) , one may write

$$\int \mathcal{D}[A]e^{-S_G[A]} = \int \mathcal{D}[A]\exp\left\{-\int \mathrm{d}^4x\ \mathcal{L}_G^0(x)\right\}\left(1 - g_0\int \mathrm{d}^4y\ \mathcal{L}_G^I(y) + \dots\right), \tag{1.24}$$

$$\begin{aligned}\int \mathcal{D}\left[\overline{\psi},\psi\right]e^{-S_F\left[\overline{\psi},\psi,A\right]} = & \int \mathcal{D}\left[\overline{\psi},\psi\right]\ \exp\left\{-\int \mathrm{d}^4x\ \mathcal{L}_F^0(x)\right\} \\ & \times\left(1 - g_0\int \mathrm{d}^4y\ \mathcal{L}_F^I(y) + \dots\right). \end{aligned} \tag{1.25}$$

If we plug these equations into formulae (1.6),(1.7), we can express the expectation value $\langle\mathcal{O}\rangle$ of any observable $\mathcal{O}$ asymptotically in a power series in the bare coupling g_0. This expansion is of course only valid if g_0 is sufficiently small. An individual term in the g_0 expansion of an observable may be represented pictorially as a Feynman diagram Feynman [1949]. Figure 1.1 shows a contribution of order g_0^2 to a quantity called the fermion self-energy. A summation over all intermediate indices including the coordinates z and z' is implicit. The computational rules given in the figure are called Feynman rules. The straight and curly lines symbolize the free fermion and gluon propagator, given by the lowest order of the expectation value of $\langle\psi^b(y)\overline{\psi}^c(y)\rangle$ and $\langle A_\mu^{a_1}(x)A_\nu^{a_2}(y)\rangle$. They can be calculated by inverting the free actions, albeit one has to first go through the gauge fixing procedure to be able to invert the free gluon action.

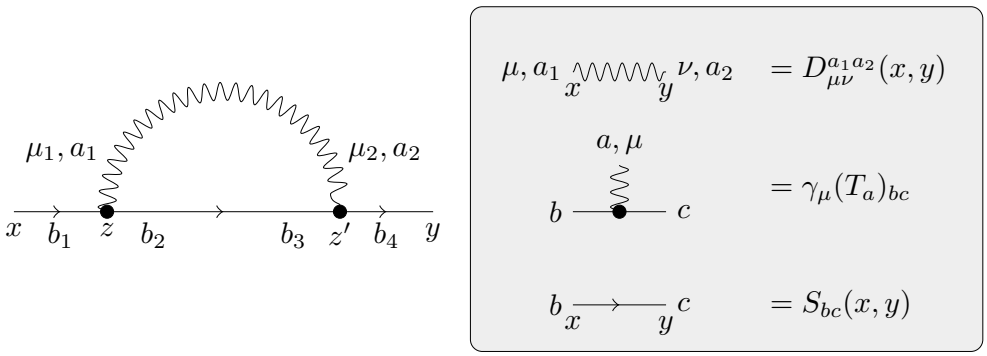

Figure 1.1.: Example Feynman Diagram.

1.7. Gauge Fixing

There is still a piece missing before we can evaluate (1.7). This last ingredient, gauge fixing, is connected to the gauge freedom of the theory and the fact that in (1.7) we integrate over infinitely many gauge equivalent fields A_μ. Let us write a gauge transformation Ω explicitly as

$$\Omega(x) = e^{-g_0 \alpha^a(x) T_a}. \tag{1.26}$$

One finds that exactly the fields $A_\mu(x)$, wich are gauge equivalent to zero are causing trouble. Using (1.14) one can see that they read, in momentum space,

$$A_\mu(k) = i k_\mu \alpha(k). \tag{1.27}$$

A few lines of algebra show that for $\alpha(-k) = \alpha(k)$ the field strength (1.18) and with it the gauge action (1.17) is zero for these gauge fields. This means that the integral (1.7) will be divergent. Equivalently, one runs into trouble when trying to obtain the free gluon propagator. This can be overcome by the method of Faddeev and Popov (Faddeev and Popov [1967], following Peskin and Schroeder [1995]) . The first step is to factor out the integration over gauge equivalent fields in the path integral,

$$\int \mathcal{D}A e^{-S_G[A]} = \int \mathcal{D}\alpha \int \mathcal{D}A e^{-S_G[A]} \delta(G(A)) \det\left(\frac{\delta G(A^\alpha)}{\delta \alpha}\right), \tag{1.28}$$

where A^α denotes the gauge transformed field according to (1.14). Its infinitesimal form may be written as

$$(A^\alpha)^a_\mu = A^\alpha_\mu + \partial_\mu \alpha^a + i\, f^{abc} A^b_\mu\, \alpha^c = A^a_\mu + D_\mu \alpha^a. \tag{1.29}$$

This defines the action of D_μ on a field in the adjoint representation of $SU(3)$. G is a linear function, called the gauge-fixing function and determines which of the infinitely many gauge-equivalent configurations actually contribute to the path integral. The usual choice is

$$G(A) = \partial_\mu A^a_\mu(x) - \omega^a(x), \tag{1.30}$$

with Gaussian weight functions $\omega(x)$. These are used to write the delta function in (1.28), after integration over ω, as a part of the action,

$$S_{GF}[A] = -\lambda \int \mathrm{d}^4x \ \mathrm{tr}\{D_\mu A_\mu D_\nu A_\nu\}. \tag{1.31}$$

The gauge fixing parameter λ can be chosen arbitrarily with $0 < \lambda$. The α-integration in (1.28) finally ensures that we do not alter the original integral and amounts to an infinite multiplicative factor. If we use (1.29), we may write

$$\det\left(\frac{\delta G(A^\alpha)}{\delta\alpha}\right) = \det\left(\partial_\mu D_\mu\right) = \int \mathcal{D}[\overline{c},c]\exp\left\{\int \mathrm{d}^4x\ \overline{c}\ \partial_\mu D_\mu\ c\right\} = \int \mathcal{D}[\overline{c},c]e^{-S_{FP}[\overline{c},c,A]}. \tag{1.32}$$

The Grassmann valued, single component ghost fields $c, \overline{c}$ have been introduced only to provide a simple way to include the determinant in the action but must of course be considered, just as the original quark field, when calculating expectation values. Our final formula for the gauge average then reads

$$\langle F\rangle_G = \frac{1}{Z}\int \mathcal{D}[\overline{c},c,A]e^{-S_G[A]-S_{GF}[A]-S_{FP}[\overline{c},c,A]}\mathcal{Z}_F[A]F[A], \tag{1.33}$$

in wich we also have to redefine Z, which cancels the integration over α and the path integral may then expected to be finite.

1.8. Continuum HQET

To evaluate the functional integral (1.3) even for simple observables, one usually has to resort to numerical methods. If the observable contains heavy quarks like charm or bottom, one faces a multi-scale-problem ranging from $m_\pi \approx 140$ MeV, to $m_b \approx 5$ GeV or $m_c \approx 1.3$ GeV Nakamura et al. [2010]. Evaluating the functional integral (1.3) with Monte Carlo methods, as will be described in section 2.6, is not feasible in this case with current computers and will probably stay out of reach for some time.

An interesting alternative is provided by heavy quark effective theory (abbreviated HQET, Eichten and Hill [1990a], for a review see Sommer [2011]). One considers a system with a single heavy quark or anti-quark, whose mass m_h is much bigger than all other relevant scales. Examples for such systems include the B-meson and b-baryons. After identifying the relevant degrees of freedom, one performs successive Fouldy Wouthuysen-Tani (FTW) transformations to obtain a systematic expansion of the Lagrangian in $1/m_\mathrm{h}$ Korner and Thompson [1991]. The lowest order is called the *static* limit, $m_\mathrm{h}\to\infty$. In the rest-frame of the heavy quark, one ends up with the Lagrangian Eichten and Hill [1990a]

$$\mathcal{L} = \mathcal{L}_\mathrm{h}^\mathrm{stat} + \frac{1}{2m_\mathrm{h}}\mathcal{L}_\mathrm{h}^{(1)} + \mathcal{L}_{\bar{\mathrm{h}}}^\mathrm{stat} + \frac{1}{2m_\mathrm{h}}\mathcal{L}_{\bar{\mathrm{h}}}^{(1)} + O(1/m_\mathrm{h}^2), \tag{1.34}$$

$$\mathcal{L}_\mathrm{h}^\mathrm{stat} = \overline{\psi}_\mathrm{h}(m_\mathrm{h}+D_0)\psi_\mathrm{h}, \quad \mathcal{L}_{\bar{h}}^\mathrm{stat} = \overline{\psi}_{\bar{\mathrm{h}}}(m_\mathrm{h}-D_0)\psi_{\bar{\mathrm{h}}}, \tag{1.35}$$

$$\mathcal{L}_\mathrm{h}^{(1)} = -\left(\mathcal{O}_\mathrm{kin}+\mathcal{O}_\mathrm{spin}\right), \quad \mathcal{L}_{\bar{\mathrm{h}}}^{(1)} = -\left(\overline{\mathcal{O}}_\mathrm{kin}+\overline{\mathcal{O}}_\mathrm{spin}\right), \tag{1.36}$$

with D_0 as defined in (1.16). The heavy anti-quark is no longer related to the conjugate of the heavy quark field, but completely decouples from it. The relevant components of a heavy quark or anti-quark field are given in its rest-frame by the application of the

projectors $P_\pm = (1 \pm \gamma_0)/2$,

$$P_+\psi_\mathrm{h} = \psi_\mathrm{h}, \quad \overline{\psi}_\mathrm{h}P_+ = \overline{\psi}_\mathrm{h}, \quad P_-\psi_{\bar{\mathrm{h}}} = \psi_{\bar{\mathrm{h}}}, \quad \overline{\psi}_{\bar{\mathrm{h}}}P_- = \overline{\psi}_{\bar{\mathrm{h}}}, \tag{1.37}$$

which are effectively two-component spinors, even though the static Lagrangian is formally the one for a one-dimensional fermion for each lattice point $\mathbf{x}$. The operators corresponding to the $1/m_\mathrm{h}$-corrections read

$$\mathcal{O}_\mathrm{kin}(x) = \overline{\psi}_\mathrm{h}(x)\ \mathbf{D}^2(x)\ \psi_\mathrm{h}(x), \quad \mathcal{O}_\mathrm{spin}(x) = \overline{\psi}_\mathrm{h}(x)\ \sigma\cdot\mathbf{B}(x)\ \psi_\mathrm{h}(x), \tag{1.38}$$

$$\overline{\mathcal{O}}_\mathrm{kin}(x) = \overline{\psi}_{\bar{\mathrm{h}}}(x)\ \mathbf{D}^2(x)\ \psi_{\bar{\mathrm{h}}}(x), \quad \overline{\mathcal{O}}_\mathrm{spin}(x) = \overline{\psi}_{\bar{\mathrm{h}}}(x)\ \sigma\cdot\mathbf{B}(x)\ \psi_{\bar{\mathrm{h}}}(x), \tag{1.39}$$

where $\sigma_k = \frac{1}{2}\epsilon_{ijk}\sigma_{ij}$ with $\sigma_{jk} = \frac{i}{2}\left[\gamma_j, \gamma_k\right]$ as in (B.11) and $B_k = \frac{i}{2}\epsilon_{ijk}F_{ij}$.

1.8.1. $1/m_\mathrm{h}$ Expansion of Expectation Values.

As explained in Della Morte et al. [2007], the expectation value of an observable $\mathcal{O}$ containing heavy and light quarks can be expanded according to

$$\langle\mathcal{O}\rangle = \langle\mathcal{O}\rangle_\mathrm{stat} + \frac{1}{2m_\mathrm{h}}\int \mathrm{d}x\ \langle\mathcal{O}\mathcal{O}_\mathrm{kin}(x)\rangle_\mathrm{stat} + \frac{1}{2m_\mathrm{h}}\int \mathrm{d}x\ \langle\mathcal{O}\mathcal{O}_\mathrm{spin}(x)\rangle_\mathrm{stat} + O(1/m_\mathrm{h}^2). \tag{1.40}$$

Here, $\langle\cdot\rangle_\mathrm{stat}$ denotes the expectation value in the sense of (1.6), (1.7) with (considering a system containing a single heavy quark)

$$S_F[\overline{\psi}, \psi, \overline{\psi}_\mathrm{h}, \psi_\mathrm{h}, A] = S_\mathrm{l}[\overline{\psi}, \psi, A] + S_\mathrm{h}[\overline{\psi}_\mathrm{h}, \psi_\mathrm{h}, A], \quad S_\mathrm{h} = \int \mathrm{d}^4x\ \mathcal{L}_\mathrm{h}^\mathrm{stat}(x), \tag{1.41}$$

and S_l given as before by (1.8). This expansion is very similar to what was discussed in section 1.6, since just as $\mathcal{L}_F^I$ can be treated as a correction to $\mathcal{L}_F^0$ for small values of g_0, $\mathcal{O}_\mathrm{spin}$ and $\mathcal{O}_\mathrm{kin}$ can be treated as corrections to $\mathcal{L}_\mathrm{h}^\mathrm{stat}$ for big values of m_h. One can derive (1.40) in formal analogy to the weak-coupling expansion (1.25). However, one should keep in mind that this analogy is rather superficial, since the weak-coupling expansion is renormalizable, while one needs more and more parameters when higher orders in $1/m_\mathrm{h}$ are included in (1.40).

1.9. The Schrödinger Functional

The Schrödinger functional was first introduced by Symanzik to show the existence and renormalization properties of the Schrödinger picture in quantum field theory and to calculate the Casimir force between two disjoint surfaces Symanzik [1981]. It was then formulated for $SU(N)$ Yang-Mills theory Lüscher et al. [1992] and later for full QCD Sint [1994]. One of the most prominent applications of the Schrödinger functional is the step scaling method used e.g. to calculate running couplings Lüscher et al. [1991]. A good signal-to-noise ratio and the absence of zero-modes are further benefits.

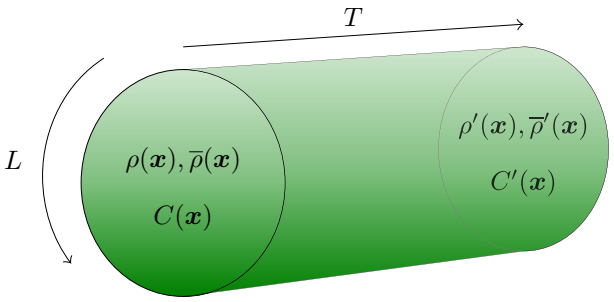

Figure 1.2.: Depiction of the Schrödinger Functional.

1.9.1. The Schrödinger Functional in Yang-Mills Theory

In the spatial directions, the gauge fields A_μ satisfy periodic boundary conditions with period L, $A_\mu(x + L\hat{k}) = A_\mu(x)$. Dirichlet boundary conditions are imposed in the temporal direction, given in terms of two smooth classical gauge fields $C_k(\mathbf{x})$, $C'_k(\mathbf{x})$. The path integral representation of the Schrödinger functional is then Lüscher et al. [1992]

$$Z[C', C] = \int \mathcal{D}[\Lambda, A] e^{-S_G}, \tag{1.42}$$

with S_G as in (1.17). The boundary conditions on the integration variables A read explicitly

$$A_k(x)|_{x_0=0} = C_k^\Lambda(\mathbf{x}), \quad A_k(x)_{x_0=T} = C'_k(\mathbf{x}). \tag{1.43}$$

Here, Λ is a gauge transformation acting on C according to (1.14),

$$C_k(\mathbf{x}) \to C_k^\Lambda(\mathbf{x}) = \Lambda(\mathbf{x}) A_k(\mathbf{x}) \Lambda^{-1}(\mathbf{x}) + \frac{1}{g_0} \Lambda(\mathbf{x}) \partial_k \Lambda(\mathbf{x})^{-1}. \tag{1.44}$$

To be compatible with the boundary conditions, Λ must be spatially periodic. The integration over Λ ensures invariance of $Z[C', C]$ under gauge transformations of the boundary fields, as can be seen from the quantum mechanical representation of the Schrödinger functional Lüscher et al. [1992]. This integration over gauge transformations will be automatically included in the lattice formulation.

1.9.2. Background Field

In the perturbative regime, when g_0 is small, the main contributions of $Z[C', C]$ are those from field configurations which are close to the classical minimum B_μ of the action. However, it is rarely possible to compute B_μ for given C, C' analytically. One rather chooses a background field B_μ, such that one can prove that it is the unique (up to gauge transformations), absolute minimum of S_G and sets

$$C_k(\mathbf{x}) = B_k(x)|_{x_0=0}, \quad C'_k(\mathbf{x}) = B_k(x)|_{x_0=T}. \tag{1.45}$$

Involved cases are possible, the minimum of the gauge action could be in a non-trivial topological sector. We will not consider these and assume B has the properties stated above. A family of Abelian background fields is given in Lüscher et al. [1992]. This type of background field will be used later on and the boundary values are specified in appendix C.2. If one now wants to use perturbation theory as explained in section 1.6, one has to decompose the gluon field A_μ into the background field B_μ and the fluctuation field q_μ,

$$A_\mu(x) = B_\mu(x) + q_\mu(x). \tag{1.46}$$

The relevant degree of freedom for the weak-coupling expansion is q_μ, with homogeneous boundary conditions

$$q_k(x)|_{x_0=0} = 0, \quad q_k(x)|_{x_0=T} = 0. \tag{1.47}$$

1.9.3. Fermions

Just like the gluons, the quark fields $\psi, \overline{\psi}$ obey Dirichlet boundary conditions in the temporal direction Sint [1994],

$$\begin{aligned} P_+\psi(x)|_{x_0=0} &= \rho(\mathbf{x}), \quad P_-\psi(x)|_{x_0=T} = \rho'(\mathbf{x}), \\ \overline{\psi}(x)P_-|_{x_0=0} &= \overline{\rho}(\mathbf{x}), \quad \overline{\psi}(x)P_+|_{x_0=T} = \overline{\rho}'(\mathbf{x}). \end{aligned} \tag{1.48}$$

The projectors ensure that only half of the components of the fields are fixed at each boundary. The equations of motion are first order differential equations for $\psi, \overline{\psi}$ and thus one can not expect to obtain a sane theory if the boundary conditions are imposed on more than half of the field components. The spatial boundary conditions for the fermion fields are L-periodic up to a phase θ_k Sint and Sommer [1996],

$$\psi(x + L\hat{k}) = e^{i\theta_k}\psi(x), \quad \overline{\psi}(x + L\hat{k}) = e^{-i\theta_k}\overline{\psi}(x). \tag{1.49}$$

This restricts the three-momenta of the fermions to

$$p_k = \frac{2\pi n_k + \theta_k}{L}, \quad n_k \in \mathbb{Z}. \tag{1.50}$$

One often chooses a common value $\theta_k = \theta, k = 1, 2, 3$. Due to translational invariance in the spatial directions it can be beneficial to work in a time-momentum representation,

$$f(x) = \frac{1}{L^3}\sum_{\mathbf{p}} e^{i\,\mathbf{p}\mathbf{x}} f(\mathbf{p}, x_0), \tag{1.51}$$

and we will make use of this later on. The fermion action for the Schrödinger functional reads Sint [1994]

$$S_F[A,\overline{\psi},\psi] = \int \mathrm{d}^4x\ \overline{\psi}(x)(\gamma_\mu D_\mu + m_0)\psi(x) \\ - \int_0^L \mathrm{d}^3\mathbf{x}\ \left\{\overline{\psi}(x)P_-\psi(x)|_{x_0=0} + \overline{\psi}(x)P_+\psi(x)|_{x_0=T}\right\}. \quad (1.52)$$

The appearance of the boundary terms in (1.52) may be understood in two ways, as was pointed out in Sint [1994]. Coming from the Wilson lattice formulation, one ends up naturally with the boundary terms in the continuum theory by taking the naive continuum limit. But the boundary terms may also be explained without any reference to the lattice. To this end, one regards the classical action as a functional acting on $\mathcal{C}^\infty$ functions with boundary conditions as specified in (1.48). Then, following the variational principle, one looks for stationary points of the action, whose solutions are required to be $\mathcal{C}^\infty$ and obey the correct boundary conditions as well. If one leaves the form of the boundary terms undetermined during this process, one finds that the exact form of these as in (1.52) is required if the action shall remain invariant under parity transformations.

Heavy Quarks

The inclusion of a heavy quark field as described in section 1.8 is rather straightforward (e.g. Sommer [2011]). We will consider a system with one single heavy quark. Inspecting the boundary conditions (1.48) and the relevant components of the heavy quark field (1.37), one finds that the boundary conditions simplify to

$$\psi_\mathrm{h}(x)|_{x_0=0} = \rho_\mathrm{h}(\mathbf{x}), \quad \overline{\psi}_\mathrm{h}(x)|_{x_0=T} = \overline{\rho}_\mathrm{h}{}'(\mathbf{x}). \quad (1.53)$$

The action for a heavy quark in the Schrödinger functional is then given in analogy to (1.52) by

$$S_\mathrm{h}[A,\overline{\psi}_\mathrm{h},\psi_\mathrm{h}] = \int \mathrm{d}^4x\ \mathcal{L}_\mathrm{h}(x) - \int \mathrm{d}^3\mathbf{x}\ \overline{\psi}_\mathrm{h}(x)\psi_\mathrm{h}(x)|_{x_0=T}. \quad (1.54)$$

The Lagrangian $\mathcal{L}_\mathrm{h}$ is as in (1.35), respecting the boundary conditions (1.53).

2. Lattice Regularization

Restricting the fermion and gauge fields to the points of an Euclidean space-time lattice with spacing a serves as an ultraviolet regulator, since the field's momentum components are restricted to the first Brillouin zone. This opens the door to numerical methods to evaluate the path integral. To be able to perform calculations on a computer, one has to restrict the extent of the lattice as well. One usually sets the spatial extent to L, and the temporal one to T, where L and T both must be an integer multiple of a. Often periodic boundary conditions are used or, as in the case of the Schrödinger functional, Dirichlet ones, as discussed in section 1.9.

2.1. Quarks

Inspecting (1.13), one finds that there are at first glance different choices to define a discretized version of the covariant derivative. The obvious choices are the forward and backward covariant derivative,

$$\nabla_\mu \psi(x) = \frac{1}{a}\Big[U_\mu(x)\psi(x+a\hat{\mu}) - \psi(x)\Big], \tag{2.1}$$

$$\nabla^*_\mu \psi(x) = \frac{1}{a}\Big[\psi(x) - U^{-1}_\mu(x-a\hat{\mu})\psi(x-a\hat{\mu})\Big], \tag{2.2}$$

approximating (1.15), with an error of order a, by

$$U_\mu(x) = e^{a g_0 A_\mu(x)}. \tag{2.3}$$

However, one finds that the symmetric derivative

$$\tilde{\nabla}_\mu = \frac{1}{2}(\nabla_\mu + \nabla^*_\mu) \tag{2.4}$$

must be used to obtain the correct continuum theory in the limit $a \to 0$. Note that in contrast to the forward and backward derivatives, the symmetric one only introduces a discretization error of $O(a^2)$ instead of $O(a)$. One may now try to use

$$S_F^{\text{naive}}[U, \overline{\psi}, \psi] = a^4 \sum_x \overline{\psi}(x)\ (\gamma_\mu \tilde{\nabla}_\mu + m_0)\ \psi(x) \tag{2.5}$$

as the lattice version of (1.8) but this fermion action leads to a phenomenon called *doubling* Wilson [1974]. When one calculates the free propagator using the discretization above, one ends up with 16 fermion-like field excitations at finite lattice spacing. The solution by Wilson Wilson [1974] involves adding an *irrelevant* term to the action

vanishing in the continuum limit $a \to 0$, such that the full action reads

$$S_F^W = a^4 \sum_x \left\{ \overline{\psi}(x)(\gamma_\mu \tilde{\nabla}_\mu + m_0)\psi(x) - a\,\overline{\psi}(x)\nabla_\mu^* \nabla_\mu \psi(x) \right\}. \tag{2.6}$$

This action does not give rise to doublers.

Generally, irrelevant terms with the correct symmetries may be included in the lattice action to modify the theory at non-zero lattice spacing without changing the continuum limit. This can be used for example to speed up the convergence of the lattice theory to the continuum one as $a \to 0$ (c.f. Lüscher et al. [1996] for a discussion of $O(a)$-improvement). The point we want to make here is that various lattice formulations of the same continuum theory are possible, each of which has different properties at finite a and a different perturbative expansion in the sense of (1.21). Our aim is to set up a framework for lattice perturbation theory that can handle rather general actions. We assume a typical bilinear fermion action, given by

$$S_F[U, \overline{\psi}, \psi] = \sum_i \overline{\psi}(x_i)\; w_i\, \Gamma_i\, \mathcal{U}_i(x_i, y_i)\; \psi(y_i). \tag{2.7}$$

Here, w_i are complex weights, Γ_i spin matrices in the Pauli or Dirac algebra, and $\mathcal{U}_i$ parallel transporters on the lattice. A generic parallel transporter $\mathcal{U}(x, y)$ (being the

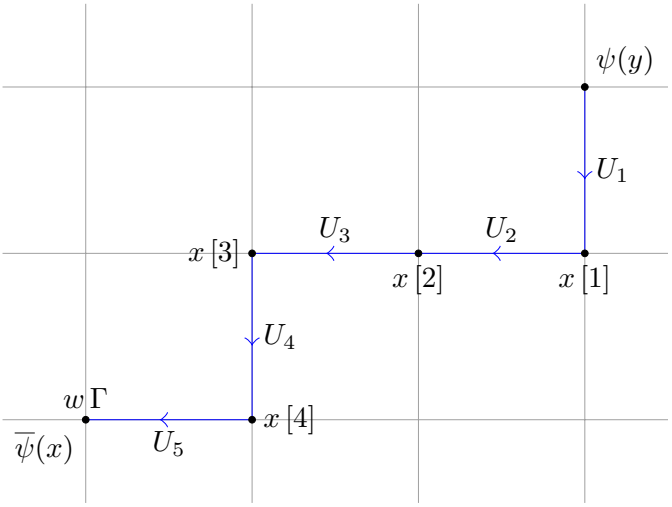

Figure 2.1.: A single parallel transporter contributing to a bilinear quark action.

lattice version of (1.15)) is a product of links U_i and may be fully specified by giving a starting point $x[0] = y$ and a sequence of *signed directions* $\mathcal{C} = (s[1]\mu[1], \ldots, s[l]\mu[l])$, $\mu[i] \in \{0, 1, 2, 3\}$, $s[i] = \pm 1$. These directions lead us, starting form y, to the lattice point x. Since some of them may be negative, we have to take some care on how to define the corresponding sequence of links U_i connecting x and y,

$$\mathcal{U}(x, y) = U_l\, U_{l-1}\, \ldots\, U_1. \tag{2.8}$$

We define

$$U_i = U_{s[i]\mu[i]}(x[i]), \quad U_{-\mu}(x) = U_\mu^{-1}(x - a\hat{\mu}), \tag{2.9}$$

where

$$x[i-1] - x[i] = a\, s[i]\, \hat{\mu}[i]. \tag{2.10}$$

With this nomenclature, a generic contribution to (2.7) may be depicted as in figure 2.1. As an explicit example, let us reconstruct the Wilson fermion action (2.6) in terms of (2.7). To this end, one uses the sequences $\mathcal{C}_i$ with weights w_i and spin matrix Γ_i that are given in table 2.1. As the starting points, all lattice points x must be chosen successively.

i	w_i	$\mathcal{C}_i$	Γ_i
μ	$a^3/2$	(μ)	γ_μ
$4+\mu$	$-a^3/2$	$(-\mu)$	γ_μ
$8+\mu$	$-a^3/2$	(μ)	1
$12+\mu$	$-a^3/2$	$(-\mu)$	1
16	$4a^3 + a^4 m$	()	1

Table 2.1.: Parameters specifying the Wilson lattice action. The Greek letter μ in the first column simply acts as a running index, $\mu = 0, 1, 2, 3$.

2.2. Gluons

As we stated in the previous section, the link variable (2.3) is a natural choice for representing the gauge field on the lattice. To construct a gauge invariant quantity of link variables, one may choose the trace over a closed loop, such as Wilson's plaquette Wilson [1974],

$$U_{\mu\nu}(x) = U_\mu(x)\, U_\nu(x + a\hat{\mu})\, U_\mu^{-1}(x + a\hat{\nu})\, U_\mu^{-1}(x). \tag{2.11}$$

If one assumes the existence of a smooth continuum gauge field, such that the lattice gluon field is the restriction of the continuum one to a hypercubic lattice, one finds that

$$U_{\mu\nu}(x) = \exp\{a^2 g_0 F_{\mu\nu}(x) + O(a^3)\}, \tag{2.12}$$

and hence we have

$$\frac{1}{g_0^2} \sum_{x,\mu,\nu} \mathrm{tr}\,[1 - U_{\mu\nu}(x)] = -\frac{1}{2} \int \mathrm{d}^4x \ \mathrm{tr}\,[F_{\mu\nu}(x) F_{\mu\nu}(x)] + O(a^2). \tag{2.13}$$

A careful analysis shows that the $O(a^3)$ term in (2.12) actually vanishes, such that we only get corrections of $O(a^2)$ in (2.13). Wilson's choice for the gluon action then reads

Wilson [1974]

$$S_G^W[U] = \frac{1}{g_0^2} \sum_{x,\mu,\nu} \operatorname{tr}\left[1 - U_{\mu\nu}(x)\right]. \tag{2.14}$$

As in the fermionic case, other choices are possible, and thus we assume the gluon action to be of the more generic form

$$S_G[U] = \frac{1}{g_0^2} \sum_i w_i \operatorname{tr}\left[1 - \mathcal{U}_i(x_i)\right]. \tag{2.15}$$

The parallel transporters $\mathcal{U}_i$ are required to be closed now, $\mathcal{U}_i(x_i) = \mathcal{U}_i(x_i, x_i)$, but otherwise we use the same nomenclature as in the last section (c.f. figure 2.2). The weights w_i must be chosen correctly to reproduce the Yang-Mills continuum action. The Wilson gauge action (2.14) is represented in this notation by the terms

$$w_{\mu+4\nu} = 1, \quad \mathcal{C}_{\mu+4\nu} = (\mu, \nu, -\mu, -\nu), \quad \mu, \nu = 0, \ldots, 3. \tag{2.16}$$

Again, all lattice points x must be chosen as the starting point in turn.

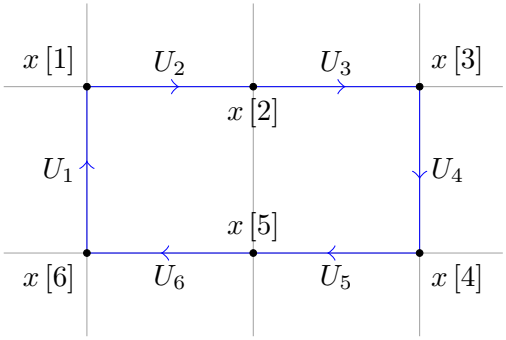

Figure 2.2.: Pictorial representation of a closed gluon loop.

2.3. Improvement and Renormalization

In Symanzik [1983a,b], Symanzik described how to remove the cut-off effects of on-shell observables in a lattice theory, describing them in terms of an effective continuum theory sharing the symmetries of the original lattice theory. Irrelevant lattice operators with the correct symmetries are then used to remove the cut-off effects up to some order in a Lüscher and Weisz [1985], Sheikholeslami and Wohlert [1985]. Counter-terms must be added to the lattice action and to composite fields Heatlie et al. [1991], Martinelli et al. [1991], Lüscher et al. [1996]. Furthermore, when working with Dirichlet boundary conditions, more improvement terms may arise from the boundary Lüscher et al. [1996]. We will only discuss the terms to be included in the bulk action here and leave the discussion of the boundary counter-terms to section 2.5.4. Operator improvements will be given when the respective operators are introduced.

The lattice gluon action (2.14) already reproduces the continuum gauge action up to corrections of $O(a^2)$. To improve the fermion action, only the so-called Sheikholeslami-Wohlert or clover term Sheikholeslami and Wohlert [1985] needs to be included (other terms amount to a redefinition of the bare mass and coupling),

$$S_{SW}\left[U,\overline{\psi},\psi\right] = a^5 c_{SW} \sum_{x,\mu,\nu} \overline{\psi}(x)\frac{i}{4}\sigma_{\mu\nu}\mathcal{F}_{\mu\nu}(x)\psi(x), \tag{2.17}$$

with $\sigma_{\mu\nu}$ as in (B.11) and

$$\mathcal{F}_{\mu\nu}(x) = \frac{1}{8a^2}\{U_{\mu\nu}(x) - U_{\nu\mu}(x) + U_{\nu(-\mu)}(x) - U_{\mu(-\nu)}(x) + U_{(-\mu)(-\nu)} - U_{(-\nu)(-\mu)} + U_{(-\nu)\mu}(x) - U_{(-\mu)\nu}(x)\}. \tag{2.18}$$

$U_{\mu\nu}$ is given by (2.11) and the negative subscripts are to be understood in the sense of (2.9). A pictorial representation of the clover term can be found in figure 2.3. The

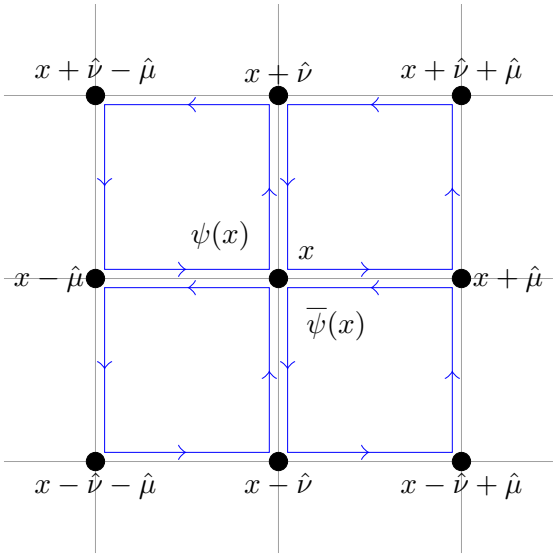

Figure 2.3.: Pictorial representation of the Sheikholeslami-Wohlert or clover term.

improvement term S_{SW} is added to the fermion action with a coefficient $c_{SW}(g_0)$, which has to be computed.

It turns out that one has to take some care that the improvement of the lattice action is compatible with renormalization Lüscher et al. [1996], since some of the $O(a)$ improvement terms amount to a redefinition of the bare parameters and fields. A mass-independent renormalization scheme compatible with improvement is given in Lüscher

et al. [1996], where the renormalized coupling and mass read

$$g_{\mathrm{R}}^2 = \tilde{g}_0^2 Z_g(\tilde{g}_0^2, a\mu), \tag{2.19}$$

$$m_{\mathrm{R}} = \widetilde{m}_q Z_m(\tilde{g}_0^2, a\mu), \tag{2.20}$$

where μ is the renormalization scale and the modified bare parameters $\tilde{g}_0, \widetilde{m}_q$ are given by

$$\tilde{g}_0^2 \;= g_0^2 \left[1 + a\, b_g(g_0^2)\, m_{\mathrm{q}}\right] \tag{2.21}$$

$$\widetilde{m}_q \;= m_{\mathrm{q}} \left[1 + a\, b_m(g_0^2)\, m_{\mathrm{q}}\right], \quad m_{\mathrm{q}} = m_0 - m_{\mathrm{c}}. \tag{2.22}$$

To give the critical bare mass m_{c} a precise meaning, we have to go through some more definitions. The $O(a)$ improved axial current and the pseudoscalar density read

$$(A_I)_\mu(x) = \overline{\psi}_{\mathrm{l}}(x)\gamma_\mu\gamma_5\psi_{\mathrm{h}}(x) + ac_{\mathrm{A}}\,\tilde{\partial}_\mu P(x), \tag{2.23}$$

$$P(x) = \overline{\psi}_{\mathrm{l}}(x)\gamma_5\psi_{\mathrm{h}}(x). \tag{2.24}$$

We labeled the two quark flavors involved *heavy* and *light* for later convenience. The symmetric lattice derivative is defined in terms of the forward and backward derivatives, $\tilde{\partial}_\mu = 1/2(\partial_\mu + \partial_\mu^*)$, which in turn read

$$\partial_\mu\psi(x) = \frac{1}{a}\Big[\psi(x + a\hat{\mu}) - \psi(x)\Big], \tag{2.25}$$

$$\partial_\mu^*\psi(x) = \frac{1}{a}\Big[\psi(x) - \psi(x - a\hat{\mu})\Big]. \tag{2.26}$$

The renormalization of (2.23) and (2.24) will be explained in section 4.1.1. For now it is enough to say that we can define the renormalized quark masses $(m_{\mathrm{h}})_{\mathrm{R}}$ and $(m_{\mathrm{l}})_{\mathrm{R}}$ through the PCAC relation

$$\langle\tilde{\partial}(A_R)_\mu(x)\mathcal{O}\rangle = [(m_{\mathrm{h}})_{\mathrm{R}} + (m_{\mathrm{l}})_{\mathrm{R}}]\,\langle P_R(x)\mathcal{O}\rangle + O(a^2). \tag{2.27}$$

Here, $\mathcal{O}$ can be any product of renormalized, improved fields, which are separated from each other and x by a non-zero physical distance. Assuming two mass degenerate flavors for now, we may define the critical mass through

$$m_{\mathrm{R}}(m_0 = m_{\mathrm{c}}) \equiv 0. \tag{2.28}$$

2.4. HQET

The lattice discretization of HQET is rather straight forward. Using the identities (1.37), one infers from (1.35) and (2.6) that the static lattice actions reads Eichten and Hill

[1990a]

$$S_{\mathrm{h}}\Big[U,\overline{\psi}_{\mathrm{h}},\psi_{\mathrm{h}}\Big]=\frac{1}{1+a\,\delta m}a^4\sum_x\overline{\psi}_{\mathrm{h}}(x)(\nabla_0^*+\delta m)\psi_{\mathrm{h}}(x), \tag{2.29}$$

$$S_{\bar{\mathrm{h}}}\Big[U,\overline{\psi}_{\bar{\mathrm{h}}},\psi_{\bar{\mathrm{h}}}\Big]=\frac{1}{1+a\,\delta m}a^4\sum_x\overline{\psi}_{\bar{\mathrm{h}}}(x)(\nabla_0+\delta m)\psi_{\bar{\mathrm{h}}}(x), \tag{2.30}$$

where we have a specific (but ultimately irrelevant) normalization factor $1/(1+a\,\delta m)$. The term δm is an additive mass renormalization like m_{c} in (2.22), but of course defined differently. If we calculate the static propagator $G_{\mathrm{h}}(x,y)$ by solving

$$\frac{1}{1+a\,\delta m}(\nabla_0^*+\delta m)G_{\mathrm{h}}(x,y)=\delta_{xy}P_+, \tag{2.31}$$

we find that

$$G_{\mathrm{h}}(x,y)=\theta(x_0-y_0)\,\delta_{\mathbf{x},\mathbf{y}}\,e^{-\widehat{\delta m}(x_0-y_0)}\,\mathcal{U}_0(y,x)^\dagger\,P_+,\quad \widehat{\delta m}=\frac{1}{a}\log(1+a\,\delta m), \tag{2.32}$$

with

$$\theta(x)=\begin{cases}1 & \text{if } x\geq 0,\\ 0 & \text{else.}\end{cases} \tag{2.33}$$

The parallel transporter $\mathcal{U}_0$ is a straight line in the time direction and can be constructed recursively,

$$\mathcal{U}_0(x,x)=1,\quad \mathcal{U}_0(x,y+\hat{0})=\mathcal{U}_0(x,y)\,U_0(y). \tag{2.34}$$

The counter-term δm just shifts all energy levels in the static theory, as in (2.32). It is then sufficient to perform all calculations with $\delta m=0$ and account for the energy shift in the final results by setting Sommer [2011]

$$E^{QCD}=E^{\mathrm{stat}}|_{\delta m=0}+\widehat{\delta m}+m_{\mathrm{h}}. \tag{2.35}$$

One finds that the only $O(a)$-improvement term entering the theory can be absorbed by a redefinition of δm Kurth and Sommer [2001]. However, one often considers observables where δm cancels and thus no $O(a)$-effects are present.

2.4.1. $1/m_{\mathrm{h}}$ Corrections

To include the operators $\mathcal{O}_{\mathrm{kin}}$ and $\mathcal{O}_{\mathrm{spin}}$ from (1.36), we first have to find the corresponding lattice versions. The Laplacian is translated to $(\nabla_k^*\nabla_k)$, such that

$$\mathcal{O}_{\mathrm{kin}}(x)=\overline{\psi}_{\mathrm{h}}(x)\nabla_k^*\nabla_k\psi_{\mathrm{h}}(x),\quad \overline{\mathcal{O}}_{\mathrm{kin}}(x)=\overline{\psi}_{\bar{\mathrm{h}}}(x)\nabla_k^*\nabla_k\psi_{\bar{\mathrm{h}}}(x). \tag{2.36}$$

For the field strength $F_{\mu\nu}$, we already have the clover prescription, $\mathcal{F}_{\mu\nu}$ in equation (2.18). We set as in (1.38)

$$\mathcal{O}_{\mathrm{spin}}(x)=\overline{\psi}_{\mathrm{h}}(x)\,\sigma\cdot\mathbf{B}(x)\,\psi_{\mathrm{h}}(x),\quad \overline{\mathcal{O}}_{\mathrm{spin}}(x)=\overline{\psi}_{\bar{\mathrm{h}}}(x)\,\sigma\cdot\mathbf{B}(x)\,\psi_{\bar{\mathrm{h}}}(x), \tag{2.37}$$

but now with $B_k = \frac{i}{2}\epsilon_{ijk}\mathcal{F}_{ij}$. It is known that renormalization introduces no new operators in the Lagrangian, and thus treating the coefficients $\omega_{\mathrm{kin}}, \omega_{\mathrm{spin}}$ of $\mathcal{O}_{\mathrm{kin}}$ and $\mathcal{O}_{\mathrm{spin}}$ as free parameters is sufficient Sommer [2011]. The $1/m_{\mathrm{h}}$ expansion of expectation values (1.40) then reads in the lattice theory

$$\langle \mathcal{O} \rangle = \langle \mathcal{O} \rangle_{\mathrm{stat}} + \omega_{\mathrm{kin}} a^4 \sum_x \langle \mathcal{O}\mathcal{O}_{\mathrm{kin}}(x) \rangle_{\mathrm{stat}} + \omega_{\mathrm{spin}} a^4 \sum_x \langle \mathcal{O}\mathcal{O}_{\mathrm{spin}}(x) \rangle_{\mathrm{stat}} + O\left(\frac{1}{m_{\mathrm{h}}^2}\right) \quad (2.38)$$

and in fact performing this expansion is required, else the continuum limit of the theory does not exist Thacker and Lepage [1991].

2.5. Schrödinger Functional

To formulate the Schrödinger functional on the lattice we can use the lattice gauge and fermion action as defined in (2.14) and (2.6), c.f. Lüscher et al. [1992], Sint [1994]. The boundary term in the quark action (1.52) can be included in an elegant way. The quark field boundary conditions are like in the continuum (1.48), given in terms of the lattice fields $\overline{\rho}, \rho, \rho', \overline{\rho}'$. We pad the other components with zeros, setting

$$\psi(x) = 0, \quad \text{for } x_0 < 0,\ x_0 > T, \quad P_- \psi(x)|_{x_0=0} = P_+ \psi(x)|_{x_0=T} = 0, \quad (2.39)$$

and for the anti-quark field correspondingly

$$\overline{\psi}(x) = 0, \quad \text{for } x_0 < 0,\ x_0 > T, \quad \overline{\psi}(x) P_+|_{x_0=0} = \overline{\psi}(x) P_-|_{x_0=T} = 0. \quad (2.40)$$

With these conventions, the Wilson action or any reasonable fermion action (2.7) may be used.

In the gauge sector, one must relate the boundary conditions on the algebra fields (1.43) to corresponding boundary conditions on the lattice gauge fields. Taking the formula for the continuum parallel transporter (1.15) as a point of reference, one sees that Lüscher et al. [1992]

$$W_k(\mathbf{x}) = P \exp\left\{ a g_0 \int_0^1 \mathrm{d}t\ C_k(\mathbf{x} + a\hat{\mathbf{k}} - ta\hat{\mathbf{k}}) \right\}, \quad (2.41)$$

and W' defined as above with C replaced by C' are the correct choices. One sets

$$U_k(x)|_{x_0=0} = W_k(\mathbf{x}), \quad U_k(x)|_{x_0=T} = W'_k(\mathbf{x}). \quad (2.42)$$

The integration over gauge transformations of the boundary values in (1.42) is obsolete in the lattice formulation, since the lattice version of the Schrödinger functional is already invariant under these Lüscher et al. [1992]. The gluon action (2.14) or (2.15) may then be used.

2.5.1. Expectation Values

The boundary values $\rho, \rho', \overline{\rho}, \overline{\rho}'$ allow for the definition of boundary fields Lüscher et al. [1996],

$$\zeta(\mathbf{x}) = \frac{\delta}{\delta\overline{\rho}(\mathbf{x})}, \quad \overline{\zeta}(\mathbf{x}) = -\frac{\delta}{\delta\rho(\mathbf{x})}, \quad \zeta'(\mathbf{x}) = \frac{\delta}{\delta\overline{\rho}'(\mathbf{x})}, \quad \overline{\zeta}'(\mathbf{x}) = -\frac{\delta}{\delta\rho'(\mathbf{x})}, \tag{2.43}$$

which can be included in observables. We may then write down the generating functional

$$\mathcal{Z}_F[\overline{\eta}, \eta, \overline{\rho}, \rho, \overline{\rho}', \rho', U] = \int \mathcal{D}\Big[\overline{\psi}, \psi\Big]\, e^{-S_F[U,\overline{\psi},\psi] + a^4 \sum_x \{\overline{\eta}(x)\psi(x) + \overline{\psi}(x)\eta(x)\}}. \tag{2.44}$$

The fermion average of any function $\mathcal{O}$ of the quark and boundary fields (2.43) can now be calculated replacing $\psi, \overline{\psi}$ with derivatives with respect to the source fields as in (1.5) and then use

$$\langle \mathcal{O} \rangle_F = \frac{1}{\mathcal{Z}_F[U]}\, \mathcal{O}\, \mathcal{Z}_F[\overline{\eta}, \eta, \overline{\rho}, \rho, \overline{\rho}', \rho', U]\Big|_{\overline{\eta}=\ldots=\rho'=0}, \tag{2.45}$$

again with

$$\mathcal{Z}_F[U] = \mathcal{Z}_F[0,0,0,0,0,0,U] = \int \mathcal{D}\Big[\overline{\psi}, \psi\Big]\, e^{-S_F[U,\overline{\psi},\psi]}\Big|_{\overline{\rho}=\rho=\overline{\rho}'=\rho'=0}. \tag{2.46}$$

The gauge average is then obtained as in equation (1.7), now using the partition function

$$Z_G[C', C] = \int \mathcal{D}[U] e^{-S_G[U]} \mathcal{Z}_F[U]. \tag{2.47}$$

One uses the Haar measure for compact Lie groups (such as $SU(N)$, see any textbook on lattice QCD, e.g. Gattringer and Lang [2010]), defined by the basic properties

$$\mathrm{d}U = \mathrm{d}(UV) = \mathrm{d}(VU), \quad \int \mathrm{d}U = 1. \tag{2.48}$$

The point is that we now integrate over a compact group and thus the infinities mentioned in section 1.7 are absent, and therefore the gauge fixing procedure described there is not needed in general. However, if we want to apply the weak-coupling expansion as in section 1.6 to the lattice theory, we still need to fix the gauge. The reason for this is that the bilinear part (in terms of q_μ) of the gluon action is still not invertible and thus the free gluon propagator is not defined before fixing the gauge.

2.5.2. Background Field

If the boundary values C, C' are chosen such that the background field B has the desired properties stated in section 1.9.2, we can assume that the lattice gauge configuration V_μ minimizing the action $S_G[U]$ should be unique just as B_μ and most importantly it should be in correspondence with its continuum counterpart Lüscher et al. [1992],

$$V_\mu(x) = 1 + a\, B_\mu(x) + O(a^2). \tag{2.49}$$

From now on, we will assume that the boundary conditions are chosen either to produce an Abelian background field as described in appendix C.2 or are set to zero, such that the background field is trivial, $B_\mu \equiv 0$.

A link variable U_μ close to V_μ may then be written in terms of the background and fluctuation field q_μ analogous to (1.46),

$$U_\mu(x) = \exp\{a\, g_0\, q_\mu(x)\} V_\mu(x). \tag{2.50}$$

To be compatible with the boundary conditions, q must then obey homogeneous boundary conditions as in the continuum,

$$q_\mu(x)|_{x_0=0} = q_\mu(x)|_{x_0=T} = 0. \tag{2.51}$$

2.5.3. Gauge Fixing in the Schrödinger Functional

Before performing perturbative calculations, we have to fix the gauge as explained in section 1.7. This procedure is rather involved in the Schrödinger functional. Only periodic gauge transformations which do not change the boundary fields are allowed and this fact must be taken into account when fixing the gauge. We refer the reader to Lüscher et al. [1992] and only state the most important results from this reference here for brevity.

For the gauge fixing function $F(U)$, one chooses a linear mapping from the space $\mathcal{H}$ of gauge fields in an infinitesimal neighborhood of the background field V to the Lie algebra $\mathcal{L}$ of the gauge group $\mathcal{G}$ as defined in Lüscher [1990]. We parametrize the gauge fields in $\mathcal{H}$ as in (2.50), and similarly an infinitesimal gauge transformation Ω may be written in terms of an element $\omega \in \mathcal{L}$,

$$\Omega(x) = 1 - g_0 w(x) + O(g_0^2). \tag{2.52}$$

We then define the gauge fixing function

$$F(U) = \mathrm{d}^* q \tag{2.53}$$

in terms of the mapping $\mathrm{d} : \mathcal{L} \to \mathcal{H}$,

$$\omega(x) \mapsto (\mathrm{d}\omega)_\mu(x) = \nabla_\mu \omega(x). \tag{2.54}$$

It is defined through action of the operators ∇_μ and ∇^*_μ on elements of the Lie *algebra* $su(3)$ of $SU(3)$ (note these are different operators than (2.1) and (2.2)),

$$\nabla_\mu f(x) = \frac{1}{a}\left\{V_\mu(x)\, f(x + a\hat{\mu})\, V_\mu^{-1}(x) - f(x)\right\}, \tag{2.55}$$

$$\nabla^*_\mu f(x) = \frac{1}{a}\left\{f(x) - V_\mu^{-1}(x - a\hat{\mu})\, f(x - a\hat{\mu})\, V_\mu(x - a\hat{\mu})\right\}. \tag{2.56}$$

The adjoint action of d may then be defined using the scalar product in the algebra,

$$(q, r) = -2a^4 \sum_{x,\mu} \mathrm{tr}\,[q_\mu(x) r_\mu(x)]. \tag{2.57}$$

Setting $(\mathrm{d}^* q, \omega) = -(q, \mathrm{d}\omega)$, the gauge fixing term finally reads

$$S_{GF}[B, q] = \frac{\lambda_0}{2} (\mathrm{d}^* q, \mathrm{d}^* q). \tag{2.58}$$

We need to add this to the gauge action (2.15) to be able to invert the bilinear part and obtain the tree level gluon propagator. Explicitly, one finds that in the bulk

$$\mathrm{d}^* q(x) = \nabla^*_\mu q_\mu(x), \quad 0 < x_0 < T \tag{2.59}$$

and at the boundary for $x_0 = 0$ or $x_0 = T$

$$[\mathrm{d}^* q(x)]_{\alpha\beta} = \begin{cases} \frac{a^2}{L^3} \sum_{\mathbf{y}} [q_0(0, \mathbf{y})]_{\alpha\beta}, & \text{if } \alpha = \beta \text{ and } x_0 = 0, \\ 0 & \text{else.} \end{cases} \tag{2.60}$$

The Faddeev-Popov action is given in terms of the ghost field $\overline{c}, c$ by

$$S_{FP}[B, q, \overline{c}, c] = -(\overline{c}, \mathrm{d}^* \delta_c q), \tag{2.61}$$

with the first order variation $\delta_c q$ of q under the gauge transformation generated by c (c.f. 1.32)),

$$\delta_c q_\mu = \nabla_\mu c + g_0 \mathrm{Ad} q_\mu c + \left\{ \frac{1}{2} g_0\, a\, \mathrm{Ad} q_\mu + \frac{1}{12} (g_0\, a\, \mathrm{Ad} q_\mu)^2 + \ldots \right\} \nabla_\mu c. \tag{2.62}$$

The adjoint representation of $SU(3)$ is defined in the usual way, i.e. we have

$$\mathrm{Ad} X(Y) = [X, Y], \quad X, Y \in SU(3). \tag{2.63}$$

The terms in (2.62) yield the perturbative expansion of the ghost action up to order g_0^2. As it turns out, the ghost contribution to processes at $O(g_0^2)$ vanishes for a trivial background field Lüscher and Weisz [1996].

2.5.4. $O(a)$ Improvement

As stated in Lüscher et al. [1992], $O(a)$-improvement in the gauge sector may be implemented by including a factor $w(x, \mu, \nu)$ in the gauge action (2.14) to adjust the weight of the plaquettes at the boundaries. Equivalently, one may introduce the boundary counter-terms Lüscher et al. [1996]

$$\delta S_{G,s}[U] = \frac{1}{2g_0^2} (c_s - 1) \sum_{p_s} \mathrm{tr}\,[1 - U(p_s)] + \frac{1}{2g_0^2} (c_t - 1) \sum_{p_t} \mathrm{tr}\,[1 - U(p_t)]. \tag{2.64}$$

The summations run over all time-like and space-like plaquettes p_t, p_s at the boundaries. For more complicated gauge actions (2.15), more operators may be included Aoki et al. [1999] to achieve improvement. For the fermion sector, the boundary counter-terms read Lüscher et al. [1996]

$$\hat{\mathcal{O}}_t(\mathbf{x}) = \frac{1}{a}\left\{\overline{\psi}(y)\,\psi(y) - \overline{\psi}(y)\,U_0(y-\hat{0})^{-1}\rho(\mathbf{x}) - \overline{\rho}(\mathbf{x})\,U_0(y-\hat{0})\,\psi(y)\right\}_{y=(a,\mathbf{x})}, \tag{2.65}$$

$$\hat{\mathcal{O}}'_t(\mathbf{x}) = \frac{1}{a}\left\{-\overline{\psi}(y)\,\psi(y) + \overline{\psi}(y)\,U_0(y)\,\rho'(\mathbf{x}) + \overline{\rho}'(\mathbf{x})\,U_0(y)^{-1}\psi(y)\right\}_{y=(T-a,\mathbf{x})}, \tag{2.66}$$

$$\hat{\mathcal{O}}_s(\mathbf{x}) = \frac{1}{2}\,\overline{\rho}(\mathbf{x})\,\gamma_k\,(\nabla_k^* + \nabla_k)\,\rho(\mathbf{x}), \tag{2.67}$$

$$\hat{\mathcal{O}}'_s(\mathbf{x}) = \frac{1}{2}\,\overline{\rho}'(\mathbf{x})\,\gamma_k\,(\nabla_k^* + \nabla_k)\,\rho'(\mathbf{x}). \tag{2.68}$$

They are included in the fermion action with coefficients $(\tilde{c}_t - 1)$ and $(\tilde{c}_s - 1)$ respectively, such that the boundary correction to the fermion action reads

$$\delta S_{F,b} = a^4 \sum_{\mathbf{x}} \left\{(\tilde{c}_t - 1)\left[\hat{\mathcal{O}}_t(\mathbf{x}) - \hat{\mathcal{O}}'_t(\mathbf{x})\right] + (\tilde{c}_s - 1)\left[\hat{\mathcal{O}}_s(\mathbf{x}) + \hat{\mathcal{O}}'_s(\mathbf{x})\right]\right\}. \tag{2.69}$$

Further correction terms may be absorbed in the renormalization factor of the boundary fields (2.43), such that the renormalized fields read Lüscher et al. [1996]

$$\zeta_R(\mathbf{x}) = Z_\zeta(\tilde{g}_0^2, a\mu)\,(1 + b_\zeta\,a\,m_\mathrm{q})\,\zeta(\mathbf{x}), \tag{2.70}$$

and for the other boundary fields accordingly. The bare parameters are renormalized according to (2.19), (2.20) and the clover term (2.17) must be included as well (again with a factor $c_{SW}(g_0)$).

2.6. Monte Carlo Methods

Even though the main focus of this thesis is on the weak-coupling expansion, we feel that we should spend a little time to explain the most basic principles of the Monte Carlo method to evaluate the path integral, since it is probably the most important tool in lattice QCD. Furthermore, we will rely on Monte Carlo methods for the cross checks discussed in section 4.3. However, we will only mention the most important aspects here and refer the reader to the literature, e.g. Gattringer and Lang [2010].

First, we write down the gauge average again,

$$\langle\mathcal{O}\rangle_G = \frac{1}{Z}\int \mathcal{D}[U] e^{-S[U]}\mathcal{O}[U], \tag{2.71}$$

with

$$\exp\{-S\} = \exp\{-S_G\}\det[D] = \exp\{-S_G + \mathrm{tr}\,[\log D]\} = \exp\{-S_G - S_F^{\mathrm{eff}}\}. \tag{2.72}$$

The symbol D stands for the lattice Dirac operator. The key observation is that we can

calculate (2.71) using a sum,

$$\langle \mathcal{O} \rangle_G = \lim_{N\to\infty} \frac{1}{N} \sum_{n=1}^{N} \mathcal{O}[U_n], \tag{2.73}$$

if we draw random gauge configurations U_n with probability density

$$\mathrm{d}P(U) = \frac{1}{Z} e^{-S[U]} \mathcal{D}[U]. \tag{2.74}$$

The main problem here is that the probability density must be positive and real, which is not always guaranteed. However, in most cases the lattice Dirac operator obeys γ_5-hermiticitiy,

$$\gamma_5 \, D \, \gamma_5 = D^\dagger, \tag{2.75}$$

which ensures that the determinant is real. To satisfy the second condition, one can e.g. choose to use two mass-degenerate flavors, which makes the determinant a square and thus positive.

To obtain the random gauge configurations U_n in (2.73), one usually uses a Markov chain, which will generate the U_n sequentially,

$$\ldots \longrightarrow U_{n-1} \longrightarrow U_n \longrightarrow U_{n+1} \longrightarrow \ldots, \tag{2.76}$$

starting from some initial configuration U_0. If the algorithm to produce the Markov chain is chosen with care, the probability distribution of the generated sequence will after some initial thermalization converge towards the desired one given by (2.74). The subject how to choose a correct and efficient algorithm is a broad field and we refer the reader to the literature at this point Gattringer and Lang [2010], Kennedy [2006], Lüscher [2011].

Choosing boundary conditions such as the Schrödinger functional ones one may, for a modest number of lattice points of say $L/a = O(10)$, store the gauge field on a computer (up to a given numerical precision). In the past, one usually applied the quenched approximation by setting the fermion determinant in (2.72) to unity. Generating configurations with weight proportional to $\exp(-S_G)$, one may then approximate the gluon path integral (2.71) numerically, truncating (2.73) at some large N. This will introduce a statistical error of $O(1/\sqrt{N})$. Quarks then only enter as propagators through the fermion average (2.45) and thus the quenched approximation amounts to neglecting vacuum loops of quarks. A simple method to generate gauge configurations that is guaranteed to yield the correct distribution is the Metropolis algorithm Metropolis et al. [1953]. In practice, it turns out to be rather slow in decorrelating[1] the gauge field configurations. Very efficient alternatives exists, for example the hybrid overrelaxation algorithm Adler [1981], Horvath and Kennedy [1998], Wolff [1992], with which it is pos-

[1] A problem of many algorithms is that subsequent configurations are correlated. This has to be taken into account in the computation of the statistical error. We will not discuss this further and refer the reader to e.g. Wolff [2004], Schaefer et al. [2011].

sible to generate many thousands of uncorrelated configurations. A variety of quenched simulations have been successfully performed Bowler et al. [2000], Aoki et al. [2003]. We will use quenched Monte Carlo data to perform our cross check in section 4.3 as well. Neglecting the quark vacuum loops will introduce no systematic error in our case since we are only interested in extracting the one loop result.

The inclusion of dynamical fermions is not a straight forward task. One usually rewrites the fermion determinant as a Gaussian integral over a boson field. The new variables are then called pseudo-fermions and may be represented on a computer. This comes at the cost that the resulting action is non-local, which means that its calculation after a Monte Carlo step is relatively costly, even if only local changes in the gauge field were applied. There are efficient methods for simulations of QCD with dynamical fermions available, such as the much used hybrid Monte Carlo algorithm Duane and Kogut [1985, 1986].

3. Automated Lattice Perturbation Theory in the Schrödinger Functional

The author developed the `pastor` software package for automated lattice perturbation theory calculations in the Schrödinger functional. The package consists of two parts. The front end written in Python is a code generator that will produce computer programs for calculating all terms in the perturbative expansions of observables in the Schrödinger functional up to and including order g_0^2. The back end is a C++ library used by these programs to generate Feynman rules for general fermion and gluon actions given in the form of (2.7), (2.15).

3.1. Preliminaries

Before we discuss details of the algorithms used to perform the weak-coupling expansion for Schrödinger functional observables, we give a brief introduction to this rather technical chapter, explaining which objects we have to deal with and at what stage they enter.

3.1.1. Some Examples

We start with a few examples of interesting Schrödinger functional observables involving two quark flavors, which we call heavy and light. The light mass is always chosen such that $m_\mathrm{q} = 0$, and the heavy mass is given by the parameter $z = L\, m_\mathrm{R}$. The two flavors obey the boundary conditions (1.49) with phase angles θ_h and θ_l. We will frequently choose $\theta_\mathrm{h} = \theta_\mathrm{l} = \theta$, and only indicate the dependence on one angle. A bigger set of relevant correlation functions will be discussed in more detail in section 4.1.

In the following we will frequently refer to *boundary kernels*. These enter through the inclusion of boundary fields (2.43) in our observables and will be formally introduced in section 3.2. For now, one can think of them as gauge links connecting the boundary and the bulk. As the first observable, consider the boundary to bulk correlator shown in figure 3.1 Lüscher et al. [1996],

$$f_\mathrm{A}(x_0;\theta_\mathrm{h},\theta_\mathrm{l},z) = -\frac{a^6}{2}\sum_{\mathbf{y}_1,\mathbf{y}_2}\langle (A_I)_0(x)\overline{\zeta_\mathrm{h}}(\mathbf{y}_1)\gamma_5\zeta_\mathrm{l}(\mathbf{y}_2)\rangle, \tag{3.1}$$

involving the improved axial vector current (2.23). For our second example, shown in figure 3.1 as well, we choose a correlator involving an order $1/m_\mathrm{h}$ correction operator Della Morte et al. [2007] and a static quark (also labeled by the subscript h on the fields),

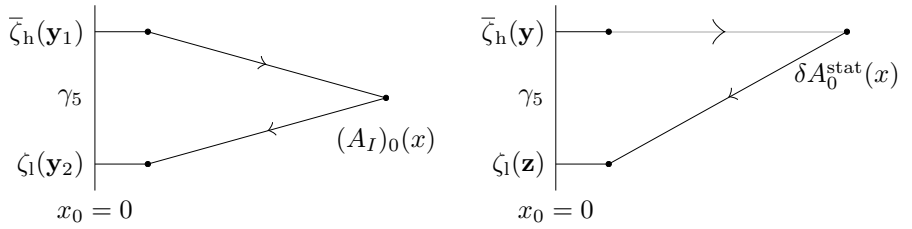

Figure 3.1.: The correlation functions f_{A} (left) and $f_{\delta\mathrm{A}}^{\mathrm{stat}}$ (right). Double fermion lines depict the propagation of a static quark, the dotted lines represent the boundary kernels.

$$f_{\delta\mathrm{A}}^{\mathrm{stat}}(x_0;\theta_{\mathrm{h}},\theta_{\mathrm{l}}) = -\frac{a^6}{2}\sum_{\mathbf{y},\mathbf{z}}\langle\delta A_0^{\mathrm{stat}}(x)\overline{\zeta_{\mathrm{h}}}(\mathbf{y})\gamma_5\zeta_{\mathrm{l}}(\mathbf{z})\rangle_{\mathrm{stat}}. \tag{3.2}$$

The static expectation value was defined in section 2.4.1 and the correction δA^{stat} reads

$$\delta A_0^{\mathrm{stat}}(x) = \overline{\psi}_{\mathrm{l}}(x)\frac{1}{2}\left(\overleftarrow{\nabla}_k + \overleftarrow{\nabla}_k^*\right)\gamma_k\gamma_5\psi_{\mathrm{h}}(x). \tag{3.3}$$

Lastly, we have the observable (c.f. figure 3.2)

$$F_{\mathrm{A}}(x_0;\theta,z) = \frac{a^{18}}{4L^6}\sum_{\substack{\mathbf{y}_1,\mathbf{y}_2,\mathbf{y}_3,\\ \mathbf{y}_4,\mathbf{y}_5,\mathbf{y}_6}}\langle(A_I)_0(x)\overline{\zeta_{\mathrm{h}}}(\mathbf{y}_1)\gamma_5\zeta_{\mathrm{l}}(\mathbf{y}_2)\overline{\zeta}'_1(\mathbf{y}_3)\gamma_5\zeta'_2(\mathbf{y}_5)\overline{\zeta}_2(\mathbf{y}_5)\gamma_5\zeta_1(\mathbf{y}_6)\rangle, \tag{3.4}$$

which involves two more light flavors, labeled by 1 and 2. For convenience, we set all

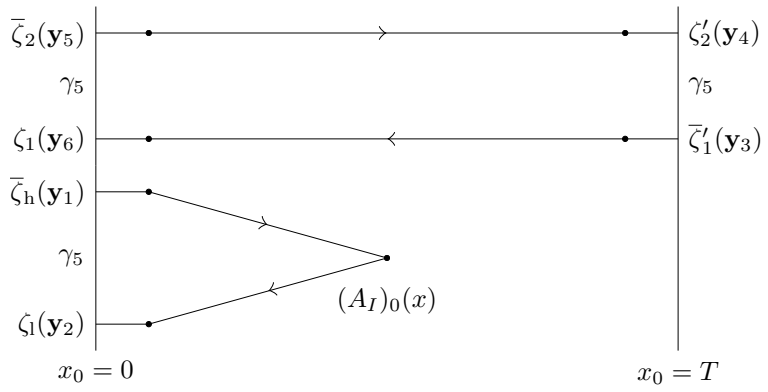

Figure 3.2.: The correlation functions F_{A}. Dotted lines represent the boundary kernels.

phase angles $\theta = \theta_{\mathrm{h}} = \theta_{\mathrm{l}} = \theta_{\mathrm{l}_1} = \theta_{\mathrm{l}_2}$ equal.

These examples show us the nature of the objects, that we expect to appear in Schrödinger functional observables.

One or more fermion traces. Multiple Dirac traces can occur in an observable like (3.4) after taking the fermion average $\langle\cdot\rangle_F$. Each trace may contain:

Quark fields. We can encounter bulk fields $\psi, \overline{\psi}$ and boundary fields $\zeta, \overline{\zeta}, \zeta', \overline{\zeta}'$, defined in (2.43). As it is the case in all examples, one usually projects to zero momentum at the boundary by summing over all spatial points. Even though this is the standard situation, other choices are possible in `pastor`.

Operator insertions. Terms like the one containing the covariant derivative in (3.2) may be written in the form

$$\mathcal{I}(x) = a^4 \sum_y \overline{\psi}(x)\kappa(x,y)\psi(y). \tag{3.5}$$

After performing the fermion Wick contractions, the kernel κ remains as an insertion in the trace. We may define κ as a sum over paths just as in the fermion action (2.7) and due to this similarity the method we will use to expand S_F in powers of g_0 carries over to $\mathcal{I}$ literally.

The method employed in Lüscher and Weisz [1996] may be used to obtain the g_0-expansion of any observable $\mathcal{O}$ up to a given order r. It may be described as follows: The first step is to take the fermion average, which we will discuss in section 3.2. Then, $\langle\mathcal{O}\rangle_F$ must be expanded in g_0 up to and including order r, with the methods we will discuss in sections 3.2.3 and 3.4. We will see that this procedure leaves us with expressions containing up to r free gluon indices. The last step is to take the gauge average $\langle\langle\mathcal{O}\rangle_F\rangle_G$. This is done by expanding the gauge action (2.15) up to order r as well (section 3.4) and performing all the possible gluon Wick contractions in $\langle\langle\mathcal{O}\rangle_F\rangle_G$. We will comment on this step in section 3.3. The C++ back end of `pastor` may be used to expand S_G and S_F in their generic forms up to any order in g_0.

However, the Python front end will apart from the tree level contribution only generate diagrams at order g_0^2, which fall into two categories. The first category contains loops like the one shown in figure 3.3, which is a contribution to f_A. Summations run over all

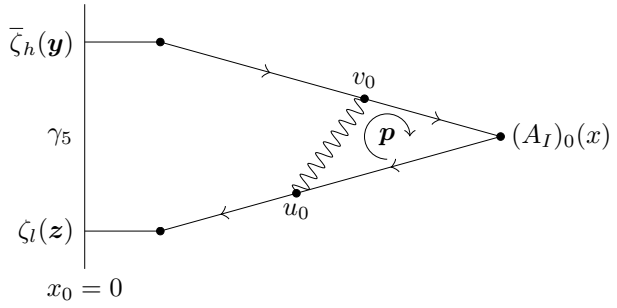

Figure 3.3.: Example for a loop diagram.

intermediate indices. Due to the momentum cut-off introduced by the lattice, we have

a finite set of momenta $\mathbf{p}$ as in (1.50) with $0 \leq n_k < L$. Further sums run over the time coordinates u_0, v_0 and the color indices, which are not shown explictly, but need to be included as well. The common choice $x_0 = T/2$ thus leads to a numerical effort of $O(L^3T^2)$ for the evaluation of this diagram.

The second category of order g_0^2 diagrams stems from terms in the action which depend explicitly or through their coefficients on the coupling. This dependence can enter through renormalization, e.g. in the mass parameter (2.20), or due to $O(a)$ improvement, such as in $c_{SW}(g_0)$ (3.45). All terms of this type are called counter-terms.

3.1.2. Including Counter-Terms

The improved Wilson fermion action is a sum of the terms (2.6), (2.17), (2.69),

$$S_{F,I} = S_F^W(m_0) + S_{SW}(c_{SW}) + \delta S_{F,b}(\tilde{c}_t, \tilde{c}_s). \tag{3.6}$$

One should note that the form of the $O(a)$ correction terms is dictated by the symmetries, such that one will end up with the same structure if any sensible generic action of the form (2.7) is used. We will collectively denote the parameters $(m_0, c_{SW}, \tilde{c}_t, \tilde{c}_s)$ with the vector $c(g_0)$. We assume that all parameters of the action depending on g_0 are contained in c. If we want to calculate the weak-coupling expansion of an observable $\mathcal{O}$, it is of advantage to keep the g_0-dependence of c separate from the powers of g_0 entering the action through the link variables. To this end, we write $c(g_0) = c^{(0)} + g_0^2 c^{(1)} + O(g_0^4)$, and

$$S_{F,I}(c) = S_{F,I}\left(c^{(0)}\right) + g_0^2 \sum_i c_i^{(1)} \partial_{c_i} S_{F,I}\left(c^{(0)}\right) + O(g_0^4). \tag{3.7}$$

We introduce the correction operators Δ,

$$\partial_{c_i} S_{F,I}\left(c^{(0)}\right) = -a^4 \sum_x \Delta_{c_i}(x), \tag{3.8}$$

wich allow us to express the fermion average of an operator $\mathcal{O}$ in the following way,

$$\langle \mathcal{O} \rangle_F = \langle \mathcal{O} \rangle_{F,c^{(0)}} + g_0^2 \sum_i c_i a^4 \sum_x \langle \mathcal{O} \Delta_i(x) \rangle_{F,c^{(0)}} + O(g_0^4). \tag{3.9}$$

The fermion average $\langle \cdot \rangle_{F,c^{(0)}}$ is taken using the action $S_{F,I}\left(c^{(0)}\right)$ in the Boltzmann factor, and we will call this the tree level improved fermion average. In the next sections, we will explain how a systematic weak-coupling expansion of the tree level improved fermion average may be performed. We will then deal with the counter-terms in section 3.5.

3.2. Fermion Average

We will now work out the fermion average (2.45) for a generic fermion action (2.7) in detail. To keep the notation short, we will use the following sum convention in this section: All lattice four- or three-vectors occurring more than once in an equation are

summed,

$$f(x)g(x) \equiv a^4 \sum_x f(x)g(x), \quad f(\mathbf{y})g(\mathbf{y}) \equiv a^3 \sum_{\mathbf{y}} f(\mathbf{y})g(\mathbf{y}). \tag{3.10}$$

We will essentially follow the steps taken in Lüscher and Weisz [1996] with a more general fermion action. Let $S_F[U, \overline{\psi}, \psi]$ be a lattice quark action as in (2.7). The fermion fields obey the boundary conditions (1.48), (2.39). The Dirac operator and its adjoint are for $0 < x_0 < T$ given by

$$\frac{\delta}{\delta\overline{\psi}(x)} S_F = (D+m)\psi(x), \quad -\frac{\delta}{\delta\psi(x)} S_F = \overline{\psi}(x)(\overleftarrow{D}^\dagger + m). \tag{3.11}$$

We define the kernels $K, K', \tilde{K}$, and $\tilde{K}'$ through the action of the Dirac operator at the boundary,

$$\begin{aligned} -\frac{\delta}{\delta\rho(\mathbf{x})} S_F &= -\overline{\psi}(y)\ K(y,\mathbf{x}), \quad \frac{\delta}{\delta\overline{\rho}(\mathbf{x})} S_F = -\tilde{K}(\mathbf{x},y)\ \psi(y) \\ -\frac{\delta}{\delta\rho'(\mathbf{x})} S_F &= -\overline{\psi}(y)\ K'(y,\mathbf{x}), \quad \frac{\delta}{\delta\overline{\rho}'(\mathbf{x})} S_F = -\tilde{K}'(\mathbf{x},y)\ \psi(y), \end{aligned} \tag{3.12}$$

where we understand $0 \le y_0 \le T$ and we have the boundary conditions

$$\begin{aligned} P_+\ K(y,\mathbf{x})|_{y_0=0} &= \tilde{K}(\mathbf{x},y)\ P_-|_{y_0=0} = 0, \\ P_- K'(y,\mathbf{x})|_{y_0=T} &= \tilde{K}(\mathbf{x},y)\ P_+|_{y_0=T} = 0. \end{aligned} \tag{3.13}$$

The explicit form of these kernels for improved Wilson fermions is given in appendix C.1. It is worth pointing out that the newly introduced kernels have some overlap at the boundaries,

$$\begin{aligned} K(x,\mathbf{y})|_{x_0=0} &= \tilde{K}(\mathbf{x},y)|_{y_0=0}, \\ K'(x,\mathbf{y})|_{x_0=T} &= \tilde{K}'(\mathbf{x},y)|_{y_0=T}. \end{aligned} \tag{3.14}$$

We define the Green's function S,

$$(D+m)S(x,y) = a^{-4}\delta_{xy}, \quad 0 < x_0 < T, \tag{3.15}$$

with the boundary conditions

$$\begin{aligned} P_+\ S(x,y)|_{x_0=0} &= P_-\ S(x,y)|_{x_0=T} = 0, \\ S(x,y)\ P_-|_{y_0=0} &= S(x,y)\ P_+|_{y_0=T} = 0. \end{aligned} \tag{3.16}$$

One may introduce a generalized version of the *classical solution* ψ_{cl} to the field equations as in Lüscher and Weisz [1996], defined by

$$(D+m)\psi_{\mathrm{cl}}(x) = 0, \quad 0 < x_0 < T, \tag{3.17}$$

with the boundary conditions

$$P_+\psi_{\rm cl}(x)|_{x_0=0} = \rho(\mathbf{x}), \quad P_-\psi_{\rm cl}(x)|_{x_0=T} = \rho'(\mathbf{x}). \tag{3.18}$$

Using the boundary kernels K and K', we may write explicitly

$$\psi_{\rm cl}(x) = S(x,y)\{K(y,\mathbf{z})\,\rho(\mathbf{z}) + K'(y,\mathbf{z})\,\rho'(\mathbf{z})\}, \quad 0 < x_0 < T. \tag{3.19}$$

Note that due to the boundary conditions of S (3.16) and K (3.13), there is no reference to the components at $y_0 = 0$ or $y_0 = T$. We will need the adjoint classical solution as well, defined by

$$\overline{\psi}_{\rm cl}(x)(\overleftarrow{D}^\dagger + m)|_{0<x_0<T} = 0, \quad \overline{\psi}_{\rm cl}(x)P_-|_{x_0=0} = \overline{\rho}(\mathbf{x}), \quad \overline{\psi}_{\rm cl}(x)P_+|_{x_0=T} = \overline{\rho}'(\mathbf{x}). \tag{3.20}$$

For $0 < x_0 < T$, $\overline{\psi}_{\rm cl}$ reads explicitly

$$\overline{\psi}_{\rm cl}(x) = \left\{\overline{\rho}(\mathbf{z})\,\tilde{K}(\mathbf{z},y) + \overline{\rho}'(\mathbf{z})\,\tilde{K}'(\mathbf{z},y)\right\} S(y,x). \tag{3.21}$$

3.2.1. Generating Functional

One may now use the classical solution to write the fermion action for a given gauge field explicitly. From equations (3.17), (3.18) one can see that the decomposition

$$\psi = \psi_{\rm cl} + \chi, \quad \overline{\psi} = \overline{\psi}_{\rm cl} + \overline{\chi}, \tag{3.22}$$

with

$$P_+\chi(x)|_{x_0=0} = P_-\chi(x)|_{x_0=T} = \overline{\chi}(x)P_-|_{x_0=0} = \overline{\chi}(x)P_+|_{x_0=T} = 0, \tag{3.23}$$

yields

$$S_F[\overline{\psi},\psi] = S_F[\overline{\chi},\chi] + S_F[\overline{\psi}_{\rm cl},\psi_{\rm cl}]. \tag{3.24}$$

One now proceeds as in standard quantum field theory and completes the square in the Boltzmann factor of (2.44) by making the substitution

$$\chi(x) \to \chi(x) + S(x,y)\,\eta(y), \quad \overline{\chi}(x) \to \overline{\chi}(x) + \overline{\eta}(y)\,S(y,x). \tag{3.25}$$

This leaves us with

$$\log \mathcal{Z}_F = \log \mathcal{Z}_F[U] - S_F[\overline{\psi}_{\rm cl},\psi_{\rm cl}] + \overline{\eta}(x)\,S(x,y)\,\eta(y) + \overline{\eta}(x)\,\psi_{\rm cl}(x) + \overline{\psi}_{\rm cl}(x)\,\eta(x), \tag{3.26}$$

All that is left to do now is to evaluate $S_F[\overline{\psi}_{\rm cl},\psi_{\rm cl}]$ by writing down the action at the boundary. From the definitions (3.12), we may infer that

$$-S_F[\overline{\psi}_{\rm cl},\psi_{\rm cl}] = \left\{\overline{\rho}(\mathbf{x})\tilde{K}(\mathbf{x},y) + \overline{\rho}'(\mathbf{x})\tilde{K}'(\mathbf{x},y)\right\}\psi_{\rm cl}(y). \tag{3.27}$$

With the representation of ψ_{cl} given in (3.19), we may write the Boltzmann factor of the generating functional ((2.44), also c.f. (2.46)) in a more explicit form,

$$\begin{aligned}\log \mathcal{Z}_F[\overline{\eta},\eta,\overline{\rho},\rho,\overline{\rho}',\rho',U] \\ = \log \mathcal{Z}_F[U] + \Big\{\overline{\rho}(\mathbf{x})\tilde{K}(\mathbf{x},y) + \overline{\rho}'(\mathbf{x})\,\tilde{K}'(\mathbf{x},y) + \overline{\eta}(y)\Big\}\, S(y,y') \\ \times \Big\{K(y',\mathbf{z})\,\rho(\mathbf{z}) + K'(y',\mathbf{z})\,\rho'(\mathbf{z}) + \eta(y')\Big\} \\ + \overline{\rho}(\mathbf{x})\,\tilde{K}(\mathbf{x},y)\,\rho(\mathbf{y})|_{y_0=0} + \overline{\rho}'(\mathbf{x})\,\tilde{K}'(\mathbf{x},y)\,\rho'(\mathbf{y})|_{y_0=T}. \end{aligned} \tag{3.28}$$

3.2.2. Functional Derivatives

Before extracting expectation values by differentiation with respect to the boundary values and source fields using (2.45), one should note that since only half of the components of the boundary fields are non-vanishing, it is necessary to impose further restrictions to ensure that the functional derivatives are well defined. As explained in appendix C of Lüscher et al. [1996], we may choose

$$\frac{\delta}{\delta\rho(\mathbf{x})}FP_+ = 0, \quad P_+\frac{\delta}{\delta\overline{\rho}(\mathbf{x})}F = 0 \tag{3.29}$$

for any polynomial $F[\overline{\rho},\rho]$ and for the boundary fields at $x_0 = T$ accordingly.

We may then compute the fermion expectation value $\langle P\rangle_F$ for a given gauge configuration with the recipe laid out in section 2.5.1.

3.2.3. Perturbative Expansion of Two Point Functions

The next step towards constructing Feynman diagrams is to expand the fermion averages in powers of the bare coupling g_0 Lüscher and Weisz [1996]. One should in principle calculate the expansions for all basic Wick contractions involving bulk and boundary fields. Instead of producing the whole list, we will work out a few examples,

$$\langle\psi(x)\overline{\psi}(y)\rangle_F = \frac{1}{\mathcal{Z}}\left(\frac{\delta}{\delta\overline{\eta}(x)}\right)\left(-\frac{\delta}{\delta\eta(y)}\right)\mathcal{Z}\Big|_{\overline{\rho}=\ldots=\eta=0} = S(x,y) \tag{3.30}$$

$$\langle\psi(x)\overline{\zeta}(\mathbf{z})\rangle_F = \frac{1}{\mathcal{Z}}\left(\frac{\delta}{\delta\overline{\eta}(x)}\right)\left(-\frac{\delta}{\delta\rho(\mathbf{z})}\right)\mathcal{Z}\Big|_{\overline{\rho}=\ldots=\eta=0} = S(x,y)\,K(y,\mathbf{z})\,P_+ \tag{3.31}$$

$$\langle\zeta(\mathbf{x})\overline{\psi}(z)\rangle_F = \frac{1}{\mathcal{Z}}\left(\frac{\delta}{\delta\overline{\rho}(\mathbf{x})}\right)\left(-\frac{\delta}{\delta\eta(z)}\right)\mathcal{Z}\Big|_{\overline{\rho}=\ldots=\eta=0} = P_-\tilde{K}(\mathbf{x},y)\,S(y,z) \tag{3.32}$$

$$\begin{aligned}\langle\zeta(\mathbf{x})\overline{\zeta}(\mathbf{y})\rangle_F &= \frac{1}{\mathcal{Z}}\left(\frac{\delta}{\delta\overline{\rho}(\mathbf{x})}\right)\left(-\frac{\delta}{\delta\rho(\mathbf{y})}\right)\mathcal{Z}\Big|_{\overline{\rho}=\ldots=\eta=0} \\ &= P_-\,\tilde{K}(\mathbf{x},x')\,S(x',y')\,K(y',\mathbf{y})\,P_+ + P_-\,\tilde{K}(\mathbf{x},y)\,P_+|_{y_0=0}\end{aligned} \tag{3.33}$$

The remaining contractions can be obtained by substituting the correct boundary kernels. The projectors come in due to the constraint in the definition of the variational

derivative with respect to the boundary fields. They are actually redundant in the last term of the r.h.s. of (3.33) due to the projectors in $\tilde{K}, K$ at the boundary. We will now explain how the perturbative expansion of the contractions given above may be obtained.

Bulk to Bulk

The bulk to bulk contraction (3.30) is given by

$$\langle \psi(x)\overline{\psi}(y)\rangle_F = S(x,y). \tag{3.34}$$

Using the definition of S, eq. (3.15), we can construct its expansion by solving

$$\left(D^{(0)} + m + \sum_{i=1}^{\infty} g_0^i \; D^{(i)}\right) \left(\sum_{i=0}^{\infty} g_0^i \; S^{(i)}(x,y)\right) = a^{-4}\delta_{xy} \tag{3.35}$$

order by order in g_0 Lüscher and Weisz [1996]. This involves the inversion of $(D^{(0)}+m)$ to obtain $S^{(0)}$ and then the explicit form of $D^{(i)}$ is needed to construct the higher order contributions, e.g.

$$S^{(1)}(x,z) = -S^{(0)}(x,y)\, D^{(1)}\, S^{(0)}(y,z). \tag{3.36}$$

A method to construct the Feynman rules $D^{(k)}$ automatically will be discussed in section 3.4. Even though the inverse of the Dirac operator $(D^{(0)}+m)$ is known for many actions, we perform a numerical inversion to obtain $S^{(0)}$ in order to not restrict ourselves to certain actions. Since we will work in time momentum space, the matrices that have to be inverted are of a manageable size, and one can use a QR decomposition to get the exact inverse up to round-off errors.

Bulk To Boundary

For the bulk to boundary Wick contractions such as in (3.31),

$$\langle \psi(x)\, \overline{\zeta}(\mathbf{z})\rangle_F = S(x,y)\; K(y,\mathbf{z})\; P_+, \tag{3.37}$$

little additional work is required once the expansion of S is constructed as explained above. Expanding the kernel K in powers of g_0, we get

$$\langle \psi(x)\, \overline{\zeta}(\mathbf{z})\rangle_F = \left(\sum_i g_0^i \; S^{(i)}(x,y)\right) \left(\sum_i g_0^i \; K^{(i)}(y,\mathbf{z})\right) \; P_+. \tag{3.38}$$

The method to construct the Feynman rules $D^{(i)}$ automatically may be used to obtain the expansion coefficients $K^{(j)}$ as well. This can be seen by comparing the definitions of a generic action (2.7) and of the boundary kernels (3.12).

Boundary To Boundary

As the last example for a basic Wick contraction, we consider the boundary to boundary one (3.33),

$$\langle \zeta(\mathbf{x})\,\overline{\zeta}(\mathbf{y})\rangle_F = P_- \left(\sum_i g_0^i\, \tilde{K}^{(i)}(\mathbf{x},x')\right) \left(\sum_i g_0^i\, S^{(i)}(x',y')\right) \left(\sum_i g_0^i\, K^{(i)}(y',\mathbf{y})\right) P_+ + P_- \left(\sum_i g_0^i\, \tilde{K}^{(i)}(\mathbf{x},y)\right) P_+\Big|_{y=(0,\mathbf{y})} . \quad (3.39)$$

All the terms in this formula may be constructed as explained above, no new contributions appear.

3.3. Gauge Average

The `pastor` front end will only produce diagrams up to order g_0^2, and taking the gauge average is in fact not a difficult task in this case. Let $\mathcal{O}$ be an observable consisting of a single fermion trace. The machinery explained above is then used to extract the first three terms in the expansion

$$\langle \mathcal{O}\rangle_F = \langle \mathcal{O}\rangle_F^{(0)} + g_0 \langle \mathcal{O}\rangle_F^{(1)} + g_0^2 \langle \mathcal{O}\rangle_F^{(2)} + O(g_0^3) \quad (3.40)$$

The gauge average of the tree level contribution $\langle \mathcal{O}\rangle_F^{(0)}$ is trivial. The g_0 coefficient $\langle \mathcal{O}\rangle_F^{(1)}$ has one free gluon index. This free index must be contracted with the tadpole diagram depicted in figure 3.4. The dashed line represents the ghost propagator, which

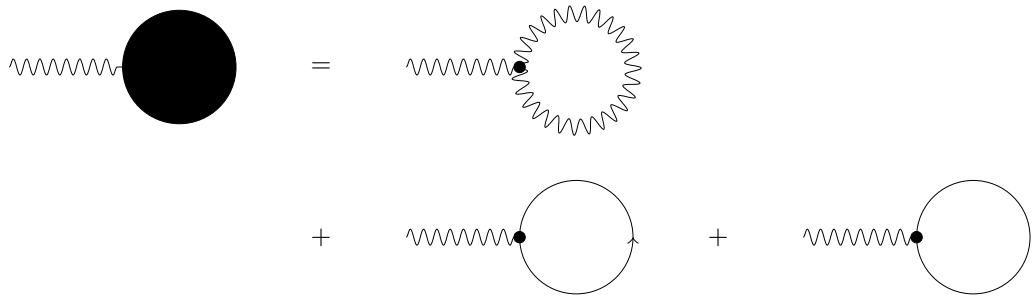

Figure 3.4.: Tadpole diagrams contributing at order g_0.

can be obtained by inverting the bilinear term in (2.61). The ghost-gluon vertex may be extracted fromm the same equation. When using a trivial background field, this contribution vanishes Lüscher and Weisz [1996]. Even though `pastor` includes code to calculate the ghost propagator and vertices, this feature is not yet well tested at the time of writing and hence the usage of the code generator with an Abelian background field is discouraged. The diagram generator will omit the tadpole depicted in 3.4 by default.

The second order coefficient $\langle\mathcal{O}\rangle_F^{(2)}$ has two free gluons, $q_\mu^a(x)$ and $q_\nu^b(y)$, which must be contracted into a propagator $D_{\mu\nu}^{ab}(x,y)$. This is done automatically and the gluon propagator is calculated by `pastor` after gauge fixing by inverting the bilinear term in the gauge action (2.15) numerically. The resulting diagram then contains a closed loop. It has to be evaluated by summing over all intermediate indices, as described at the beginning of this chapter. The details of the construction of the diagram and the summations are taken into account by the `pastor` front end and the user does not have to deal with this. The final step to obtain the contribution of a given diagram to $\langle\mathcal{O}\rangle$ is taking the trace. If the fermion average $\langle\cdot\rangle_F$ of the original observable has more than one fermion trace, the gluon contraction will vanish for a trivial background field if the free gluons come from different traces. This is implemented in `pastor`, such that one can investigate observables with multiple traces for a trivial background field as well.

3.4. Automatic Generation of Vertices

In this section we will discuss how to obtain the g_0-expansion of a generic fermion or gluon action as in (2.7), (2.15). This will then yield the $D^{(i)}$ as defined in (3.35) and the corresponding gluonic vertices, but will also provide us with a method to perform the perturbative expansion of the boundary kernels and insertions defined in the last section. The first such method was introduced by Lüscher and Weisz in Lüscher and Weisz [1986], further developed in Hart et al. [2009], and finally extended to the Schrödinger functional and applied to the gauge sector in Takeda [2009]. Inspecting the definitions of the actions (2.7), (2.15), it becomes clear that it is sufficient to perform the perturbative expansion for each parallel transporter and then sum over the individual contributions. The trace operation in the gluon action may then either be performed before the summation for each term individually or after performing the sum over the Wilson lines.

Let us start with spending some time to investigate the explicit form of the vertices $\mathcal{V}$ coming from the g_0-expansion of a Wilson line $\mathcal{U}$, defined in time-momentum space by

$$\mathcal{U}(x,y) = \sum_r \frac{g_0^r}{r!}\left(\frac{a}{L}\right)^{3r} \sum_{\mathbf{k}_1,a_1,\mu_1,t_1} \dots \sum_{\mathbf{k}_r,a_r,\mu_r,t_r} q_{\mu_1}^{a_1}(\mathbf{k}_1;t_1)\,\dots\,q_{\mu_r}^{a_r}(\mathbf{k}_r;t_r) \times \mathcal{V}_{\mu_1\,\dots\,\mu_r}^{a_1\,\dots\,a_r}(\mathbf{k}_1,t_1;\,\dots;\mathbf{k}_r,t_r). \tag{3.41}$$

Interchanging the gluon fields leaves the equation above invariant. We may thus require the vertices $\mathcal{V}_{\mu_1\,\dots\,\mu_r}^{a_1\,\dots\,a_r}(\mathbf{k}_1,t_1;\,\dots;\mathbf{k}_r,t_r)$ themselves to be symmetric under simultaneous exchange of the indices associated with any of the gluons,

$$\begin{aligned}\sigma\cdot\mathcal{V}_{\mu_1\,\dots\,\mu_r}^{a_1\,\dots\,a_r}(\mathbf{k}_1,t_1;\,\dots;\mathbf{k}_r,t_r) &= \mathcal{V}_{\mu_{\sigma(1)}\,\dots\,\mu_{\sigma(r)}}^{a_{\sigma(1)}\,\dots\,a_{\sigma(r)}}(\mathbf{k}_{\sigma(1)},t_{\sigma(1)};\,\dots;\mathbf{k}_{\sigma(r)},t_{\sigma(r)}) \\ &= \mathcal{V}_{\mu_1\,\dots\,\mu_r}^{a_1\,\dots\,a_r}(\mathbf{k}_1,t_1;\,\dots;\mathbf{k}_r,t_r)\end{aligned} \tag{3.42}$$

where $\sigma\in\mathcal{P}_r$ is a permutation of r elements Lüscher and Weisz [1986].

3.4.1. Weak-Coupling Expansion of a Wilson Line

We assume that the Wilson line $\mathcal{U}(x,y)$ of length l is given as explained in section 2.1 by a starting point $x_0 = y$ and the signed directions $s[i]\mu[i]$. The points $x[i]$ are defined exactly as explained before, additionally we will use the mid-points [1]

$$\tilde{x}[i] = (x[i] + x[i-1])/2, \quad 0 < i \leq l. \tag{3.43}$$

We use the exponential form (2.50) of the link variable for small g_0, setting now

$$U_i = \exp\{a\, g_0\, q_i\} V_i, \quad 0 < i \leq l, \tag{3.44}$$

with

$$V_i = V_{s[i]\mu[i]}(x[i]), \quad q_i = q_{s[i]\mu[i]}(x[i]). \tag{3.45}$$

We define

$$q_{-k}(x) = -\sum_b e^{-i\phi_b(x_0)}\, q_k^b(x - a\,\hat{k})\; I_b, \tag{3.46}$$

$$q_{-0}(x) = -\, q_0(x - a\,\hat{0}), \tag{3.47}$$

$$V_{-\mu} = V_\mu^{-1}(x - a\,\hat{\mu}), \tag{3.48}$$

with ϕ as given in table C.1 and the color components of q read

$$q_\mu(x) = \sum_b q_\mu^b(x)\, I_b, \tag{3.49}$$

with I_b given in (B.5). To write the links in this form, we have used the commutation relations (C.12). We proceed with writing the Wilson line $\mathcal{U}(x,y) = U_l \ldots U_1$ order by order in g_0,

$$\begin{aligned}\mathcal{U}(x,y) &= \sum_r \frac{g_0^r}{r!}\, \mathcal{U}^{(r)}(x,y) = \sum_{n_l} \frac{g_0^n}{n_l!}\, q_l^{n_l}\, V_l \ldots \sum_{n_1} \frac{g_0^{n_1}}{n_1!}\, q_1^{n_1} V_1 \\ &= \sum_{r,\{\alpha\}} \frac{g_0^r}{r!} \frac{r!}{\alpha_1! \ldots \alpha_l!} q_l^{\alpha_l} V_l \;\ldots\; q_1^{\alpha_1} V_1. \end{aligned} \tag{3.50}$$

The sum is understood to be over all non-negative integers $\alpha_1, \ldots, \alpha_l$, such that $\sum_j \alpha_j = r$. To make the connection between (3.41) and (3.50) we first have to switch to time-momentum space. We define the Fourier components of the q_μ field such that

$$q_k^b(x) = \left(\frac{a}{L}\right)^3 \sum_{\mathbf{p}} e^{i\mathbf{p}\mathbf{x}}\, e^{i(ap_k + \phi_b(x_0))/2}\, q_k^b(\mathbf{p}; x_0), \tag{3.51}$$

$$q_0^b(x) = \left(\frac{a}{L}\right)^3 \sum_{\mathbf{p}} e^{i\mathbf{p}\mathbf{x}}\, q_0^b(\mathbf{p}; x_0). \tag{3.52}$$

[1] In a computer program, one preferably stores $2\tilde{x}[i]$, which are integer vectors.

Setting

$$\tilde{s}[i] = s[i](1 - \delta_{\mu[i],0}), \quad t[i] = x[i]_0, \tag{3.53}$$

we may express the fluctuation fields q_j in a more generic way,

$$q_j = s[j] \left(\frac{a}{L}\right)^3 \sum_{\mathbf{k},t,b,\mu} \delta_{t[j],t}\, \delta_{\mu[j],\mu}\, e^{i\mathbf{k}\,\tilde{\mathbf{x}}[j]}\, e^{i\tilde{s}[j]\,\phi_b(t)/2}\, q_\mu^b(\mathbf{k};t)\, I_b. \tag{3.54}$$

The last step is to bring (3.50) in a slightly different form,

$$\mathcal{U}^{(r)}(x,y) = \sum_{0<u_1\leq\ldots\leq u_r\leq l} \frac{r!}{\alpha_1!\,\ldots\,\alpha_l!} \underbrace{q_{u_r}\,\ldots}_{\alpha_l \text{ factors}} V_l\ \ldots V_2\ \underbrace{\ldots q_{u_1}}_{\alpha_1 \text{ factors}}\ V_1. \tag{3.55}$$

We may now define $\alpha_j = \sum_k \delta_{j,u_k}$ but they have the same meaning as in (3.50). Plugging (3.54) into (3.55), we get

$$\begin{aligned}\mathcal{U}^{(r)}(x,y) = \left(\frac{a}{L}\right)^{3r} &\sum_{\mathbf{k}_1,a_1,\mu_1,t_1} \ldots \sum_{\mathbf{k}_r,a_r,\mu_r,t_r} q_{\mu_1}^{a_1}(\mathbf{k}_1;t_1)\ \ldots\ q_{\mu_r}^{a_r}(\mathbf{k}_r;t_r) \\ &\times \sum_{0<u_1\leq\ldots\leq u_r\leq l} \left\{ \underbrace{I_{a_r}\,\ldots}_{\alpha_l \text{ factors}}\, V_l \ldots V_1 \right\} e^{i\sum_{j=1}^r \phi_{a_j}(t_j)\tilde{s}[u_j]/2} \\ &\times \frac{r!}{\alpha_1!\,\ldots\,\alpha_l!} \prod_{j=1}^r s[u_j]\, \delta_{t[u_j],t_j}\, \delta_{\mu[u_j],\mu_j}\, e^{i\,\mathbf{k}_j\tilde{\mathbf{x}}[u_j]}.\end{aligned} \tag{3.56}$$

To illustrate this formula, one of the $O(g_0^3)$ contributions to the expansion (3.56) of the

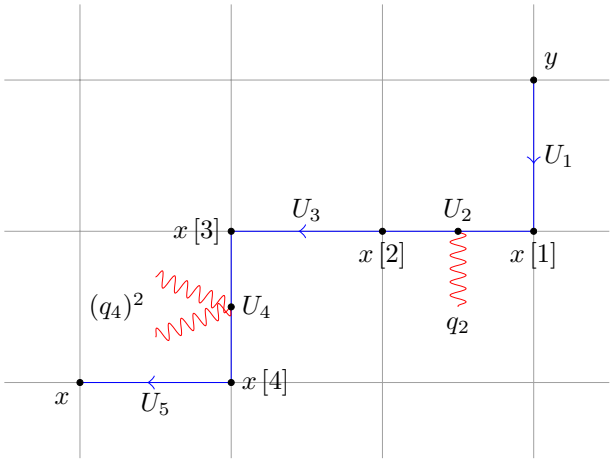

Figure 3.5.: Pictorial representation of an individual contribution to the perturbative expansion of a Wilson line at order g_0^3.

Wilson line that was shown in figure 2.1, is depicted in figure 3.5.

Trivial Background Field

If we set $V_\mu(x) \equiv 1$, (3.56) simplifies to

$$\mathcal{U}^{(r)}(x,y) = \left(\frac{a}{L}\right)^{3r} \sum_{\mathbf{k}_1,a_1,\mu_1,t_1} \dots \sum_{\mathbf{k}_r,a_r,\mu_r,t_r} q_{\mu_1}^{a_1}(\mathbf{k}_1;t_1) \dots q_{\mu_r}^{a_r}(\mathbf{k}_r;t_r)$$
$$\times I_{a_r} I_{a_{r-1}} \dots I_{a_1} \sum_{0<u_1\le\dots\le u_r\le l} \frac{r!}{\alpha_1!\dots\alpha_l!} \prod_{j=1}^{r} s[u_j]\,\delta_{t[u_j],t_j}\,\delta_{\mu[u_j],\mu_j}\,e^{i\,\mathbf{k}_j\tilde{\mathbf{x}}[u_j]}. \tag{3.57}$$

Thus, we can express the vertices as a product of a color factor $\mathcal{C}^{a_1\dots a_r}$ and what is usually called the reduced vertex $\mathcal{Y}_{\mathcal{U};\mu_1\dots\mu_r}(\mathbf{k}_1,t_1;\dots;\mathbf{k}_r,t_r)$ Lüscher and Weisz [1986],

$$\mathcal{V}_{\mu_1\dots\mu_r}^{a_1\dots a_r}(\mathbf{k}_1,t_1;\dots;\mathbf{k}_r,t_r) = \frac{1}{r!}\sum_{\sigma\in\mathcal{P}_r} \sigma\cdot\mathcal{C}^{a_1\dots a_r}\;\sigma\cdot\mathcal{Y}_{\mathcal{U};\mu_1\dots\mu_r}(\mathbf{k}_1,t_1;\dots;\mathbf{k}_r,t_r). \tag{3.58}$$

The permutations σ of the r arguments are necessary to guarantee symmetry under interchange of the indices as mentioned earlier. We have

$$\mathcal{C}^{a_1\dots a_r} = I_{a_r} I_{a_{r-1}} \dots I_1, \tag{3.59}$$
$$\mathcal{Y}_{\mathcal{U};\mu_1\dots\mu_r}(\mathbf{k}_1,t_1;\dots;\mathbf{k}_r,t_r) = \sum_{0<u_1\le\dots\le u_r\le l} \frac{r!}{\alpha_1!\dots\alpha_l!} \times \prod_{j=1}^{r} s[u_j]\,\delta_{t[u_j],t_j}\,\delta_{\mu[u_j],\mu_j}\,e^{i\,\mathbf{k}_j\tilde{\mathbf{x}}[u_j]}. \tag{3.60}$$

Iterative Construction of the Reduced Vertex

The key observation to derive an algorithm to compute the vertices for a given Wilson line automatically is the following. The reduced vertex (3.60) may be constructed by summing over a collection of lists Lüscher and Weisz [1986],

$$\Lambda^{(r)} = \left\{ \lambda^{\{u\}} \middle| \, 0 < u_1 \le \dots \le u_r \le l \right\}, \tag{3.61}$$
$$\lambda^{\{u\}} = \left(f^{\{u\}};\; s\{u\};\; \mu\{u\};\; \tilde{\mathbf{x}}\{u\};\; t\{u\} \right) \tag{3.62}$$
$$s\{u\} = s[u_1],\dots,s[u_r],\ \text{etc.}, \quad f^{\{u\}} = \frac{r!}{\alpha_1!\dots\alpha_l!}. \tag{3.63}$$

We want to stress that $X\{u\}$ should be understood in the sense of the first equation in (3.63), while $X^{\{u\}}$ is reserved to merely indicate dependence on the u_i. We can relabel the lists in the collections with a single index,

$$\Lambda^{(r)} = \{\, \lambda_i |\, i = 1,\dots,n_r \}. \tag{3.64}$$

We do the same with the lists of indices in each of the λ,

$$\lambda_i = \left(f^{(i)};\ s^{(i)};\ \mu^{(i)};\ \tilde{\mathbf{x}}^{(i)};\ t^{(i)}\right), \quad s^{(i)} = \left(s_1^{(i)}, \ldots, s_r^{(i)}\right), \text{ etc.}, \tag{3.65}$$

such that we can rewrite the reduced vertex,

$$\mathcal{Y}_{\mathcal{U};\mu_1 \ldots \mu_r}(\mathbf{k}_1, t_1; \ldots; \mathbf{k}_r, t_r) = \sum_l f^{(l)} \prod_{j=1}^{r} s_j^{(l)} \delta_{t_j, t_j^{(l)}}\, \delta_{\mu_j, \mu_j^{(l)}}\, e^{i\,\mathbf{k}_j \tilde{\mathbf{x}}_j^{(l)}}. \tag{3.66}$$

We choose not to label the order of the λ_i (3.65) explicitly, it corresponds exactly to the length of the lists they contain. We observe that for a single link $\mathcal{U}(x + s[1]\hat{\mu}[1], x)$, there is only one list per order in g_0, whose entries read

$$f^{(1)} = 1, \quad s_i^{(1)} = s[1], \quad \mu_i^{(1)} = \mu[1], \quad \tilde{\mathbf{x}}_i^{(1)} = \tilde{\mathbf{x}}[1], \quad t_i^{(1)} = t[1]. \tag{3.67}$$

Given two sets of these lists, Λ and Λ', belonging to two Wilson lines, $\mathcal{U}'(x, y)$ and $\mathcal{U}(y, z)$, we can easily construct the lists $\Lambda' \cdot \Lambda$ for the product of the Wilson lines $\mathcal{U}'(x, y)\mathcal{U}(y, z)$. It is the union of the products of the original collections of lower order,

$$(\Lambda' \cdot \Lambda)^{(r)} = \bigcup_{j=1}^{r-1} \Lambda'^{(j)} \Lambda^{(r-j)}. \tag{3.68}$$

The product of the individual collections consists mainly of concatenations of the original lists Lüscher and Weisz [1986],

$$\Lambda'^{(j)} \Lambda^{(r-j)} = \left\{ \lambda_k\, \lambda_l \middle| \lambda_k \in \Lambda^{(j)},\ \lambda_l \in \Lambda'^{(r-j)} \right\}, \tag{3.69}$$

$$\lambda_k \lambda_l = \left(f^{(k)} f^{(l)} \binom{r}{j};\ s^{(k)} \oplus s^{(l)};\ \mu^{(k)} \oplus \mu^{(l)};\ \tilde{\mathbf{x}}^{(k)} \oplus \tilde{\mathbf{x}}^{(l)};\ t^{(k)} \oplus t^{(l)} \right). \tag{3.70}$$

We define the direct sum of two lists in the canonical way,

$$(\alpha_1, \ldots, \alpha_n) \oplus (\beta_1, \ldots, \beta_m) = (\alpha_1, \ldots, \alpha_n, \beta_1, \ldots, \beta_m). \tag{3.71}$$

It is convenient to write a computer program that performs the multiplication (3.69), and builds up the perturbative expansion of any Wilson line link by link with (3.67) as starting point.

Abelian Background Fields

The main obstacle that catches one's eye inspecting (3.56) for a non-trivial background field is that the product of color matrices does not factor out as it was the case in (3.57). This can be overcome with some manipulations of the color factor Takeda [2009]. First,

we use (C.9) to rewrite all the background field factors as

$$V_j = e^{i\,a\,\tilde{s}[j]\,t[j]\,\mathcal{E}}\; V^{\tilde{s}[j]}(0). \tag{3.72}$$

With (C.12) we then get

$$V_j\, I_b = I_b\, \underbrace{e^{i\,a\,\tilde{s}[j]\,t[j]\,\mathcal{E}} V^{\tilde{s}[j]}(0)}_{V_j}\; e^{i\,\tilde{s}[j]\,\{a\,t[j]\phi'_b + \phi_a(0)\}}. \tag{3.73}$$

Then (3.56) may be rewritten as

$$\begin{aligned}\mathcal{U}^{(r)}(x,y) = \left(\frac{a}{L}\right)^{3r} \sum_{\mathbf{k}_1,a_1,\mu_1,t_1} \dots \sum_{\mathbf{k}_r,a_r,\mu_r,t_r} q^{a_1}_{\mu_1}(\mathbf{k}_1;t_1)\,\dots\, q^{a_r}_{\mu_r}(\mathbf{k}_r;t_r) \\ \times I_{a_r}\dots I_{a_1} \sum_{0<u_1\le\dots\le u_r\le l} V(0)^{A\{u\}} e^{ia^2\mathcal{E}B\{u\}} e^{i/2\left(C\{u\}\cdot\Phi' + D\{u\}\cdot\Phi\right)} \\ \times \frac{r!}{\alpha_1!\,\dots\,\alpha_l!} \prod_{j=1}^{r} s[u_j]\,\delta_{t[u_j],t_j}\,\delta_{\mu[u_j],\mu_j}\, e^{i\,\mathbf{k}_j\tilde{\mathbf{x}}[u_j]}.\end{aligned} \tag{3.74}$$

A, B are scalars and C, D are r-vectors. We have introduced the notation

$$C\cdot\Phi' = \sum_{i=1}^{r} C_i\,\phi'_{a_i}, \quad D\cdot\Phi = \sum_{i=1}^{r} D_i\,\phi_{a_i}(0). \tag{3.75}$$

The superscript $\{u\}$ indicates, as explained before, dependence on the u_i but does not say anything about the vector indices of C and D. The original factor of $e^{i\sum_{j=1}^{r}\phi_{a_j}(t_j)\tilde{s}[u_j]/2}$ in (3.56) can be absorbed in the vector D. Extracting A, B, C, and D for a given parallel transporter is not straightforward. However, we may proceed as in the last section and construct them link by link. First, we have to multiply each summand of the vertex function $\mathcal{Y}_{\mathcal{U}}$, exactly as in (3.60), with a color factor of the form

$$\mathcal{C}_{bg}(A,B,C,D) = V(0)^A e^{ia^2\mathcal{E}B} e^{i/2(C\cdot\Phi' + D\cdot\Phi)}. \tag{3.76}$$

To this end, we define new collections of lists

$$\tilde{\Lambda}^{(r)} = \left\{\tilde{\lambda}_i \mid i = 1,\dots,n_r\right\}, \quad \tilde{\lambda}_i = \left(A^{(i)}; B^{(i)}; C^{(i)}; D^{(i)}\right), \tag{3.77}$$

and get a modified reduced vertex from the direct sums $\lambda \oplus \tilde{\lambda}$,

$$\begin{aligned}\tilde{\mathcal{Y}}^{a_1,\dots,a_r}_{\mathcal{U};\mu_1\dots\mu_r}(\mathbf{k}_1,t_1;\,\dots;\mathbf{k}_r,t_r) = \sum_j V(0)^{A^{(j)}} e^{ia^2\mathcal{E}B^{(j)}} e^{i/2\left(C^{(j)}\cdot\Phi' + D^{(j)}\cdot\Phi\right)} \\ \times f^{(j)} \prod_{l=1}^{r} s^{(j)}_l\,\delta_{t_l,t^{(j)}_l}\,\delta_{\mu_l,\mu^{(j)}_l}\, e^{i\,\mathbf{k}_l\tilde{\mathbf{x}}^{(j)}_l}.\end{aligned} \tag{3.78}$$

Again, we can start with the simple lists for a single link $U_{s[1]\mu[1]}(x[1])$, (c.f. (3.67), Takeda [2009])

$$A^{(1)} = \tilde{s}[1], \quad B^{(1)} = \tilde{s}[1]t[1], \quad C_j^{(1)} = 0, \quad D_i^{(1)} = \tilde{s}[1]. \tag{3.79}$$

Inspecting (3.76) one observes that a multiplication rule for the lists (3.77) can be defined exactly as in (3.68), (3.69), with (3.70) replaced by the product Takeda [2009]

$$\tilde{\lambda}_k\tilde{\lambda}_l = \Big(A^{(k)} + A^{(l)};\ B^{(k)} + B^{(l)};\\ C^{(k)} \oplus \Big(C^{(l)} + 2B^{(k)}\Big);\ D^{(k)} \oplus \Big(D^{(l)} + 2A^{(k)}\Big)\Big). \tag{3.80}$$

The direct sum of two lists was defined in (3.71), and we have introduced the sum of a scalar and a list,

$$(a_1, a_2, \ldots, a_r) + \alpha = (a_1 + \alpha, a_2 + \alpha, \ldots, a_r + \alpha). \tag{3.81}$$

Using the lists (3.64), (3.77) and their respective multiplication rules, we can now construct the vertices for any parallel transporter link by link. The stating point is given by (3.67) and (3.79).

3.4.2. Expansion of the Full Actions

Turning back to the generic actions (2.7) and (2.15), a few points should be mentioned. The vertices may be constructed just as in (3.58), where the reduced vertex can be constructed as the sum over the contributions (3.78),

$$\mathcal{Y}^{a_1,\ldots,a_r}_{\mu_1\ldots\mu_r}(\mathbf{k}_1, t_1; \ldots; \mathbf{k}_r, t_r) = \sum_i \tilde{\mathcal{Y}}^{a_1,\ldots,a_r}_{\mathcal{U}_i;\mu_1\ldots\mu_r}(\mathbf{k}_1, t_1; \ldots; \mathbf{k}_r, t_r). \tag{3.82}$$

In the gluon case we have to perform the color trace and are done. If we deal with fermions, the vertices will depend on their indices as well,

$$S_F\Big[U, \overline{\psi}, \psi\Big] = \sum_r \frac{g_0^r}{r!}\left(\frac{a}{L}\right)^{3(r+2)} \sum_{\mathbf{p},\mathbf{q},t,u,b,c} \sum_{\mathbf{k}_1,a_1,\mu_1,t_1} \cdots \sum_{\mathbf{k}_r,a_r,\mu_r,t_r} q^{a_1}_{\mu_1}(\mathbf{k}_1; t_1) \ldots q^{a_r}_{\mu_r}(\mathbf{k}_r; t_r)\\ \times\overline{\psi}^b(\mathbf{p}, t)\mathcal{V}^{a_1\ldots a_r;b,c}_{\mu_1\ldots\mu_r}(\mathbf{k}_1, t_1; \ldots; \mathbf{k}_r, t_r; \mathbf{p}, t; \mathbf{q}, u)\psi^c(\mathbf{q}, u), \tag{3.83}$$

where the indices b, c are color indices of the fermions. Hence, $b, c \in \{1, 2, 3\}$ are associated with the adjoint representation of the color group, while the $a_i = 1, \ldots, 8$ refer to members of the fundamental one. One should also keep in mind that $\mathcal{V}$ acquires a Dirac structure trough the spin matrices Γ_i in (2.7). The inclusion of the fermion indices except for the color ones is accomplished path by path through an extension of the reduced vertex (remember that x_i and y_i are the end-points of the parallel transporter

$\mathcal{U}_i$),

$$\tilde{\mathcal{Y}}^{a_1,\ldots,a_r}_{\mathcal{U}_i(x_i,y_i);\mu_1\ldots\mu_r}(\mathbf{k}_1,t_1;\ldots;\mathbf{k}_r,t_r;\mathbf{p},t;\mathbf{q},u) = \delta_{t,(x_i)_0}\delta_{u,(y_i)_0}e^{i(\mathbf{p}\mathbf{x}_i+\mathbf{q}\mathbf{y}_i)}\tilde{\mathcal{Y}}^{a_1,\ldots,a_r}_{\mathcal{U}_i(x_i,y_i);\mu_1\ldots\mu_r}(\mathbf{k}_1,t_1;\ldots;\mathbf{k}_r,t_r) \quad (3.84)$$

The indices b and c then merely select one entry of the resulting color matrix.

3.5. Counter-Terms

3.5.1. Boundary Corrections

Note that the $O(a)$ boundary correction to the Dirac operator acts on the bulk quark fields like (c.f. (2.65), (2.66)),

$$\delta D_b\psi(x) = (\tilde{c}_t-1)\frac{1}{a}\{\delta_{x_0,a}\left[\psi(x)-U_0(x-\hat{0})^{-1}\rho(\mathbf{x})\right] \quad (3.85)$$

$$+\delta_{x_0,T-a}\left[\psi(x)-U_0(x)\rho'(\mathbf{x})\right]\}. \quad (3.86)$$

The terms involving the boundary fields can be included in the kernels $K, K', \tilde{K}, \tilde{K}'$. However, the rest must be treated separately. First, one should note that the corrections will only enter at order g_0^2, since $\tilde{c}_t = 1+O(g_0^2)$. We may set $\hat{c}_t = (\tilde{c}_t - 1)$, and using the notation of section 3.1.2, we get

$$\Delta_{\hat{c}_t}(x) = -\frac{1}{a}\left\{\delta_{x_0,a}+\delta_{x_0,T-a}\right\}\overline{\psi}(x)\psi(x). \quad (3.87)$$

The `pastor` code generator then takes the corrections into account in the spirit of (3.9). For each propagator $S(x,y)$ occurring in the expansion of a given observable $\mathcal{O}$, a new diagram is produced, given by replacing

$$S^{(0)}(x,z) \to -a^4\sum_y S^{(0)}(x,y)\frac{1}{a}\left\{\delta_{y_0,a}+\delta_{y_0,T-a}\right\}S^{(0)}(y,z), \quad (3.88)$$

in the tree level diagram corresponding to $\mathcal{O}$. In the analysis, this diagram then has to be multiplied by $\tilde{c}_t^{(1)}$ and added to the final result to remove the $O(a)$ effects coming from the boundary at $O(g_0^2)$.

3.5.2. Volume Corrections

Since the field strength $\mathcal{F}_{\mu\nu}$ (2.18) vanishes at tree level for a trivial background field, the `pastor` front end will not generate any diagrams taking $\Delta_{c_{SW}}$ into account by default. However, this behavior could be implemented (e.g. when working with an Abelian background field) without much effort, treating the clover term as an operator insertion and considering the tree level diagram as a correction.

3.5.3. Mass Counter-Term

The mass renormalization as in (2.20) can be dealt with in a similar fashion. Here, the critical mass m_c, as well as Z_m and b_m, carries a dependence on the bare coupling g_0. Given $m_\mathrm{R} = z/L$ as the mass parameter for our calculation, we first write $m_\mathrm{q} = m_\mathrm{q}^{(0)} + g_0^2 m_\mathrm{q}^{(1)}$, taking into account the respective g_0-expansions of m_c, Z_m, and b_m. We get

$$z/L = m_\mathrm{q}^{(0)}\left(1 + a\, b_\mathrm{m}^{(0)} m_\mathrm{q}^{(0)}\right) + g_0^2\Big\{ m_\mathrm{q}^{(1)}\left(1 + 2\, a\, b_\mathrm{m}^{(0)} m_\mathrm{q}^{(0)}\right) + m_\mathrm{q}^{(0)}\left(Z_\mathrm{m}^{(1)}(1 + a\, b_\mathrm{m}^{(0)} m_\mathrm{q}^{(0)}) + a\, m_\mathrm{q}^{(0)} b_\mathrm{m}^{(1)}\right)\Big\}. \quad (3.89)$$

One may now evaluate any function $f(m_0)$ using

$$f\left(m_0\right) = f\left(m_0^{(0)}\right) + g_0^2 m_0^{(1)} \partial_m f\left(m_0^{(0)}\right) + O(g_0^4), \quad (3.90)$$

where $m_0^{(0)}$ is given as the solution of

$$z/L = m_\mathrm{q}^{(0)}\left(1 + a\, b_\mathrm{m}^{(0)} m_\mathrm{q}^{(0)}\right), \quad (3.91)$$

and the g_0^2-correction reads

$$m_0^{(1)} = m_\mathrm{c}^{(1)} - m_\mathrm{q}^{(0)} \frac{Z_\mathrm{m}^{(1)}\left(1 + a\, m_\mathrm{q}^{(0)} b_\mathrm{m}^{(0)}\right) + a\, m_\mathrm{q}^{(0)} b_\mathrm{m}^{(1)}}{1 + 2\, a\, b_\mathrm{m}^{(0)} m_\mathrm{q}^{(0)}}. \quad (3.92)$$

The expansions of the improvement coefficient b_m Sint and Weisz [1997] and the renormalization factor Z_m in the lattice (lat) scheme Peskin and Schroeder [1995], Gabrielli et al. [1991] read (using $g_R^2 = g_0^2 + O(g_0^4)$)

$$b_\mathrm{m} = -0.5 - 0.07217(2)\, C_F\, g_0^2 + O(g_0^4), \quad (3.93)$$

$$Z_{\mathrm{m,lat}}(\mu = 1/L) = 1 - \frac{1}{2\,\pi^2} \log(a/L) g_0^2 + O(g_0^4). \quad (3.94)$$

All calculations in `pastor` are performed with z as input parameter. The bare mass $m_0^{(0)}$ is then determined by (3.91). To take into account the g_0^2 correction, we note that

$$\Delta_m(x) = -\overline{\psi}(x)\psi(x). \quad (3.95)$$

Performing the fermion Wick contractions one then sees that the derivative acts on the propagator like

$$\partial_m S(x,z) = -a^4 \sum_y S(x,y) S(y,z). \quad (3.96)$$

For each propagator S in a given observable $\mathcal{O}$, `pastor` thus generates a new diagram, obtained from the tree level result $\langle\mathcal{O}\rangle^{(0)}$ with S replaced according to (3.96) with $\partial_m S$. This diagram then has to be multiplied by $m_0^{(1)}$ as given in (3.92) and added to the final result. One might want to keep in mind that the b_m contribution to (3.92) is merely an $O(a)$ correction, while the critical mass $m_\mathrm{c}^{(1)}$ and the renormalization factor $Z_\mathrm{m}^{(1)}$ have to be taken into account to obtain the correct continuum limit.

3.6. Implementation

The implementation of the respective parts of the code that deal with vertex and diagram generation have rather different requirements.

The low level vertex code should be efficient, but its maintenance and extension should not be too involved. This is the reason the author decided to use the C++ language, which allows to write highly efficient code but still profits from the flexibility of being object oriented and offering features such as templates, which can not only improve the usability of the code but may also be employed to leave less room for errors in case the user wants to build his own applications using the pastor library.

The generation of Feynman diagrams is much less demanding from the numerical point of view but is challenging in a completely different way. The objects that we introduced in the previous sections fall from the computer's point of view in only two categories, propagators and vertices (operator insertions and even static propagators may be considered as generalized vertices). However, one has to be careful to establish the flow of momentum and color through the diagram correctly. Another layer of complexity is then added when one wants to generate not only valid but also efficient C++ code. The Python language was thus chosen because of its flexibility and the ease with which compact and clear code may be written. As a scripting language it also provides the advantage that the programs are easy to maintain and extend.

We will briefly discuss how the techniques introduced in this chapter are implemented in `pastor` in some more detail. The generation of diagrams is mostly a problem of bookkeeping of the indices, as was discussed in section 3.3.

Generating the vertices is more involved and we will sketch how this is done in `libsculptr`, the C++ back end of `pastor`. The reader might use figures 3.6 and 3.7 as a point of reference.

The basic ingredients to construct gluon and fermion actions are the weights, paths and, in the fermion case, spin matrices as mentioned repeatedly before. The usual way to construct an action is to omit the starting point, `pastor` will then assume that a summation is intended. A fixed starting point may be given as well, which is useful to construct insertions as in (3.5). The signed directions are represented by the integers $\pm1, \pm2, \pm3, \pm4$, where the four-direction is the temporal one. Furthermore, the keywords `mu`, `nu`, `rho`, and `sigma` may be used. `pastor` then sums over these, keeping them different if multiple keywords are given in one path. The weights are complex numbers, there is only one subtlety concerning the weights for the gluon paths. As discussed briefly in section 2.5.4 and in depth in Aoki et al. [1999], one might want to modify the weight

of the loops used to construct the gluon action depending on their position. `pastor` allows for three different weights w_1, w_2, w_3 and the actual weight $w_{\mathcal{U}}$ of a given loop $\mathcal{U}$ is chosen according to

$$w_{\mathcal{U}} = \begin{cases} w_2 & \text{if } \mathcal{U} \text{ touches the boundary,} \\ w_3 & \text{if } \mathcal{U} \text{ is completely on the boundary,} \\ w_1 & \text{else.} \end{cases} \tag{3.97}$$

Then, out of a given parallel transporter, an object named FermionTerm or GluonTerm is created. These can be thought of as representations of the collections Λ, now containing the combined lists $\lambda \oplus \tilde{\lambda}$. They are broken down to (adopting the nomenclature of Hart et al. [2009]) Entities, which are representations of the lists $\lambda \oplus \tilde{\lambda}$. The Entities contain what we will call a kinetic part λ and the color part $\tilde{\lambda}$. After symmetrization, the parts are stored in two separate containers in an object called FermionAction (or GluonAction, respectively). This is done to keep the overhead small. Many of the Entities have identical color parts, but different kinetic ones. It is thus of advantage to store those parts only once. Otherwise one would waste CPU cycles when calculating the reduced vertices (3.78) for a given set of external momenta and color indices. We call this operation a *dispatch*, during which the resulting vertex is written to an array or associative array. The storage key types are multi-indices consisting of a number of time and Lorentz indices, and the value types are either spin matrices for fermions or complex numbers in the gauge case. Associative arrays[2] are most useful to store vertices, which are due to the locality of the action sparse objects. The same holds for the bilinear contributions to the actions, but since we have to invert them (to calculate the tree level propagators) one should use a simple array, which was implemented as well. As mentioned before, we use the QR-decomposition as inverter, two more advanced solvers, conjugate gradient and BICGSTAB, are included as well. A single GluonAction or FermionAction can contain an arbitrary number of terms, and various short-hand notations are implemented to allow the user to define custom actions in a compact way. The FermionAction object is then used to expand the boundary kernels $K, K', \tilde{K}, \tilde{K}'$ and insertions κ as in (3.5).

[2]More precisely, we use the boost unordered map, a hashmap type Boost Project [2012] to get a good performance. An alternative is the TR1 unordered map which ships with most modern C++ compilers. However we found that the latter performs worse and used the boost implementation.

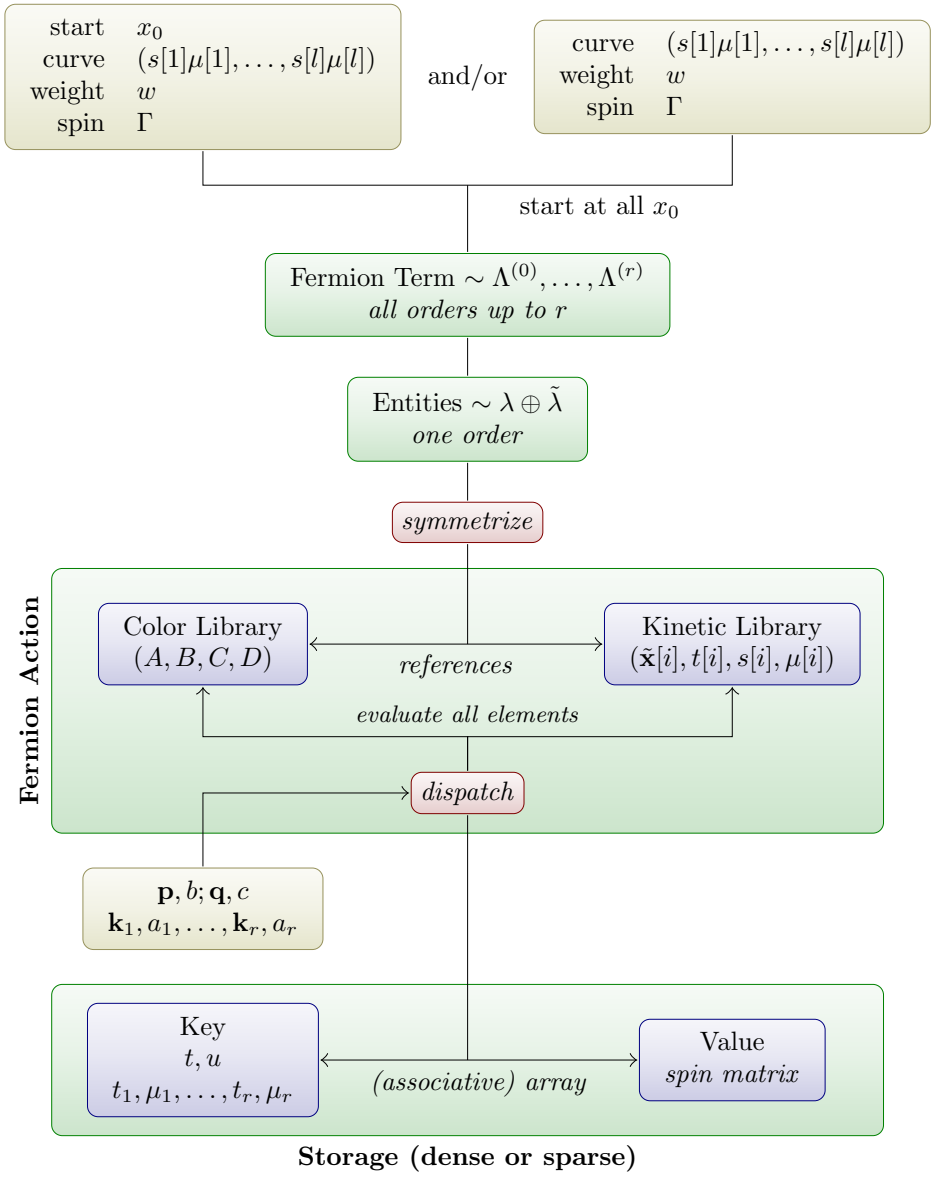

Figure 3.6.: Flowchart illustrating the construction of a fermion vertex in `libsculptr`.

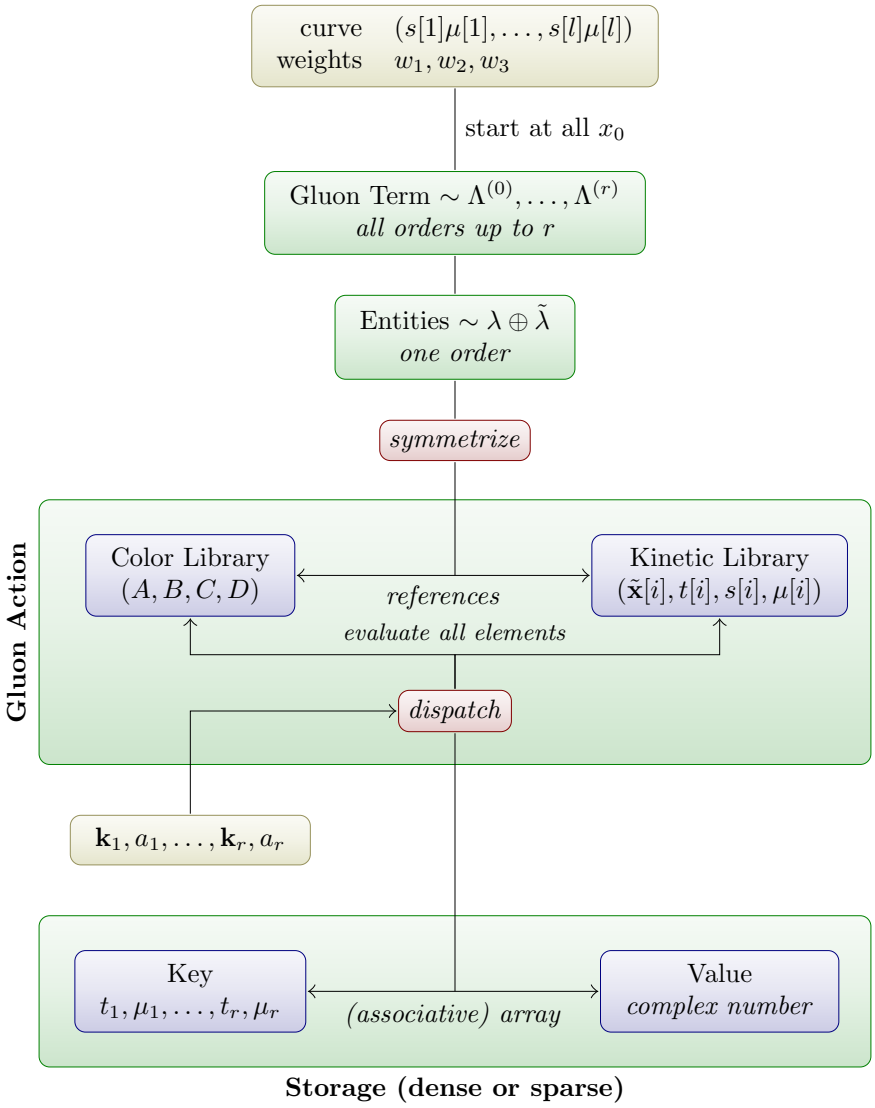

Figure 3.7.: Flowchart illustrating the construction of a gluon vertex in `libsculptr`.

4. Cross Checks

4.1. Relevant Correlation Functions

For convenience, we collect the definitions of a number of two-point functions defined in Della Morte et al. [2007], Lüscher et al. [1996], involving heavy and light quark flavors, just as introduced in section 3.1.1. They will be of importance throughout this and the next chapter. The first set of quantities are correlators involving the pseudoscalar and vector channel, similar to f_{A} (3.1),

$$f_{\mathrm{P}}(x_0;\theta_{\mathrm{h}},\theta_{\mathrm{l}},z) = -\frac{a^6}{2}\sum_{\mathbf{y}_1,\mathbf{y}_2}\langle P(x)\overline{\zeta_{\mathrm{h}}}(\mathbf{y}_1)\gamma_5\zeta_{\mathrm{l}}(\mathbf{y}_2)\rangle, \tag{4.1}$$

$$k_{\mathrm{V}}(x_0;\theta_{\mathrm{h}},\theta_{\mathrm{l}},z) = -\frac{a^6}{6}\sum_{\mathbf{y}_1,\mathbf{y}_2,k}\langle (V_I)_k(x)\overline{\zeta_{\mathrm{h}}}(\mathbf{y}_1)\gamma_k\zeta_{\mathrm{l}}(\mathbf{y}_2)\rangle, \tag{4.2}$$

with the improved vector current

$$(V_I)_\mu(x) = \overline{\psi}_{\mathrm{l}}(x)\gamma_\mu\psi_{\mathrm{h}}(x) + ac_V\tilde{\partial}_\mu\Big[i\overline{\psi}_{\mathrm{l}}(x)\sigma_{\mu\nu}\psi_{\mathrm{h}}(x)\Big], \tag{4.3}$$

and the pseudoscalar density (2.24). Furthermore, we need the boundary-to-boundary correlation functions

$$f_1(\theta_{\mathrm{h}},\theta_{\mathrm{l}},z) = -\frac{a^{12}}{2L^6}\sum_{\mathbf{y}_1,\mathbf{y}_2,\mathbf{y}_3,\mathbf{y}_4}\langle\overline{\zeta_{\mathrm{l}}}'(\mathbf{y}_1)\gamma_5\zeta_{\mathrm{h}}'(\mathbf{y}_2)\overline{\zeta_{\mathrm{h}}}(\mathbf{y}_3)\gamma_5\zeta_{\mathrm{l}}(\mathbf{y}_4)\rangle, \tag{4.4}$$

$$k_1(\theta_{\mathrm{h}},\theta_{\mathrm{l}},z) = -\frac{a^{12}}{6L^6}\sum_{\mathbf{y}_1,\mathbf{y}_2,\mathbf{y}_3,\mathbf{y}_4,k}\langle\overline{\zeta_{\mathrm{l}}}'(\mathbf{y}_1)\gamma_k\zeta_{\mathrm{h}}'(\mathbf{y}_2)\overline{\zeta_{\mathrm{h}}}(\mathbf{y}_3)\gamma_k\zeta_{\mathrm{l}}(\mathbf{y}_4)\rangle. \tag{4.5}$$

4.1.1. Renormalization

The quantities defined above are bare quantities that have to be renormalized. We assume, that a mass-independent renormalization scheme is employed, such that renormalization and improvement are compatible. In such a scheme the renormalized, $O(a)$ improved boundary fields read Lüscher et al. [1996] (reproducing (2.70) for convenience)

$$\zeta_R(\mathbf{x}) = Z_\zeta(\tilde{g}_0^2, a\mu)(1 + ab_\zeta m_{\mathrm{q}})\zeta(\mathbf{x}). \tag{4.6}$$

The pseudoscalar (2.24) density and improved axial (2.23) and vector currents are renormalized according to Lüscher et al. [1996]

$$(A_R)_\mu(x) = Z_\mathrm{A}(\tilde{g}_0^2, a\mu)(1 + a\, b_\mathrm{A} m_\mathrm{q,h}/2)(A_I)_\mu(x), \tag{4.7}$$
$$(P_R)_\mu(x) = Z_\mathrm{P}(\tilde{g}_0^2, a\mu)(1 + a\, b_\mathrm{P} m_\mathrm{q,h}/2)P(x), \tag{4.8}$$
$$(V_R)_\mu(x) = Z_\mathrm{V}(\tilde{g}_0^2, a\mu)(1 + a\, b_\mathrm{V} m_\mathrm{q,h}/2)(V_I)_\mu(x). \tag{4.9}$$

Note that the light flavor plays no role in the improvement only because we choose it to be massless in our examples. In many cases, one considers ratios of correlation functions in which some renormalization factors cancel, e.g. $f_\mathrm{A}/\sqrt{f_1}$, which is free of Z_ζ.

$1/m_\mathrm{h}$ Expansion

The $1/m_\mathrm{h}$ expansion (2.38) of some of the quantities defined above will be of interest in the following as well. In addition to the $1/m_\mathrm{h}$-expansion of the Lagrangian (1.34), we also have to take into account the expansions of the operators appearing in (3.1), (4.1), Heitger and Sommer [2004]. They read (using the notation of Sommer [2011])

$$\left(A_R^\mathrm{HQET}\right)_0(x) = Z_\mathrm{A}^\mathrm{HQET}\left[A_0^\mathrm{stat} + \sum_{i=1}^{2} c_\mathrm{A}^{(i)} A_0^{(i)}(x)\right], \tag{4.10}$$
$$A_0^\mathrm{stat}(x) = \overline{\psi}_\mathrm{l}(x)\gamma_0\gamma_5\psi_\mathrm{h}(x), \tag{4.11}$$
$$A_0^{(1)}(x) = \overline{\psi}_\mathrm{l}(x)\frac{1}{2}\gamma_5\gamma_i\left(\nabla_i^S - \overleftarrow{\nabla}_i^S\right)\psi_\mathrm{h}(x), \tag{4.12}$$
$$A_0^{(2)}(x) = \overline{\psi}_\mathrm{l}(x)\frac{1}{2}\gamma_5\gamma_i\left(\nabla_i^S + \overleftarrow{\nabla}_i^S\right)\psi_\mathrm{h}(x), \tag{4.13}$$

and for the spatial components, one has

$$\left(A_R^\mathrm{HQET}\right)_k(x) = Z_\mathbf{A}^\mathrm{HQET}\left[A_k^\mathrm{stat} + \sum_{i=3}^{6} c_\mathrm{A}^{(i)} A_k^{(i)}(x)\right], \tag{4.14}$$
$$A_k^{(3)}(x) = \overline{\psi}_\mathrm{l}(x)\frac{1}{2}\gamma_k\gamma_5\gamma_i\left(\nabla_i^S - \overleftarrow{\nabla}_i^S\right)\psi_\mathrm{h}(x), \tag{4.15}$$
$$A_k^{(4)}(x) = \overline{\psi}_\mathrm{l}(x)\frac{1}{2}\left(\nabla_k^S - \overleftarrow{\nabla}_k^S\right)\gamma_5\psi_\mathrm{h}(x), \tag{4.16}$$
$$A_k^{(5)}(x) = \overline{\psi}_\mathrm{l}(x)\frac{1}{2}\gamma_k\gamma_5\gamma_i\left(\nabla_i^S + \overleftarrow{\nabla}_i^S\right)\psi_\mathrm{h}(x), \tag{4.17}$$
$$A_k^{(6)}(x) = \overline{\psi}_\mathrm{l}(x)\frac{1}{2}\left(\nabla_k^S + \overleftarrow{\nabla}_k^S\right)\gamma_5\psi_\mathrm{h}(x). \tag{4.18}$$

The same expressions hold for the vector current, replacing $c_\mathrm{A}^{(i)} \to c_\mathrm{V}^{(i)}$ and dropping γ_5. The Schrödinger functional's periodic boundary conditions in the spatial directions then imply

$$a^3\sum_\mathbf{x} A_0^{(1)}(x) = a^3\sum_\mathbf{x} \overline{\psi}_\mathrm{l}(x)\overleftarrow{\nabla}_i^S\gamma_i\gamma_5\psi_\mathrm{h}(x), \quad a^3\sum_\mathbf{x} A_0^{(2)}(x) = 0. \tag{4.19}$$

According to (2.38), we may now write Della Morte et al. [2007] up to order $1/m_\mathrm{h}$

$$[f_A]_R = Z_A^{\mathrm{HQET}} Z_{\zeta_\mathrm{h}} Z_{\zeta_\mathrm{l}} e^{-m_\mathrm{bare} x_0} \Big[f_A^{\mathrm{stat}} + c_\mathrm{A}^{(1)} f_{\delta A}^{\mathrm{stat}} + \omega_\mathrm{kin} f_A^{\mathrm{kin}} + \omega_\mathrm{spin} f_A^{\mathrm{spin}} \Big], \tag{4.20}$$

$$[f_1]_R = Z_{\zeta_\mathrm{h}}^2 Z_{\zeta_\mathrm{l}}^2 e^{-m_\mathrm{bare} T} \Big[f_1^{\mathrm{stat}} + \omega_\mathrm{kin} f_1^{\mathrm{kin}} + \omega_\mathrm{spin} f_1^{\mathrm{spin}} \Big], \tag{4.21}$$

$$[k_1]_R = Z_{\zeta_\mathrm{h}}^2 Z_{\zeta_\mathrm{l}}^2 e^{-m_\mathrm{bare} T} \Big[f_1^{\mathrm{stat}} + \omega_\mathrm{kin} f_1^{\mathrm{kin}} - \frac{1}{3} \omega_\mathrm{spin} f_1^{\mathrm{spin}} \Big], \tag{4.22}$$

with $f_{\delta A}^{\mathrm{stat}}$ as introduced in (3.2).

4.2. Cross Checks With Known Perturbative Results

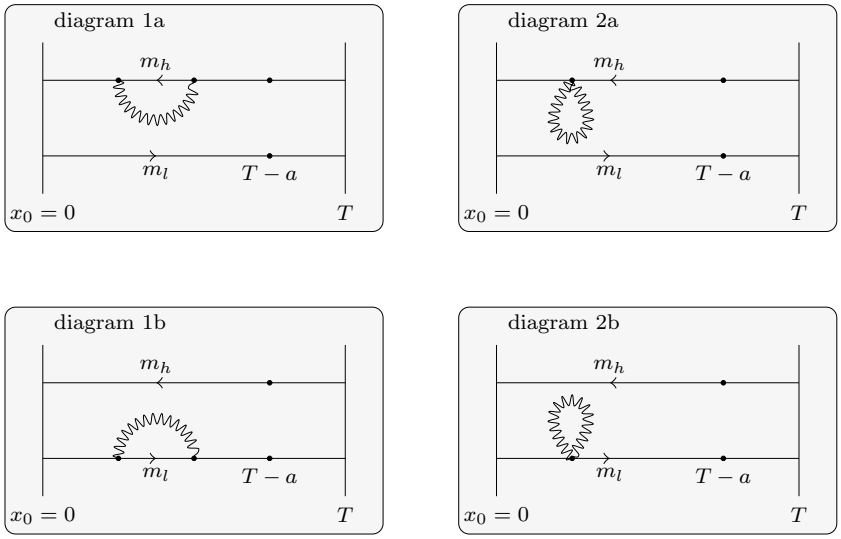

Figure 4.1.: Diagrams involved in the cross checks, numbered as in Kurth and Sommer [2002].

As a first check, we compared data calculated with `pastor` to known results for f_1 and f_A at order g_0^2 from the calculations performed for Kurth and Sommer [2002]. All available diagrams were compared for a subset of the available lattice spacings and all of them were in complete agreement within round-off errors. For brevity, we will present the comparison of the loop diagrams shown in figure 4.1, which are relevant for the correlation function f_1 (4.4). The solid fermion lines touching the boundary are a shorthand for $O(g_0^2)$ contributions of

$$H(x) = a^7 \sum_{y,\mathbf{z}} S(x,y) K(y,\mathbf{z}) P_+, \quad \tilde{H}(x) = a^7 \sum_{y,\mathbf{z}} P_- \tilde{K}(\mathbf{z},y) S(y,x). \tag{4.23}$$

The numerical values for these diagrams were provided by the authors of Kurth and Sommer [2002] and used to check against data calculated in `pastor`. The magnitude of

the relative difference in the numerical results of the two calculations for $z = 8$, $\theta = 0.5$ is plotted for a number of lattice sizes which are relevant for practical applications in figure 4.2. The differences should only come from and can indeed be explained by round-off

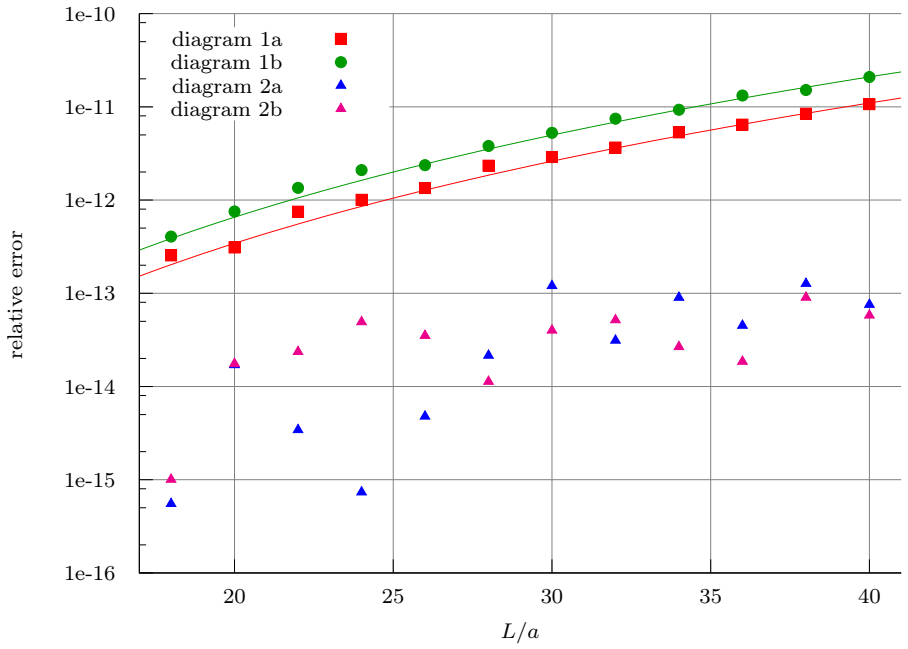

Figure 4.2.: Relative error for diagrams contributing to f_1 at $z = 8$, $\theta = 0.5$. To guide the eye, two fit functions of the form $y(L/a) = b\,(L/a)^5$ with fit parameter b are included. The temporal lattice extend was set equal to the spatial one, $T = L$.

errors. As stated before the evaluation of diagrams of the type "1" as shown in figure 4.1 requires $O(L^3T^2)$ additions. The rising of the relative errors in the figure is compatible with this behavior, as suggested by the fit functions.

Since the diagrams of type "2" have only one vertex, the number of additions decreases to $O(L^3T)$ and the round-off errors are much smaller, in fact rather close to machine precision. The spread of the errors is consequentially large and we refrain from performing a fit in this case.

4.2.1. Concerning Round-Off Errors

The `pastor` C++ back end may be instructed at compile time to use the data type `long double` instead of `double`, such that the round-off error of any observable can be estimated by performing calculations with both data types and comparing the results. For all calculations that will be presented in chapter 5, we estimated the round-off error in this fashion. For a representative set of observables, calculations in both levels of

precision were performed up to sufficiently large lattice sizes L/a. The magnitude of the relative difference δ was assumed to represent the round-off error and fitted using the function

$$\delta(L/a) = b\,(L/a)^5. \tag{4.24}$$

Then, b was increased by $\sim 50\%$ to give a safe estimate. The fits included in figure 4.2 suggest that this procedure is valid.

4.3. Cross Checks with Monte Carlo Data

With the `pastor` package, one can generate diagrams for a broad class of observables with ease. To gain more confidence in the software setup, we compared `pastor` results for a number of correlation functions to quenched Monte Carlo data at small couplings, $\beta = 50, 100$ (corresponding to $g_0^2 = 0.12$ and $g_0^2 = 0.06$, respectively). The simulations were performed by Patrick Fritzsch on the APEnext machines in Zeuthen before they were decommissioned. We investigated the correlation functions f_A, f_A^{stat}, f_A^{spin}, f_A^{kin}, f_1, f_1^{stat}, f_1^{spin}, f_1^{kin}, $f_{\delta A}^{\mathrm{stat}}$, $f_{\delta A}^{\mathrm{spin}}$, k_V, f_P, and k_1, as defined in sections 4.1 and 3.1.1. The improvement coefficient $\tilde{c}_t$ (2.69) was set to its one loop value. All quantities are calculated for $L = T = 4, 6$ and $\theta_{\mathrm{h}} = \theta_{\mathrm{l}} = \theta \in \{0.0, 0.5, 1.0\}$. The relativistic correlation functions are evaluated for two different masses for the flavor we labeled *heavy*, given by the hopping parameters $\kappa_{\mathrm{h}} \in \{\kappa_{\mathrm{c}}, 0.1\}$, where κ_{c} is the two loop critical value defined in analogy to (2.28). The light quark mass is as always kept at κ_{c}, the relation between κ and the bare mass is given by

$$\kappa = \frac{1}{2(a\,m_0 + 4)}. \tag{4.25}$$

The Monte Carlo histories contain $O(10^4)$ measurements, a binned jackknife analysis with bins of size 50 is used to extract the expectation values and extrapolations. The estimated statistical errors are negligible compared to the systematic uncertainty of the truncation in the g_0-expansion that will be introduced shortly.

We denote a generic observable out of the set given above with f. The perturbative expansion

$$f(g_0) = f^{(0)} + g_0^2\, f^{(1)} + O\left(g_0^4\right) \tag{4.26}$$

is obtained using `pastor`. The Monte Carlo result is given by $f^{MC}(g_0)$, and the two runs at different g_0 provide us with estimates for $f^{(1)}$,

$$\tilde{f}^{(1)}(g_0) = g_0^{-2}\left(f^{MC}(g_0) - f^{(0)}\right). \tag{4.27}$$

These are both valid approximations if g_0 is small. However, we may define an improved estimate by extrapolating linearly in g_0^2 to zero. We denote the extrapolated value $\tilde{f}^{(1)}_{\mathrm{ext}}$. The results of these extrapolations, together with $\tilde{f}^{(1)}$ for both $g_0^2 = 0.12$ and $g_0^2 = 0.06$, as well as the exact `pastor` results for the one loop term are presented in figures D.2

trough D.7. A fit to the Monte Carlo results of the form

$$\tilde{f}^{(1)}(g_0) = f^{(1)} + c_1\, g_0^2 + c_2\, g_0^4 \tag{4.28}$$

is performed and included in the plots. The results for $\tilde{f}^{(1)}(0.06)$ and the extrapolation $\tilde{f}^{(1)}_{\text{ext}}$, as well as the `pastor` result $f^{(0)}$ and the fit parameters c_1 and c_2 are given in tables 4.1-4.4. The only observable that shows a significant g_0^4-term is $f^{\text{stat}}_{\delta\text{A}}$ (c.f. table 4.1). However the magnitude of the coefficient c_2 is not extraordinarily large. We interpret this as an accidentally bigger higher order contribution in this observable.

f	L	θ	z	$\tilde{f}^{(1)}(0.06)$	$\tilde{f}^{(1)}_{\text{ext}}$	$f^{(1)}$	c_1	c_2
$f^{\text{spin}}_{\delta\text{A}}$	4	0.0	-	0.07671(9)	0.0830(2)	0.08236	-0.089(3)	-0.09(3)
$f^{\text{spin}}_{\delta\text{A}}$	4	0.5	-	0.04304(7)	0.0472(2)	0.04674	-0.058(2)	-0.07(2)
$f^{\text{spin}}_{\delta\text{A}}$	4	1.0	-	0.00066(4)	0.0027(1)	0.00244	-0.028(1)	-0.03(1)
$f^{\text{spin}}_{\delta\text{A}}$	6	0.0	-	0.0222(1)	0.0283(3)	0.02845	-0.104(4)	0.02(4)
$f^{\text{spin}}_{\delta\text{A}}$	6	0.5	-	0.00259(8)	0.0068(2)	0.00687	-0.072(3)	0.01(3)
$f^{\text{spin}}_{\delta\text{A}}$	6	1.0	-	-0.02136(6)	-0.0193(2)	-0.01926	-0.035(2)	0.00(2)
$f^{\text{stat}}_{\delta\text{A}}$	4	0.0	-	-0.5744(5)	-0.580(1)	-0.58124	0.12(2)	-0.1(1)
$f^{\text{stat}}_{\delta\text{A}}$	4	0.5	-	-0.2954(3)	-0.2968(6)	-0.27597	-0.498(9)	2.90(8)
$f^{\text{stat}}_{\delta\text{A}}$	4	1.0	-	-0.0354(1)	-0.0358(3)	0.00921	-1.119(4)	6.24(4)
$f^{\text{stat}}_{\delta\text{A}}$	6	0.0	-	-0.5254(3)	-0.5336(7)	-0.53273	0.11(1)	0.1(1)
$f^{\text{stat}}_{\delta\text{A}}$	6	0.5	-	-0.2969(2)	-0.3011(4)	-0.28615	-0.304(6)	2.07(5)
$f^{\text{stat}}_{\delta\text{A}}$	6	1.0	-	-0.05638(8)	-0.0583(2)	-0.02784	-0.729(3)	4.22(3)

Table 4.1.: Numerical results for the cross checks with Monte Carlo Data of $f_{\delta\text{A}^{\text{spin}}}$ and $f^{\text{stat}}_{\delta\text{A}}$. The column $\tilde{f}^{(1)}_{\text{ext}}$ denotes the linearly extrapolated value.

f	L	θ	z	$\tilde{f}^{(1)}(0.06)$	$\tilde{f}^{(1)}_{\text{ext}}$	$f^{(1)}$	c_1	c_2
f_1	4	0.0	0	-2.39(1)	-2.42(3)	-2.41702	0.5(5)	0(4)
f_1	4	0.0	2	-0.463(2)	-0.474(4)	-0.47407	0.18(5)	-0.0(5)
f_1	4	0.5	0	-0.87(1)	-0.86(1)	-0.86428	-0.0(3)	0(2)
f_1	4	0.5	2	-0.280(1)	-0.284(2)	-0.28421	0.08(4)	0.0(3)
f_1	4	1.0	0	-0.148(3)	-0.147(3)	-0.14635	-0.03(8)	0.0(4)
f_1	4	1.0	2	-0.1016(6)	-0.1025(8)	-0.10246	0.01(2)	0.0(1)
f_1	6	0.0	0	-2.318(8)	-2.33(2)	-2.32093	-0.0(3)	1(2)
f_1	6	0.0	3	-0.1555(3)	-0.1608(5)	-0.16067	0.085(8)	0.02(6)
f_1	6	0.5	0	-0.862(2)	-0.855(8)	-0.85552	-0.1(1)	0(1)
f_1	6	0.5	3	-0.0993(1)	-0.1022(3)	-0.10218	0.048(5)	0.00(4)
f_1	6	1.0	0	-0.1397(8)	-0.137(3)	-0.13828	-0.01(3)	-0.2(3)
f_1	6	1.0	3	-0.03841(5)	-0.0393(1)	-0.03933	0.015(2)	-0.00(2)
f_1^{kin}	4	0.0	-	-3.651(4)	-3.807(9)	-3.80313	2.5(1)	0(1)
f_1^{kin}	4	0.5	-	-2.351(3)	-2.444(7)	-2.44083	1.5(1)	0(1)
f_1^{kin}	4	1.0	-	-0.831(2)	-0.870(4)	-0.86833	0.60(6)	0.3(5)
f_1^{kin}	6	0.0	-	-5.810(6)	-6.17(1)	-6.18229	6.3(2)	-2(2)
f_1^{kin}	6	0.5	-	-3.905(4)	-4.14(1)	-4.14662	4.1(1)	-1(1)
f_1^{kin}	6	1.0	-	-1.568(2)	-1.669(5)	-1.67348	1.79(8)	-0.6(7)
f_1^{spin}	4	0.0	-	0.00395(1)	0.00036(4)	0.00000	0.0688(5)	-0.050(5)
f_1^{spin}	4	0.5	-	0.002342(9)	0.00015(2)	0.00000	0.0403(3)	-0.021(3)
f_1^{spin}	4	1.0	-	0.000841(4)	0.00003(1)	0.00000	0.0143(1)	-0.004(1)
f_1^{spin}	6	0.0	-	0.002361(8)	0.00028(2)	0.00000	0.0417(3)	-0.038(3)
f_1^{spin}	6	0.5	-	0.001405(8)	0.00013(2)	0.00000	0.0245(3)	-0.018(3)
f_1^{spin}	6	1.0	-	0.000499(4)	0.000034(9)	0.00000	0.0086(1)	-0.005(1)
f_1^{stat}	4	0.0	-	-2.761(1)	-2.785(3)	-2.78872	0.49(5)	-0.5(4)
f_1^{stat}	4	0.5	-	-1.8187(9)	-1.825(2)	-1.82852	0.19(3)	-0.4(2)
f_1^{stat}	4	1.0	-	-0.8676(4)	-0.8680(9)	-0.86967	0.05(1)	-0.2(1)
f_1^{stat}	6	0.0	-	-3.688(1)	-3.743(3)	-3.74485	0.96(4)	-0.2(4)
f_1^{stat}	6	0.5	-	-2.5036(7)	-2.534(2)	-2.53494	0.53(3)	-0.1(3)
f_1^{stat}	6	1.0	-	-1.1824(4)	-1.194(1)	-1.19488	0.21(2)	-0.1(2)

Table 4.2.: Numerical results for the cross checks with Monte Carlo Data of f_1 and its HQET counterpart. The column $\tilde{f}^{(1)}_{\text{ext}}$ denotes the linearly extrapolated value.

f	L	θ	z	$\tilde{f}^{(1)}(0.06)$	$\tilde{f}^{(1)}_{\text{ext}}$	$f^{(1)}$	c_1	c_2
f_{A}	4	0.0	0	1.61(1)	1.63(3)	1.63448	-0.4(5)	1(4)
f_{A}	4	0.0	2	0.539(3)	0.545(6)	0.54560	-0.12(9)	0.1(8)
f_{A}	4	0.5	0	0.37(1)	0.368(9)	0.37021	0.0(2)	0(1)
f_{A}	4	0.5	2	0.300(2)	0.300(3)	0.30068	-0.02(6)	0.1(4)
f_{A}	4	1.0	0	-0.018(2)	-0.017(3)	-0.01699	-0.02(3)	0.0(4)
f_{A}	4	1.0	2	0.0888(7)	0.0881(6)	0.08807	0.01(2)	-0.00(8)
f_{A}	6	0.0	0	1.430(5)	1.44(1)	1.42390	0.2(2)	-2(2)
f_{A}	6	0.0	3	0.3369(3)	0.3414(8)	0.34055	-0.05(1)	-0.1(1)
f_{A}	6	0.5	0	0.361(3)	0.356(5)	0.35578	0.09(8)	-0.1(8)
f_{A}	6	0.5	3	0.2151(2)	0.2168(5)	0.21655	-0.021(7)	-0.04(7)
f_{A}	6	1.0	0	-0.003(1)	-0.002(2)	-0.00139	-0.03(3)	0.1(3)
f_{A}	6	1.0	3	0.0870(1)	0.0871(4)	0.08709	-0.001(5)	0.00(6)
$f_{\text{A}}^{\text{kin}}$	4	0.0	-	3.7568(8)	3.774(2)	3.77525	-0.32(3)	0.2(3)
$f_{\text{A}}^{\text{kin}}$	4	0.5	-	2.9803(6)	2.979(1)	2.98091	-0.02(2)	0.2(2)
$f_{\text{A}}^{\text{kin}}$	4	1.0	-	1.9760(4)	1.9656(8)	1.96717	0.13(1)	0.2(1)
$f_{\text{A}}^{\text{kin}}$	6	0.0	-	5.025(1)	5.094(3)	5.09101	-1.07(5)	-0.4(5)
$f_{\text{A}}^{\text{kin}}$	6	0.5	-	3.976(1)	4.015(3)	4.01273	-0.59(4)	-0.3(4)
$f_{\text{A}}^{\text{kin}}$	6	1.0	-	2.5439(6)	2.557(2)	2.55614	-0.20(2)	-0.1(2)
$f_{\text{A}}^{\text{spin}}$	4	0.0	-	-0.3369(1)	-0.3380(3)	-0.33740	0.004(4)	0.08(4)
$f_{\text{A}}^{\text{spin}}$	4	0.5	-	-0.2674(1)	-0.2672(2)	-0.26686	-0.012(4)	0.05(3)
$f_{\text{A}}^{\text{spin}}$	4	1.0	-	-0.17175(6)	-0.1709(1)	-0.17077	-0.017(2)	0.02(2)
$f_{\text{A}}^{\text{spin}}$	6	0.0	-	-0.4446(2)	-0.4513(5)	-0.45114	0.107(6)	0.02(7)
$f_{\text{A}}^{\text{spin}}$	6	0.5	-	-0.3563(1)	-0.3603(4)	-0.36022	0.065(5)	0.01(6)
$f_{\text{A}}^{\text{spin}}$	6	1.0	-	-0.23228(8)	-0.2340(3)	-0.23399	0.028(4)	0.00(4)
$f_{\text{A}}^{\text{stat}}$	4	0.0	-	1.172(1)	1.168(2)	1.16964	0.03(4)	0.2(3)
$f_{\text{A}}^{\text{stat}}$	4	0.5	-	0.7127(6)	0.706(1)	0.70746	0.08(2)	0.2(2)
$f_{\text{A}}^{\text{stat}}$	4	1.0	-	0.3076(3)	0.3039(6)	0.30443	0.048(9)	0.08(8)
$f_{\text{A}}^{\text{stat}}$	6	0.0	-	1.5797(9)	1.572(2)	1.57217	0.12(3)	0.0(3)
$f_{\text{A}}^{\text{stat}}$	6	0.5	-	1.0747(5)	1.066(1)	1.06657	0.13(2)	0.0(2)
$f_{\text{A}}^{\text{stat}}$	6	1.0	-	0.5535(3)	0.5485(8)	0.54863	0.08(1)	0.0(1)

Table 4.3.: Numerical results for the cross checks with Monte Carlo Data of f_{A} and its HQET counterpart. The column $\tilde{f}^{(1)}_{\text{ext}}$ denotes the linearly extrapolated value.

f	L	θ	z	$\tilde{f}^{(1)}(0.06)$	$\tilde{f}^{(1)}_{\text{ext}}$	$f^{(1)}$	c_1	c_2
f_{P}	4	0.0	0	-0.53(1)	-0.53(2)	-0.53683	0.1(3)	-1(3)
f_{P}	4	0.0	2	-0.421(2)	-0.422(4)	-0.42347	0.05(7)	-0.2(6)
f_{P}	4	0.5	0	-0.172(7)	-0.17(1)	-0.17163	0.0(2)	0(1)
f_{P}	4	0.5	2	-0.285(1)	-0.286(2)	-0.28605	0.01(5)	-0.1(3)
f_{P}	4	1.0	0	0.024(2)	0.022(3)	0.02295	0.01(6)	0.2(4)
f_{P}	4	1.0	2	-0.1392(7)	-0.1390(9)	-0.13893	-0.00(2)	0.0(1)
f_{P}	6	0.0	0	-0.41(1)	-0.41(2)	-0.40609	-0.2(3)	0(3)
f_{P}	6	0.0	3	-0.2862(4)	-0.2885(9)	-0.28794	0.02(1)	0.1(1)
f_{P}	6	0.5	0	-0.126(5)	-0.122(5)	-0.12434	-0.0(1)	-0.3(7)
f_{P}	6	0.5	3	-0.2069(3)	-0.2080(4)	-0.20788	0.015(8)	0.02(6)
f_{P}	6	1.0	0	0.028(1)	0.028(4)	0.02527	0.06(3)	-0.3(5)
f_{P}	6	1.0	3	-0.1125(1)	-0.1129(3)	-0.11292	0.008(3)	-0.01(4)
k_1	4	0.0	0	-2.40(1)	-2.42(3)	-2.41702	0.3(5)	0(4)
k_1	4	0.0	2	-0.464(2)	-0.474(4)	-0.47407	0.17(5)	-0.0(5)
k_1	4	0.5	0	-0.89(1)	-0.89(1)	-0.88481	-0.1(3)	0(2)
k_1	4	0.5	2	-0.280(1)	-0.285(2)	-0.28453	0.07(4)	0.0(3)
k_1	4	1.0	0	-0.155(3)	-0.153(2)	-0.15312	-0.03(7)	0.0(3)
k_1	4	1.0	2	-0.1018(6)	-0.1028(8)	-0.10271	0.01(2)	0.0(1)
k_1	6	0.0	0	-2.326(8)	-2.33(2)	-2.32093	-0.2(3)	2(2)
k_1	6	0.0	3	-0.1555(3)	-0.1608(5)	-0.16067	0.085(8)	0.02(6)
k_1	6	0.5	0	-0.883(2)	-0.874(8)	-0.87373	-0.1(1)	0(1)
k_1	6	0.5	3	-0.0993(1)	-0.1023(3)	-0.10222	0.048(5)	0.00(4)
k_1	6	1.0	0	-0.1458(8)	-0.143(3)	-0.14404	-0.02(3)	-0.2(4)
k_1	6	1.0	3	-0.03845(5)	-0.0394(1)	-0.03936	0.015(2)	-0.00(2)
k_{V}	4	0.0	0	-1.02(1)	-1.01(2)	-1.01291	0.0(4)	-1(3)
k_{V}	4	0.0	2	-0.481(2)	-0.483(5)	-0.48408	0.07(8)	-0.1(7)
k_{V}	4	0.5	0	-0.348(8)	-0.34(1)	-0.34278	-0.1(2)	0(1)
k_{V}	4	0.5	2	-0.307(2)	-0.307(3)	-0.30763	0.01(5)	-0.1(4)
k_{V}	4	1.0	0	-0.033(2)	-0.033(2)	-0.03220	-0.02(5)	0.1(3)
k_{V}	4	1.0	2	-0.1333(7)	-0.1328(9)	-0.13281	-0.01(2)	0.0(1)
k_{V}	6	0.0	0	-0.921(8)	-0.91(1)	-0.90335	-0.3(2)	1(2)
k_{V}	6	0.0	3	-0.3173(4)	-0.3205(8)	-0.31978	0.04(1)	0.1(1)
k_{V}	6	0.5	0	-0.347(4)	-0.338(4)	-0.33849	-0.14(9)	-0.1(6)
k_{V}	6	0.5	3	-0.2212(2)	-0.2227(4)	-0.22241	0.019(7)	0.03(5)
k_{V}	6	1.0	0	-0.054(1)	-0.051(3)	-0.05267	-0.00(3)	-0.2(5)
k_{V}	6	1.0	3	-0.11149(9)	-0.1118(3)	-0.11185	0.006(3)	-0.00(4)

Table 4.4.: Numerical results for the cross checks with Monte Carlo Data of various QCD observables. The column $\tilde{f}^{(1)}_{\text{ext}}$ denotes the linearly extrapolated value.

5. Applications in HQET

After we gained confidence in the `pastor` package, we set out to demonstrate its usefulness for physics computations. Specifically, we will investigate some aspects of the matching procedure of HQET and QCD, as described in Heitger and Sommer [2004].

Here, one wants to establish the connection

$$HQET \xleftarrow{m_{\mathrm{h}}\to\infty} QCD, \tag{5.1}$$

by adjusting the parameters in the effective theory accordingly. To this end, one imposes a set of matching conditions, which can be thought of as renormalization conditions for the HQET parameters. Sections 5.2.1 and 5.2.2 contain calculations involved in this step.

Ultimately, the matching should be performed non-perturbatively through Monte Carlo simulations (as we will see in section 5.2.4). To keep the numerical effort manageable, the matching step is usually performed in a physically small volume with spatial extent L_1 Heitger and Sommer [2004], where simulations of QCD with relativistic heavy quarks are feasible. However, to obtain physical predictions, one should perform HQET simulations in a large volume with extent L_2. A finite size step scaling method Lüscher et al. [1991] is then employed to fix the HQET parameters in L_2. In section 5.2.3 we will investigate the perturbative cut-off effects of this procedure for two selected relevant quantities.

5.1. Matching of HQET and QCD

The HQET Lagrangian at order $1/m_{\mathrm{h}}$ contains tree bare parameters, δm, ω_{kin}, and ω_{spin}. While these are enough to obtain energy levels, $c_{\mathrm{A}}^{(1)}$ and $Z_{\mathrm{A}}^{\mathrm{HQET}}$ have to be included if one is interested e.g. in the leptonic decay of a B-meson, $B \to \ell\nu$. To include semi-leptonic B-decays, e.g. $B \to D\ell\nu$, the vector current and hence $Z_{\mathrm{V}}^{\mathrm{HQET}}$ and $c_{\mathrm{V}}^{(1)}$ have to be included, as well as further $1/m_{\mathrm{h}}$ coefficients $c_{\mathrm{V}}^{(i)}$, entering the expansion of the spatial components of the currents, (4.10)-(4.18). If one is furthermore interested in investigating parity changing transitions the rest of the parameters connected to the axial vector current, namely $c_{\mathrm{A}}^{(i)}, i = 3, \ldots, 6$ need to be included.

We will denote the parameters to be fixed generically by the column vector $\omega = (\omega_1, \ldots, \omega_N)^T$. The first step is to find a suitable set of N observables $\Phi_i^{\mathrm{QCD}}, i = 1, \ldots, N$, and their HQET expansion Φ. The matching conditions then read

$$\Phi_i^{\mathrm{QCD}}(L_1, m_{\mathrm{R}}, a = 0) = \Phi_i(L_1, m_{\mathrm{R}}, a). \tag{5.2}$$

The observables are assumed to be renormalized. In fact, imposing any renormalization scheme on the HQET side will determine the divergent parts of the renormalization constants. The matching conditions are then needed to fix the finite parts and thus make HQET an effective theory of QCD in the limit of a heavy quark mass. It is beneficial to take the continuum limit of the QCD quantities before performing the matching, otherwise one would have to scale a also on the QCD side of (5.2) to take the continuum limit in HQET.

As pointed out in Blossier et al. [2010a], it is of advantage to choose the observables Φ such that they are linear in ω,

$$\Phi(L, m_{\mathrm{R}}, a) = \eta(L, a) + \phi(L, a)\,\omega(m_{\mathrm{R}}, a), \tag{5.3}$$

where Φ and η are N-vectors, and ϕ is a $N \times N$ matrix. In this case, one may easily extract the parameters $\tilde{\omega}$ in L_1, inverting (5.3),

$$\tilde{\omega}(m_{\mathrm{R}}, a) = \phi^{-1}(L_1, a)\left[\Phi^{\mathrm{QCD}}(L_1, m_{\mathrm{R}}, 0) - \eta(L_1, a)\right]. \tag{5.4}$$

5.1.1. Step Scaling

As stated before, one now wishes to perform simulations with a larger lattice extent L_2. To obtain ω in L_2, one needs the observables Φ in the larger volume. With the knowledge of $\tilde{\omega}$, one may use the HQET observables to extract

$$\Phi(L_2, m_{\mathrm{R}}, 0) = \lim_{a\to 0}\left\{\eta(L_2, a) + \phi(L_2, a)\tilde{\omega}(m_{\mathrm{R}}, a)\right\}. \tag{5.5}$$

Combining this equation with (5.4), we find

$$\Phi(L_2, m_{\mathrm{R}}, 0) = \lim_{a/L_1\to 0}\left\{\eta(L_2, a) + \phi(L_2, a)\phi^{-1}(L_1, a)\left[\Phi(L_1, m_{\mathrm{R}}, 0) - \eta(L_1, a)\right]\right\}. \tag{5.6}$$

The ratio $\phi(L_2, a)\phi^{-1}(L_1, a)$ defines the step scaling functions Σ_{ij},

$$\Sigma(L_1, a) = \phi(L_2, a)\phi^{-1}(L_1, a). \tag{5.7}$$

By using only L_1 as argument, we have assumed, that one has fixed the ratio $s = L_2/L_1$. We will adopt the choice of Blossier et al. [2010a] and set $s = 2$. The last step is to obtain the parameters ω using essentially (5.4) again,

$$\omega(m_{\mathrm{R}}, a) = \phi^{-1}(L_2, a)\left[\Phi(L_2, m_{\mathrm{R}}, 0) - \eta(L_2, a)\right]. \tag{5.8}$$

The matching at order $1/m_{\mathrm{h}}$ including $Z_{\mathrm{A}}^{\mathrm{HQET}}$ and $c_{\mathrm{A}}^{(1)}$ is performed non-perturbatively in the quenched approximation in Blossier et al. [2010a]. As stated before, one would ultimately wish to extend this to the other coefficients $c_{\mathrm{A}}^{(i)}$ and the vector channel. We will not list the explicit formulae for the matching observables Φ and their expansion η, ϕ from Blossier et al. [2010a] to avoid unnecessary clutter, and rather restrict our attention to those which will play a role in the following.

5.2. Perturbative Matching

Perturbation theory can make useful contributions to the matching procedure. For example, one can check in computationally cheap perturbative studies if the z-dependence of the parameters ω is dominated by the lowest order terms z^0, z^{-1} in their $1/z$ expansion or if we have large higher order corrections. If the latter is the case, the HQET expansion for Φ may simply not be accurate. This knowledge can then be used to select the observables Φ.

In the following sections, we will present two studies that were performed using `pastor`. First, we will demonstrate how one of the matching parameters, namely ω_{kin}, may be extracted to one loop order in perturbation theory. We will study the z-dependence at tree level and at order g_0^2. In the limit $m_{\mathrm{h}} \to \infty$, the final result for ω_{kin} will be independent of the kinematic parameters θ_1, θ_2 of the observable that was used to extract it and thus a further confirmation of the validity of the $1/m_{\mathrm{h}}$-expansion to order g_0^2 will be obtained. The dependence of the round-off errors on θ_1, θ_2 may then also be used to find a choice for those parameters that represents a good compromise between a weak z-dependence and small round-off errors. This point has some importance because the round-off errors in perturbative calculations can serve as a qualitative indicator for the expected statistical errors in Monte Carlo simulations. If e.g. ω_{kin} multiplies a numerically small quantity in the matching equation (c.f. (5.12) below), this will impact the numerical precision in a perturbative calculation trough a higher round-off error in the final result and a Monte Carlo simulation will suffer from bigger statistical fluctuations in that case.

We then proceed to the analysis of two observables, Φ^{V_0} and Φ^{A_1}, which are candidates that may be used in the future for the matching of the renormalization factors $Z_{\mathrm{V}}^{\mathrm{HQET}}$ and $Z_{\mathbf{A}}^{\mathrm{HQET}}$ belonging to the vector and axial vector current respectively. We will study the z-dependence of these observables to one loop order of perturbation theory and the dependence of the magnitude of the round-off errors on the kinematic parameters, again to find a good compromise between small $1/z$-corrections and the achievable numerical precision.

5.2.1. The Parameter ω_{kin}

The matching procedure is rather simple for the parameter ω_{kin}. Inspecting (4.21), (4.22), one sees that the quantity

$$R_1(L/a, z, \theta_1, \theta_2) = \frac{1}{4}\left\{R_1^P(L/a, z, \theta_1, \theta_2) + 3R_1^V(L/a, z, \theta_1, \theta_2)\right\}, \tag{5.9}$$

with

$$R_1^P(\theta_1, \theta_2) = \log\left\{f_1(\theta_1)/f_1(\theta_2)\right\}, \quad T = L/2, \tag{5.10}$$

$$R_1^V(\theta_1, \theta_2) = \log\left\{k_1(\theta_1)/k_1(\theta_2)\right\}, \quad T = L/2, \tag{5.11}$$

is sensitive to the parameter $\omega_{\rm kin}$ Della Morte et al. [2007]. In Blossier et al. [2010a], $\Phi_4 = R_1$ is used as one of the matching observables. The $1/m_{\rm h}$ contribution to R_1 may be extracted using Della Morte et al. [2007]

$$R_1^{(1/m)}(L/a, z, \theta_1, \theta_2) = R_1 - R_1^{\rm stat} = \omega_{\rm kin}(z, L/a) R_1^{\rm kin}(L/a, \theta_1, \theta_2) + O(1/z). \quad (5.12)$$

The individual contributions to the HQET expansion are given by

$$R_1^{\rm stat}(L/a, \theta_1, \theta_2) = \log\left\{ f_1^{\rm stat}(\theta_1)/f_1^{\rm stat}(\theta_2) \right\}, \quad T = L/2, \quad (5.13)$$

$$R_1^{\rm kin}(L/a, \theta_1, \theta_2) = \frac{f_1^{\rm kin}(\theta_1)}{f_1^{\rm stat}(\theta_1)} - \frac{f_1^{\rm kin}(\theta_2)}{f_1^{\rm stat}(\theta_2)}, \quad T = L/2. \quad (5.14)$$

Equation (5.12) is the matching condition to extract $\omega_{\rm kin}$, and since all other parameters drop out when taking the ratios which define R_1, we can extract $\omega_{\rm kin}$ using this single equation. A point that needs consideration is that the operator $\mathcal{O}_{\rm kin}$ in principle has to be renormalized. In the continuum, using the $\overline{MS}$ scheme, one can however show using the so-called reparametrization invariance that the renormalization factor is one to all orders Luke and Manohar [1992], Kilian and Ohl [1994], Sundrum [1998]. In our one loop analysis, we find that the leading logarithmic term in $LR_1^{\rm kin}$ is compatible with zero within errors. Using the method described in appendix C.3 we perform fits of the form

$$L\, R_1^{\rm kin}(L/a, \theta_1, \theta_2) = r(\theta_1, \theta_2) + s(\theta_1, \theta_2) \log(L/a) + \ldots, \quad (5.15)$$

obtaining values for r as given in table 5.3 and s compatible with 0.00006(10) for all choices for θ_1 and θ_2. Thus we conclude that the renormalization factor of $\mathcal{O}_{\rm kin}$ has no divergent part at one loop level. Using the lattice minimal subtraction scheme (lat), we may then set $Z_{\mathcal{O}^{\rm kin}}$ to one at order g_0^2. The consequence for our analysis is that the absence of a divergent renormalization of $\mathcal{O}_{\rm kin}$ implies that $\omega_{\rm kin}$ will have no logarithmic z-dependence. This in turn implies that we may expect $m_{\rm h}\omega_{\rm kin}$ to be finite in the limit $m_{\rm h} \to \infty$.

Tree Level

Knowing the classical value $\omega_{\mathrm{kin}} = 1/(2m_{\mathrm{h}})$, we expect the continuum limit of the tree level relation

$$m_{\mathrm{h}}\omega^{(0)}_{\mathrm{kin}}(z, L/a) = z\left[\frac{R_1^{(1/m)}(L/a, z, \theta_1, \theta_2)}{L\, R_1^{\mathrm{kin}}(L/a, \theta_1, \theta_2)}\right]_{g_0=0} \tag{5.16}$$

to approach the value $1/2$ in the limit $a/L \to 0$, $z \to \infty$.

The tree level calculation was performed in Della Morte and Dooling [2011] for different choices of θ_1, θ_2 from ours, which we label A, B, and C, as defined in table 5.1. We thus repeated the tree level calculation with z ranging from four to 30 and lattice sizes up to $L/a = 200$. The continuum limits were extracted by a fitting procedure as explained in C.3. The round-off error plays virtually no role at tree level.

label	A	B	C
θ_1	0.5	0.0	0.0
θ_2	1.0	1.0	0.5

Table 5.1.: Choices for θ and θ'.

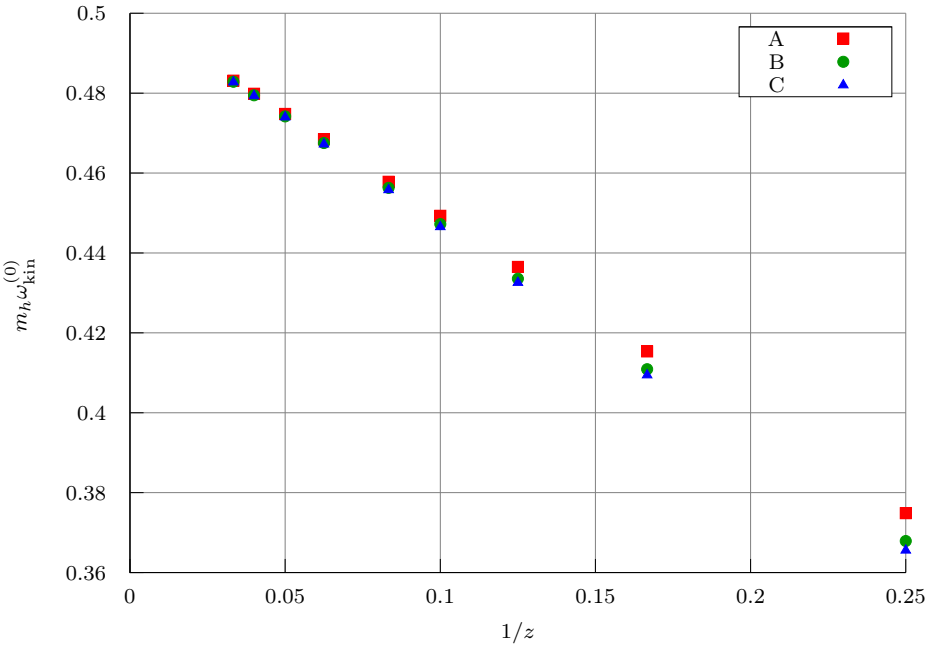

Figure 5.1.: Results for $\omega^{(0)}_{\mathrm{kin}}$.

The results are shown in figure 5.1. The data is linear in $1/z$ over the whole range of values for z that were investigated, approaching the asymptotic value as expected. At

$z = 10$ we have a $1/z$-correction of around 10%. Since $\omega_{\mathrm{kin}} R_1^{\mathrm{kin}}$ is a $1/z$-correction to R_1^{stat}, which is of order $1/2$, the 10% correction to ω_{kin} above then translates to a typical $1/z^2$ term of 1%.

One Loop

We used `pastor` to calculate the observables R_1, R_1^{stat}, and R_1^{kin} at one loop level for lattice resolutions L/a of up to 46 in steps of two, starting for R_1^{stat} and R_1^{kin} at $L/a = 4$. The QCD observable R_1 is calculated for $z = 4, 6, \ldots, 12$, the lowest value of L/a that can be used is then determined as the first one for which a solution of (3.91) exists. We present the continuum values for the one loop coefficients of R_1, R_1^{stat}, and R_1^{kin}, extracted as explained in appendix C.3, in tables 5.2 and 5.3. For sufficiently large L/a, the perturbative data shows a rather weak dependence on the lattice resolution and the uncertainty of the continuum extrapolations is then dominated by the round-off errors. As an example the one loop coefficient of R_1^P for $z = 12$ is plotted against a/L in figure 5.2.

θ	$z = 4$	$z = 6$	$z = 8$	$z = 10$	$z = 12$
A	-0.00856363(22)	-0.00755510(57)	-0.006941(45)	-0.006534(49)	-0.006228(77)
B	-0.0285850(13)	-0.0250893(19)	-0.022859(18)	-0.021361(84)	-0.02021(21)
C	-0.0200213(11)	-0.0175342(13)	-0.015920(14)	-0.014829(38)	-0.01398(14)

Table 5.2.: Results for the continuum value of R_1.

θ	A	B	C
R_1^{stat}	-0.0114056(1)	-0.016689(1)	-0.0052839(2)
LR_1^{kin}	-0.10135(1)	-0.13701(2)	-0.03566(2)

Table 5.3.: Results for the leading coefficients a_0 for $R_1^{\mathrm{stat},(1)}$ and $LR_1^{\mathrm{kin},(1)}$.

To conclude our one loop analysis, we proceed as follows. We define

$$Q_1(z, \theta_1, \theta_2) = \lim_{a/L \to 0} z R_1^{(1/m)}(L/a, z, \theta_1, \theta_2). \tag{5.17}$$

One may extract $Q_1^{(1)}$ from the data points for $R_1^{(1/m),(1)}$ at our disposal, the results are shown in figure 5.3. The quantity $Q_1^{(1)}$ is then combined with our results for R_1^{kin} at finite lattice resolutions L/a to calculate

$$m_{\mathrm{h}}\, \omega_{\mathrm{kin}}^{(1)}(z, L/a) = \frac{Q_1^{(1)}(z, \theta_1, \theta_2) - \frac{L}{2a} R_1^{\mathrm{kin},(1)}(L/a, \theta_1, \theta_2)}{L R_1^{\mathrm{kin},(0)}(L/a, \theta_1, \theta_2)}. \tag{5.18}$$

The resulting values for $m_{\mathrm{h}} \omega_{\mathrm{kin}}^{(1)}$ have a z-dependence, which only enters through the z-dependence of $Q_1^{(1)}$.

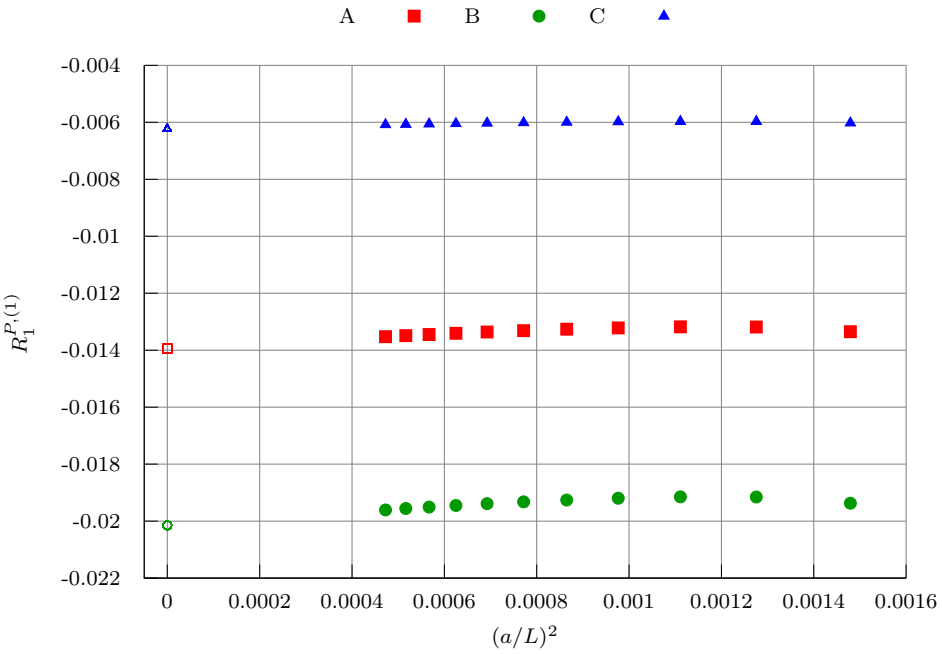

Figure 5.2.: The one loop coefficient $R_1^{P,(1)}$ for $z = 12$ and its continuum limit. The size of the round-off errors is usually much smaller than the point size.

The results for $m_\mathrm{h}\,\omega_\mathrm{kin}^{(1)}$ are presented in figures 5.4 and 5.5. The z-dependence of the data for $Q_1^{(1)}$ as seen in figure 5.3 translates to a z-dependence of the estimates for $m_\mathrm{h}\,\omega_\mathrm{kin}^{(1)}$. However, this dependence does not affect the precision of the final result significantly, since the magnitude of the one loop correction to $m_\mathrm{h}\omega_\mathrm{kin}$ is very small compared to the asymptotic tree level value of 1/2. Inspecting figures 5.4 and 5.5, we find that there is only a relative effect of order $10^{-2}g_0^2$ on ω_kin between $z = 6$ and $z = 12$. Considering that ω_kin itself has a small effect on physical observables, the z-dependence observed here is overall a very minor correction.

The dependence of the data on the lattice resolution is rather weak due to a weak a/L-dependence of LR_1^kin. The spread in the data for the different choices A,B, and C for the kinematic variables is small, which is expected. The choice of θ_1, θ_2 should not affect the parameters in the Lagrangian. However, we want to point out that this is not a trivial result. In figure 5.3, we do find a spread in the data for A,B, and C. Only the combination of Q_1 with the data for R_1^kin cancels the θ-dependence and this may be interpreted as a confirmation of the validity of the $1/z$-expansion at order $1/z$ to one loop level of perturbation theory.

If one compares the error bars in figures 5.4 and 5.5, one finds an indication that the choices B and C for the θ are the preferable ones.

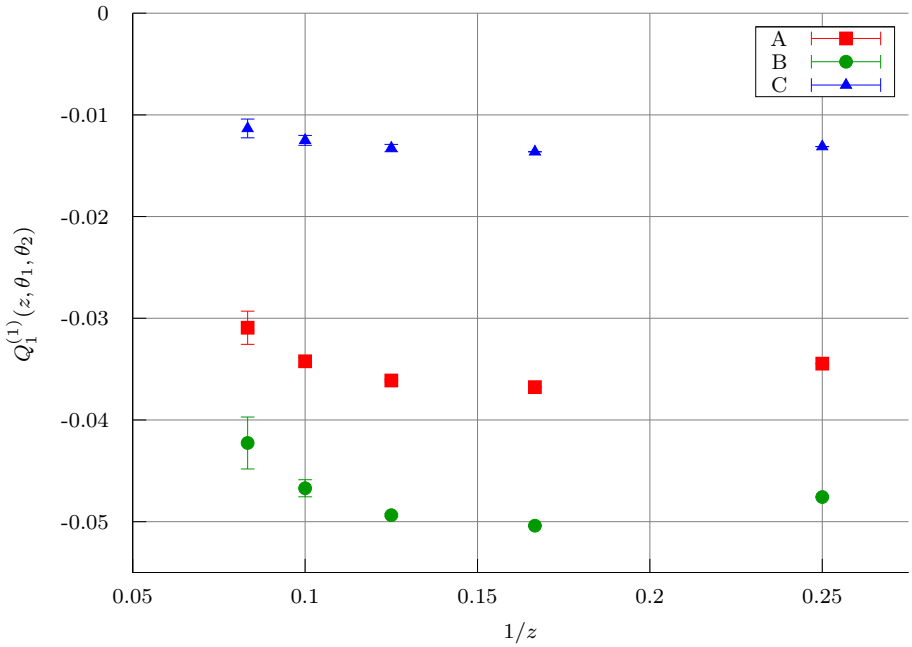

Figure 5.3.: Results for $Q_1^{(1)}$.

Performance

We found that the error on the continuum values extracted in fits using only the largest lattice sizes of, say $L/a = 40, \ldots, 46$, is dominated by the round-off errors. Thus, the largest sensible lattice size that should be used is in this range. The numerically most challenging diagram contributing to f_1 took 15 hours to be evaluated at $L/a = 46$ on a single 2 GHz CPU core. We found that using `long double` precision will yield a penalty in execution time of a factor of up to three.

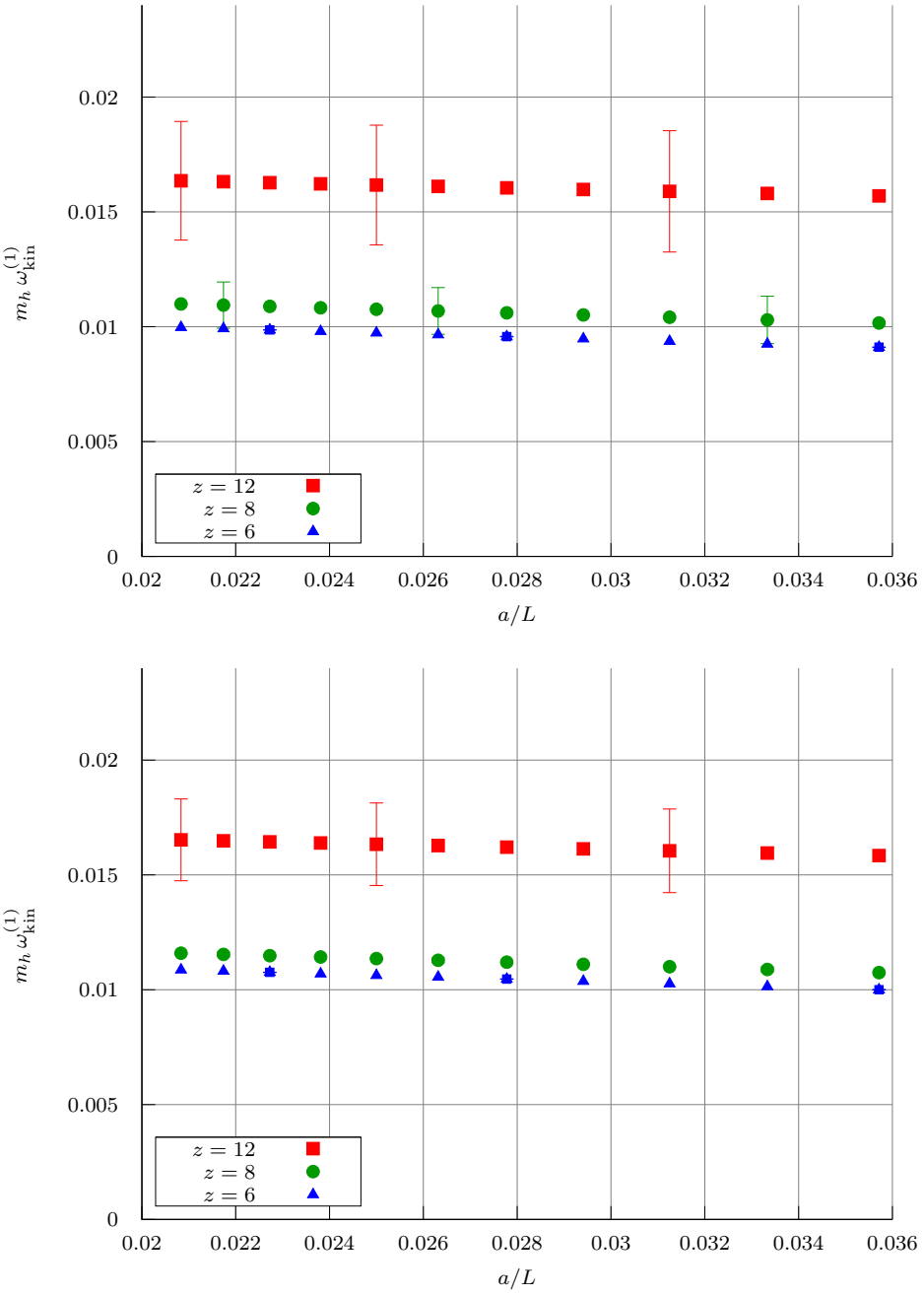

Figure 5.4.: The one loop coefficients $m_{\rm h}\,\omega^{(1)}_{\rm kin}$ for choices A (top) and B (bottom) of the angles θ_1 and θ_2. A few representative error bars are shown.

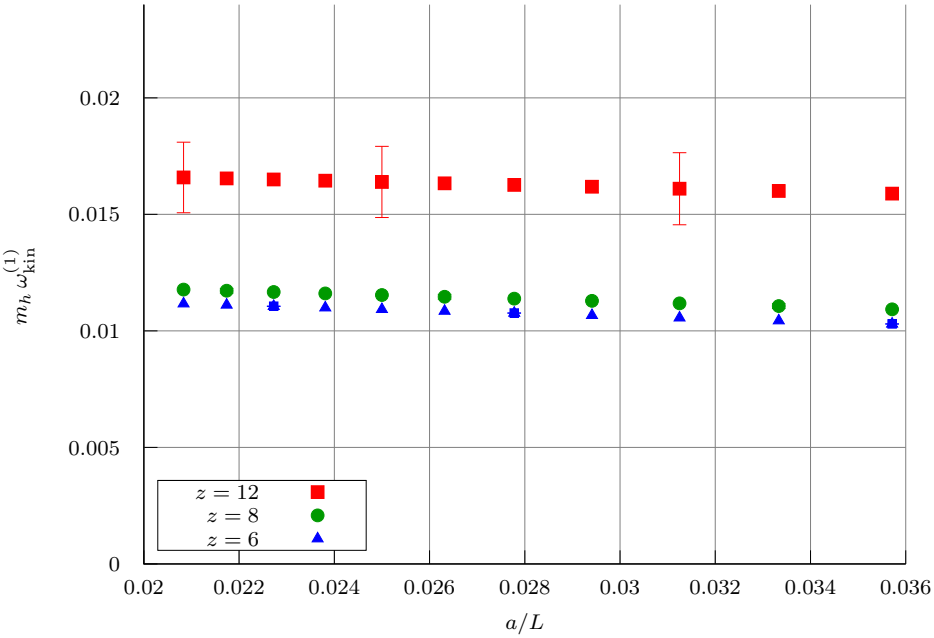

Figure 5.5.: The one loop coefficients $m_{\rm h}\,\omega^{(1)}_{\rm kin}$ for choice C of the angles θ_1 and θ_2. A few representative error bars are shown.

5.2.2. New Observables

Currently, the ALPHA collaboration makes efforts to include the missing parameters in the matching of QCD and HQET. While some of the observables that are investigated show a z-dependence which is strongly dominated by the leading terms, others have noticeable $1/z^2$ corrections Della Morte and Dooling [2011]. The z-dependence of the parameters can be anticipated by investigating the higher order corrections in z of the QCD observables that will be used for the matching. Two interesting candidates for QCD quantities whose HQET counterparts are proportional to $Z_{\mathrm{V}}^{\mathrm{HQET}}$ and $Z_{\mathbf{A}}^{\mathrm{HQET}}$ (4.10), (4.14) are the $O(a)$ improved three-point functions Hesse and Sommer [2011],

$$f_1^{\mathrm{A}_1}(x_0;\theta_1,\theta_2,\theta_3,z) = -\left(1+a\frac{m_{\mathrm{q},2}+m_{\mathrm{q},3}}{2}b_{\mathrm{A}}\right)\frac{a^3}{2}\sum_{\mathbf{x}}\langle\overline{\zeta}_1\,\gamma_5\,\zeta_3\,A_1(x)\,\overline{\zeta}_2'\,\gamma_1\,\zeta_1'\rangle \quad (5.19)$$

$$f_1^{\mathrm{V}_0}(x_0;\theta_1,\theta_2,\theta_3,z) = -\left(1+a\frac{m_{\mathrm{q},2}+m_{\mathrm{q},3}}{2}b_{\mathrm{V}}\right)\frac{a^3}{2}\sum_{\mathbf{x}}\langle\overline{\zeta}_1\,\gamma_5\,\zeta_3\,V_0(x)\,\overline{\zeta}_2'\,\gamma_5\,\zeta_1'\rangle, \quad (5.20)$$

where we introduced the shorthand

$$\zeta_i = a^3L^{-3/2}\sum_{\mathbf{x}}\zeta_i(\mathbf{x}), \quad \overline{\zeta}_i = a^3L^{-3/2}\sum_{\mathbf{x}}\overline{\zeta}_i(\mathbf{x}). \quad (5.21)$$

Two of the three flavors are light, $m_1 = m_2 = 0$, the mass of the third is as usual given by $z/L = m_3$. The QCD matching observables for the currents V_0 and A_k then read (c.f. (4.7), (4.9))

$$\Phi^{\mathrm{V}_0} = Z_{\mathrm{V}}\frac{f_1^{\mathrm{V}_0}(T/2;\theta_1,\theta_2,\theta_3,z)}{[f_1(\theta_1,\theta_3,z)f_1(\theta_1,\theta_2,0)]^{1/2}}, \quad (5.22)$$

$$\Phi^{\mathrm{A}_1} = Z_{\mathrm{A}}\frac{f_1^{\mathrm{A}_1}(T/2;\theta_1,\theta_2,\theta_3,z)}{[f_1(\theta_1,\theta_3,z)f_1(\theta_1,\theta_2,0)]^{1/2}}. \quad (5.23)$$

Note that these observables are $O(a)$-improved, since the improvement terms proportional to c_{V} and c_{A} vanish for A_k and V_0. We will set $\theta_1 = \theta_2 = \theta_3 = \theta$ in the following.

Static Approximation

In the static approximation, we can use the symmetries of the theory to relate the renormalized, renormalization group invariant (RGI) axial and vector currents Sommer [2011],

$$V_0^{\mathrm{HQET}} = C_{\mathrm{PS}}(M_b/\Lambda_{\overline{MS}})\,Z_{\mathrm{A,RGI}}^{\mathrm{stat}}(g_0)\,Z_{\mathrm{V/A}}^{\mathrm{stat}}(g_0)\,V_0^{\mathrm{stat}}, \quad (5.24)$$

$$A_k^{\mathrm{HQET}} = C_{\mathrm{V}}(M_b/\Lambda_{\overline{MS}})\,Z_{\mathrm{A,RGI}}^{\mathrm{stat}}(g_0)\,Z_{\mathrm{V/A}}^{\mathrm{stat}}(g_0)\,A_k^{\mathrm{stat}}. \quad (5.25)$$

The RGI matrix elements of an observable Φ are given by

$$\Phi_{\mathrm{RGI}} = \exp\left\{-\int^{g_R(\mu)} \mathrm{d}x\, \frac{\gamma(x)}{\beta(x)}\right\} \Phi(\mu), \tag{5.26}$$

with the γ and β function as in appendix C.4. We will not spend more time on renormalization group invariants here, since they will only play a secondary role in the following and refer to Sommer [2011] for all the details.

At one loop level, we have in the lattice minimal subtraction scheme

$$(V^{\mathrm{stat}}_{\mathrm{lat}})_0(\mu) = Z^{\mathrm{stat}}_{\mathrm{A,lat}}(\mu)\, Z^{\mathrm{stat}}_{\mathrm{V/A}} V_0^{\mathrm{stat}}, \tag{5.27}$$

$$(A^{\mathrm{stat}}_{\mathrm{lat}})_k(\mu) = Z^{\mathrm{stat}}_{\mathrm{A,lat}}(\mu)\, Z^{\mathrm{stat}}_{\mathrm{V/A}} A_k^{\mathrm{stat}}, \tag{5.28}$$

$$Z^{\mathrm{stat}}_{\mathrm{A,lat}}(\mu) = 1 - \gamma_0 \log(a\mu)\, g_0^2 + O(g_0^4), \tag{5.29}$$

$$Z^{\mathrm{stat}}_{\mathrm{V/A}} = 1 + \left(Z^{\mathrm{stat}}_{\mathrm{V/A}}\right)^{(1)} g_0^2 + O(g_0^4), \tag{5.30}$$

with (c.f. Palombi [2008], Shifman and Voloshin [1987], Politzer and Wise [1988])

$$\left(Z^{\mathrm{stat}}_{\mathrm{V/A}}\right)^{(1)} = 0.0521(1), \tag{5.31}$$

$$\gamma_0 = -\frac{1}{4\pi^2}. \tag{5.32}$$

We define

$$X_{\mathrm{A}}(\mu) = Z^{\mathrm{stat}}_{\mathrm{A,lat}}(\mu)\, Z^{\mathrm{stat}}_{\mathrm{V/A}} X^{\mathrm{bare}}_{\mathrm{A}}, \tag{5.33}$$

$$X_{\mathrm{V}}(\mu) = Z^{\mathrm{stat}}_{\mathrm{A,lat}}(\mu)\, Z^{\mathrm{stat}}_{\mathrm{V/A}} X^{\mathrm{bare}}_{\mathrm{V}}, \tag{5.34}$$

$$X^{\mathrm{bare}}_{\mathrm{A}} = \frac{\left(f_1^{\mathrm{A}_1}\right)^{\mathrm{stat}}(T/2;\theta_1,\theta_2,\theta_3,z)}{\left[f_1^{\mathrm{stat}}(\theta_1,\theta_3,z) f_1(\theta_1,\theta_2,0)\right]^{1/2}}, \tag{5.35}$$

$$X^{\mathrm{bare}}_{\mathrm{V}} = \frac{\left(f_1^{\mathrm{V}_0}\right)^{\mathrm{stat}}(T/2;\theta_1,\theta_2,\theta_3,z)}{\left[f_1^{\mathrm{stat}}(\theta_1,\theta_3,z) f_1(\theta_1,\theta_2,0)\right]^{1/2}}. \tag{5.36}$$

Note that pre-factors of $(1+a\,m_{q,2}\,b^{\mathrm{stat}}_{\mathrm{V}})$ and $(1+a\,m_{q,2}\,b^{\mathrm{stat}}_{\mathrm{A}})$ are implicit in the definitions of $\left(f_1^{\mathrm{V}_0}\right)^{\mathrm{stat}}$ and $\left(f_1^{\mathrm{A}_1}\right)^{\mathrm{stat}}$ respectively, just as in (5.19), (5.20). However, since we choose $m_{q,2}$ to vanish, these can be disregarded altogether. We then expect in analogy to Kurth and Sommer [2002] the following relations to hold at one loop level (c.f. (5.27), (5.28)),

$$\Phi^{\mathrm{V}_0}(z) = (1 + B^{\mathrm{stat}}_{\mathrm{A}} g_0^2) X_{\mathrm{V}}(z/L) + O(1/z), \tag{5.37}$$

$$\Phi^{\mathrm{A}_1}(z) = (1 + B^{\mathrm{stat}}_{\mathrm{V}} g_0^2) X_{\mathrm{A}}(z/L) + O(1/z), \tag{5.38}$$

where Kurth and Sommer [2002]

$$B_{\mathrm{A}}^{\mathrm{stat}} = -0.137(1). \tag{5.39}$$

From this, one can extract $B_{\mathrm{V}}^{\mathrm{stat}}$ using Sommer [2011]

$$\frac{C_{\mathrm{V}}}{C_{\mathrm{PS}}} = 1 + g_{\mathrm{R}}^2 \frac{\gamma_{\mathrm{match},1}^{\gamma_{\mathrm{k}}} - \gamma_{\mathrm{match},1}^{\gamma_0\gamma_5}}{2b_0} + O(g_{\mathrm{R}}^4), \tag{5.40}$$

and then we have

$$B_{\mathrm{V}}^{\mathrm{stat}} - B_{\mathrm{A}}^{\mathrm{stat}} = \frac{\gamma_{\mathrm{match},1}^{\gamma_{\mathrm{k}}} - \gamma_{\mathrm{match},1}^{\gamma_0\gamma_5}}{2b_0} = -0.016900. \tag{5.41}$$

Tree Level

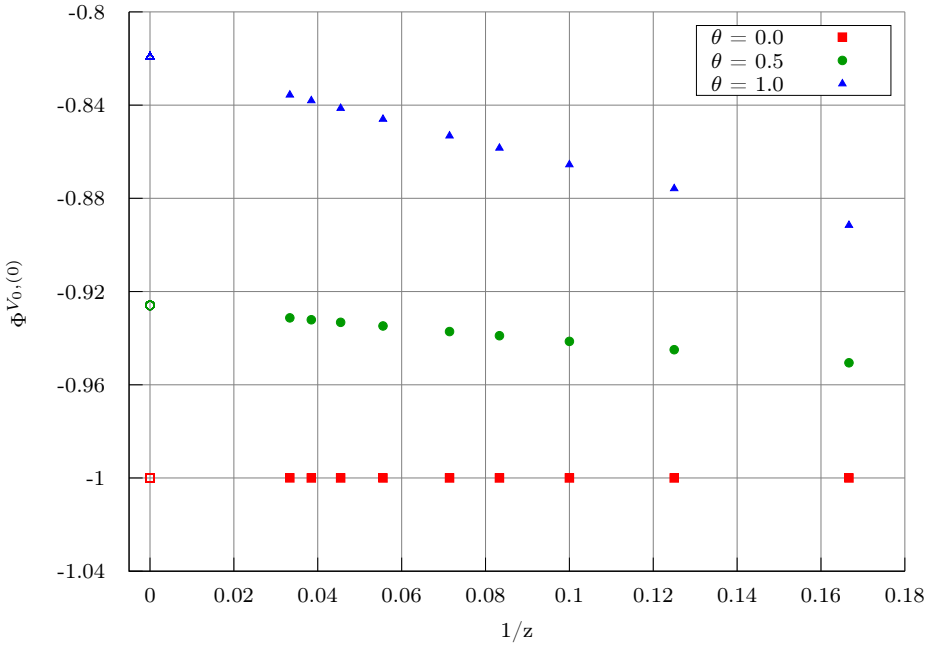

Figure 5.6.: Φ^{V_0} at tree level in the continuum limit. The point size is bigger than the error.

Tree level results for Φ^{V_0} and Φ^{A_1} are shown in figures 5.6 and 5.7, the points at $1/z = 0$ correspond to the static values $X_{\mathrm{V}}^{(0)}$ and $X_{\mathrm{A}}^{(0)}$. For $\theta = 0.5, 1.0$, the dependence on $1/z$ is linear with a small slope. In the interesting region of $z = 10$, which is the typical matching point for B physics used in Della Morte et al. [2007], the $1/z$ corrections

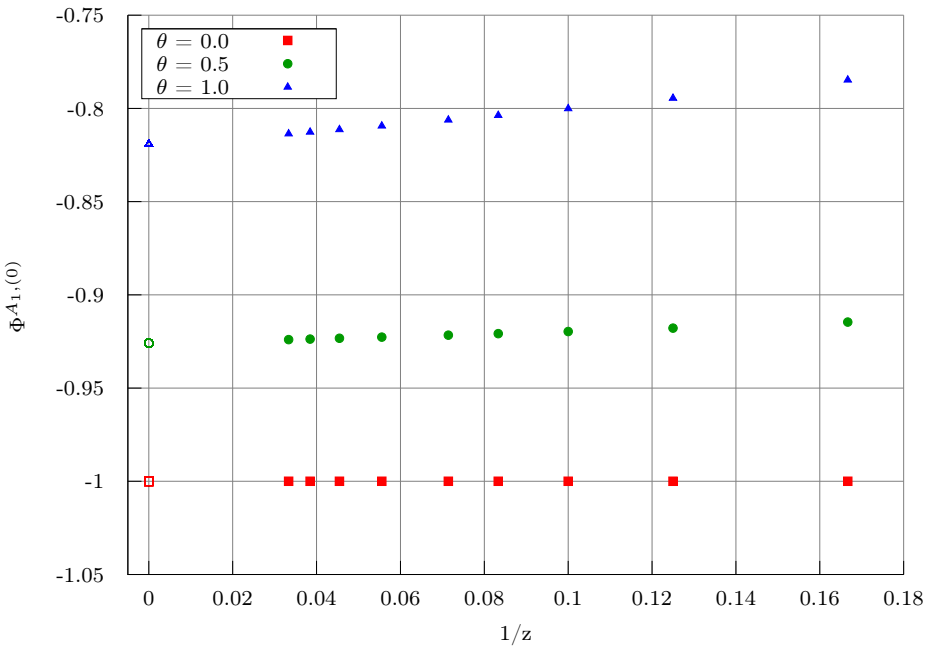

Figure 5.7.: Φ^{A_1} at tree level in the continuum limit. The point size is bigger than the error.

at tree level, defined by

$$(\Delta\Phi^{\mathrm{A}_1})^{(0)} = \left|\frac{\Phi^{\mathrm{A}_1,(0)} - \Phi^{\mathrm{A}_1,\mathrm{stat},(0)}}{\Phi^{\mathrm{A}_1,\mathrm{stat},(0)}}\right|, \quad (\Delta\Phi^{\mathrm{V}_0})^{(0)} = \left|\frac{\Phi^{\mathrm{V}_0,(0)} - \Phi^{\mathrm{V}_0,\mathrm{stat},(0)}}{\Phi^{\mathrm{V}_0,\mathrm{stat},(0)}}\right|, \tag{5.42}$$

can be found in table 5.4.

θ	$(\Delta\Phi^{\mathrm{A}_1})^{(0)}$	$(\Delta\Phi^{\mathrm{V}_0})^{(0)}$
0.5	0.7%	1.7%
1.0	2.4%	8.2%

Table 5.4.: $1/z$ corrections for Φ^{V_0} and Φ^{A_1} at tree level, $z = 10$.

For $\theta = 0$, there is no dependence on z and L/a at tree level for both observables as is easily seen by inserting the tree level propagators.

The continuum limit at tree level was extracted from computations with L/a up to 200, again using the fitting procedure explained in appendix C.3, neglecting round-off errors.

One Loop

The observables f_1, Φ^{V_0}, and Φ^{A_1} were calculated at one loop level for $z = 4, 6, 8, 10$ (and at $z = 0$ for f_1), with lattice resolutions up to $L/a = 40$, and for $\theta = 0.0, 0.5, 1.0$. Furthermore, we evaluated the static counterparts f_1^{stat}, $\Phi^{\mathrm{V}_0,\mathrm{stat}}$ and $\Phi^{\mathrm{A}_1,\mathrm{stat}}$ for lattices with L/a up to 28. No bigger lattice sizes are required for the HQET quantities, since their continuum limit is easier to obtain due to a weaker a/L-dependence. The continuum values are presented in figures 5.6 and 5.7, the points for $1/z = 0$ are again the static

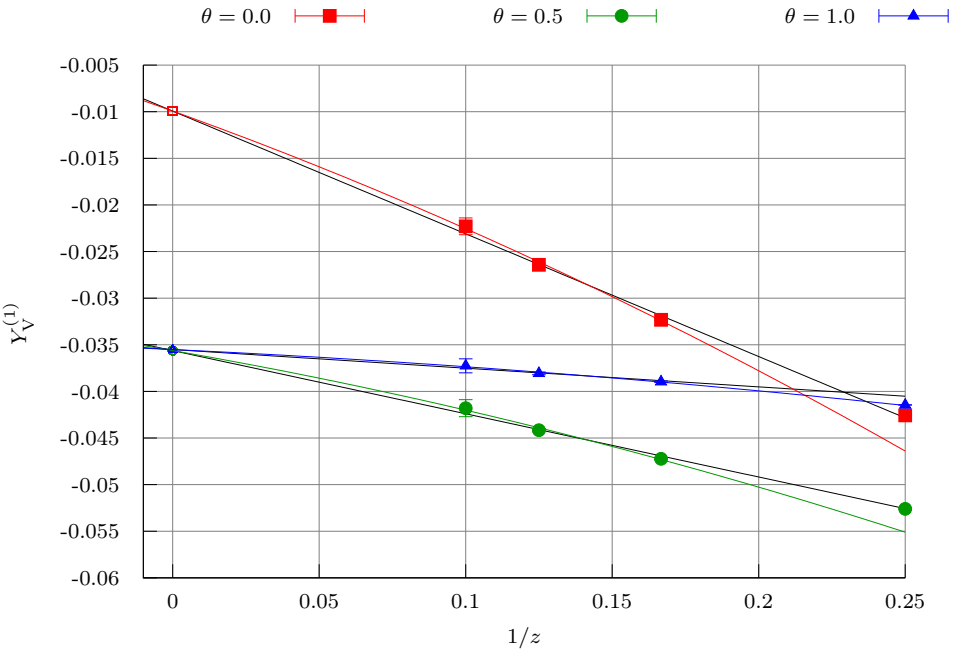

Figure 5.8.: Φ^{V_0} at one loop level in the continuum limit.

values on which we will comment shortly. The extraction of the continuum values is done with the usual method, the output of the analysis program is given for Φ^{V_0} at $z = 6$ and for its static partner in appendix C.3.1.

Coming back to the issue of establishing the connection to the static limit, we define the one loop quantities

$$Y_{\mathrm{V}}^{(1)} = \Phi^{\mathrm{V}_0,(1)}(z) - \left[B_{\mathrm{A}}^{\mathrm{stat}} - \gamma_0 \log(z) + \left(Z_{\mathrm{V/A}}^{\mathrm{stat}}\right)^{(1)}\right] X_{\mathrm{V}}^{(0)}, \tag{5.43}$$

$$Y_{\mathrm{A}}^{(1)} = \Phi^{\mathrm{A}_1,(1)}(z) - \left[B_{\mathrm{V}}^{\mathrm{stat}} - \gamma_0 \log(z) + \left(Z_{\mathrm{V/A}}^{\mathrm{stat}}\right)^{(1)}\right] X_{\mathrm{A}}^{(0)}, \tag{5.44}$$

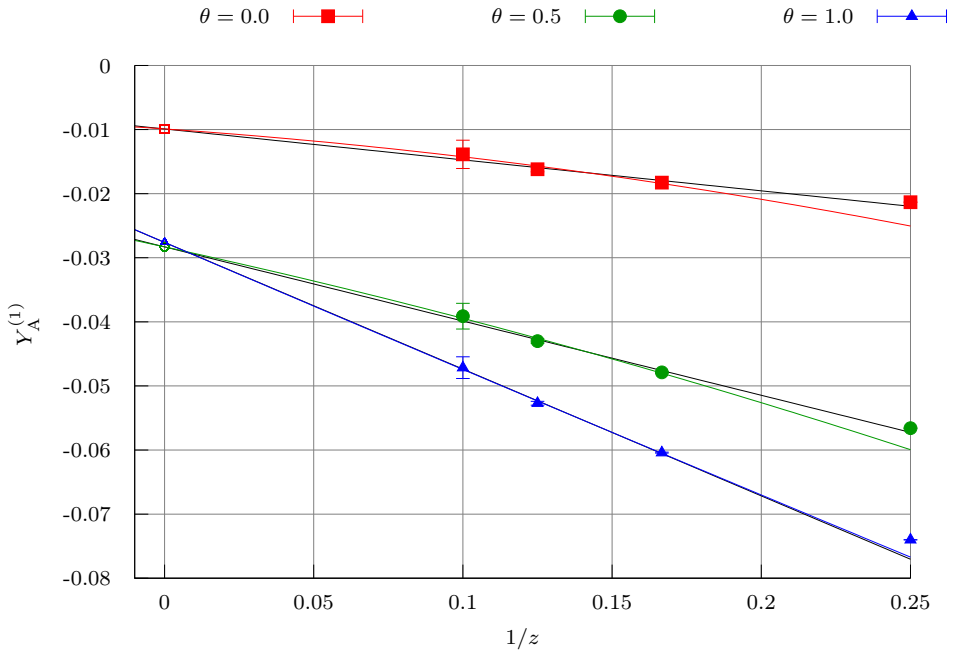

Figure 5.9.: Φ^{A_1} at one loop level in the continuum limit.

such that

$$Y_{\mathrm{V}}^{(1)}(z) \xrightarrow{1/z\to 0} X_{\mathrm{V}}^{\mathrm{bare},(1)} - \gamma_0 \log(a/L) X_{\mathrm{V}}^{\mathrm{bare},(0)} = X_{\mathrm{V,lat}}^{(1)}, \tag{5.45}$$

$$Y_{\mathrm{A}}^{(1)}(z) \xrightarrow{1/z\to 0} X_{\mathrm{A}}^{\mathrm{bare},(1)} - \gamma_0 \log(a/L) X_{\mathrm{A}}^{\mathrm{bare},(0)} = X_{\mathrm{A,lat}}^{(1)}. \tag{5.46}$$

The fit functions included in the plots are of the form

$$Y_{\mathrm{V}}^{(1)}(z) = X_{\mathrm{V,lat}}^{(1)} + c_1/z + c_2/z^2, \tag{5.47}$$

$$Y_{\mathrm{A}}^{(1)}(z) = X_{\mathrm{A,lat}}^{(1)} + c_1/z + c_2/z^2, \tag{5.48}$$

for the solid lines. The dashed lines are a linear fit in $1/z$, setting $c_2 = 0$. The data points at $z = 4$ are not included in the fits. Even though the fit is only indicative, since possible terms of the form $\log(z)/z^n$ are not included, one can anticipate that the higher order corrections corresponding to c_2 are rather small. We did not attempt to fit the logarithmic terms due to the small number of available data points.

In the case of $\Phi^{\mathrm{A_1}}$, a value of $\theta = 0$ seems to minimize the higher order corrections in $1/z$ both at tree level and at one loop. For $\Phi^{\mathrm{V_0}}$, the value $\theta = 0.5$ seems to be a good compromise considering the corrections at the two orders in perturbation theory we investigated. One should always keep in mind that the small observed dependence on $1/z$ will be eliminated once the $1/m_{\mathrm{h}}$ corrections are included in the effective theory.

Finally only the $1/z^2$-terms, manifesting themselves in the curvature of the fits, will remain as corrections.

Performance

For the evaluation of all 30 loop diagrams for $f_1^{\mathrm{V}_0}$, $f_1^{\mathrm{A}_1}$, 22 for f_1, plus 29 and 21 for the static counterparts, about two weeks real time including idle time for jobs waiting in the queue were required on the PC farm in Zeuthen for all values for the parameters combined. The farm consists of Westmere, Nehalem, and Harpertown blade systems with clock speeds varying from 2.66 GHz to 3.08 GHz.

5.2.3. Cut-off Effects of the Step Scaling Functions

The last application deals with the step scaling (5.6). We want to investigate the one loop cut-off effects of two of the step scaling functions (5.7) that were used in Blossier et al. [2010a].

Perturbative Improvement of Observables

Perturbative improvement de Divitiis et al. [1995] has been shown to be an effective method to speed up the approach to the continuum limit of a number of observables. The aim is to remove at a given order of perturbation theory all $O((a/L)^n \log(L/a)^m)$ cutoff effects. To this end, one defines the improved observable

$$\mathcal{O}_{\mathrm{I}}(a/L) = \frac{\mathcal{O}(a/L)}{1+\delta(a/L)}, \quad \delta(a/L) = \frac{\mathcal{O}(a/L)-\mathcal{O}(0)}{\mathcal{O}(0)} = \delta^{(0)}(a/L) + g_0^2\delta^{(1)}(a/L) + \dots . \tag{5.49}$$

The tree level improvements $\delta_{ij}^{(0)}$ for the step-scaling functions Σ_{ij} have already been calculated in Blossier et al. [2010a]. We want to investigate if the remaining cut-off effects that were observed non-perturbatively can be understood qualitatively as a one-loop contribution.

One Loop Analysis

We are interested specifically in the cut-off effects of Σ_{33} and Σ_{44} Blossier et al. [2010a],

$$\Sigma_{33}(L_1) = R_{\delta A}(L_2)/R_{\delta A}(L_1), \quad \Sigma_{44}(L_1) = R_1^{\mathrm{kin}}(L_2)/R_1^{\mathrm{kin}}(L_1), \tag{5.50}$$

$$R_{\delta A}(L) = \frac{f_{\delta A}^{\mathrm{stat}}(\theta, \frac{T}{2})}{f_A^{\mathrm{stat}}(\theta, \frac{T}{2})} - \frac{f_{\delta A}^{\mathrm{stat}}(\theta', \frac{T}{2})}{f_A^{\mathrm{stat}}(\theta', \frac{T}{2})}, \quad T = L, \tag{5.51}$$

$$R_1^{\mathrm{kin}}(L) = \frac{f_1^{\mathrm{kin}}(\theta)}{f_1^{\mathrm{stat}}(\theta)} - \frac{f_1^{\mathrm{kin}}(\theta')}{f_1^{\mathrm{stat}}(\theta')}, \quad T = L/2. \tag{5.52}$$

We assume again that the ratio $s = L_2/L_1$ is set to two. All relevant observables were calculated at one loop order using `pastor`. Again, the static quantities have a rather mild L/a-dependence and hence the continuum extrapolations (obtained as explained in

appendix C.3) can be performed in a straight forward way. The one loop improvements $\delta_{33}^{(1)}$ and $\delta_{44}^{(1)}$ for Σ_{33} and Σ_{44} are presented in figure 5.10, together with the tree level improved Monte Carlo data from Blossier et al. [2010b]. One should keep in mind that our investigation uses a different discretization of the static Lagrangian (Eichten-Hill, Eichten and Hill [1990b]) than the ones (HYP1/2) employed in Blossier et al. [2010a]. However, the sizes of the cutoff effects are qualitatively comparable. Perturbation theory provides an interesting hint for non-perturbative computations: the cutoff effects are minimal for $\theta = 0.5, \theta' = 1.0$.

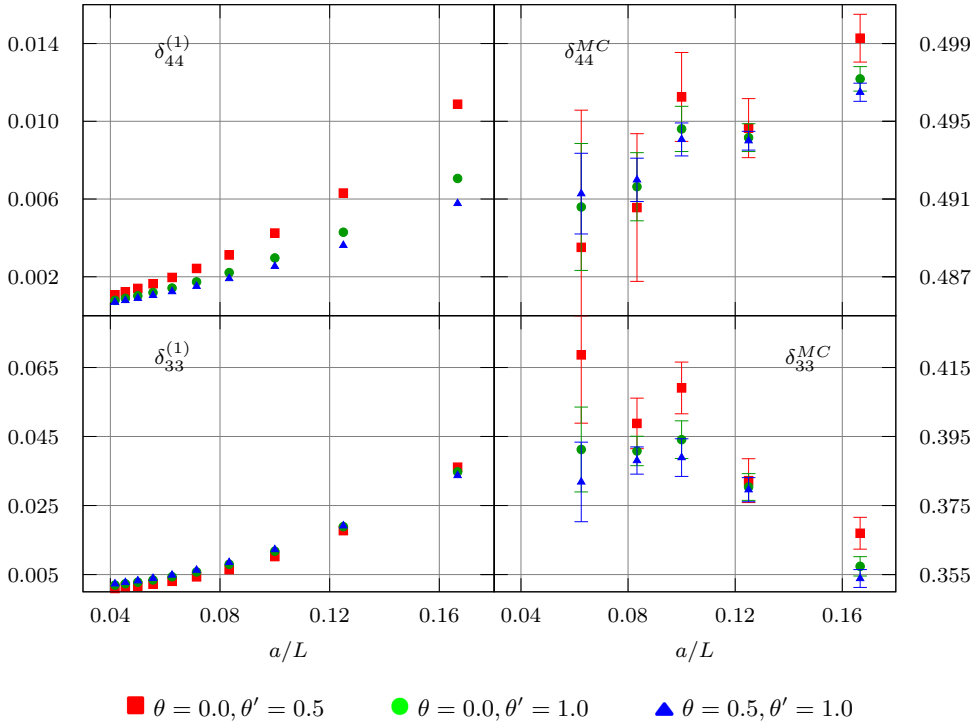

Figure 5.10.: One loop cutoff effects of Σ_{33} and Σ_{44} (Eichten-Hill action), together with the tree level improved Monte Carlo results ($N_f = 2$, $g_0 \sim 1$, HYP2 action) for comparison. The numerically most challenging diagram took 3.5 days to be evaluated for $L/a = 48$ on a single 2 GHz CPU core.

5.2.4. Outlook

It is important to keep in mind that although perturbation theory can give valuable hints for the matching procedure it ultimately has to be performed non-perturbatively if one wants to go beyond the static approximation. This may be seen as follows Sommer [2011]. The relative error on e.g. the perturbative conversion parameter C_{PS} (5.24), given the anomalous dimension (C.22) at l loops, is (choosing m_{h} as the renormalization scale)

$$\frac{\Delta C_{\mathrm{PS}}}{C_{\mathrm{PS}}} \propto [g_{\mathrm{R}}(m_{\mathrm{h}})]^l \sim \left[\frac{1}{b_0 \log(m_{\mathrm{h}}/\Lambda_{\mathrm{QCD}})}\right]^l \overset{m_{\mathrm{h}}\to\infty}{\gg} \frac{\Lambda_{\mathrm{QCD}}}{m_{\mathrm{h}}}. \tag{5.53}$$

For bigger and bigger quark masses, the perturbative error becomes dominant over the $1/m_{\mathrm{h}}$ correction. As long as the coefficient multiplying g_{R}^l is sufficiently small (such that the perturbative correction is smaller than the $1/m_{\mathrm{h}}$ one), the perturbative approach is valid. However, to be theoretically sound, a fully non-perturbative determination of the HQET parameters is needed.

We are confident that the `pastor` package will be useful to set up the matching procedure for the missing components of the vector and axial vector current. It can help in selecting suitable observables and determine preferable values for kinematic parameters, as we did in the last sections. The extension of the one loop analysis to the whole matching procedure is planned.

Of course, many other applications for `pastor` are possible. The Schrödinger functional is widely used and the flexibility of `pastor` makes it a suitable instrument for a number of investigations also beyond the standard model. For example many studies in technicolor theories are performed in a setup quite similar to ours (Hayakawa et al. [2011], see Del Debbio [2010] for a review) such that `pastor` may be employed here with little or no modifications.

Further improvements concerning performance and features are planned in the near future, for example the implementation of smeared link variables and better support for Abelian background fields.

6. Conclusions and Outlook

We made some effort in chapter 3 to explain the algorithms that were used to create the `pastor` package. This task can be quite clearly split into two parts, the generation of vertices and Feynman diagrams. We described how both tasks may be addressed and gave some overview how the vertex generation is implemented in `pastor`. The usage of only the vertex generator separate from the diagram generator may be worthwhile in some cases. The inclusion of an Abelian background field was discussed, even though the usage of such a background field with the code generator of `pastor` is not recommended at the moment, since the ghost tadpole contribution is not considered and few checks were performed. The user may however employ the pastor back-end to work with an Abelian background field.

Additionally to the self tests included in `pastor`, which check against known values of propagators and vertices for a few actions with and without background field, we confirmed in section 4.2 that we can reproduce known perturbative results with good numerical precision. In section 4.3, we demonstrated that `pastor` gives correct results for a number of observables both in QCD and HQET. A high degree of automation was reached, predictions for a whole set of observables may be obtained with rather modest effort.

We successfully employed `pastor` in the matching process of HQET and QCD in chapter 5, where we could obtain some useful information for future non-perturbative studies. The weak and very linear dependence of Φ^{V_0} and Φ^{A_1} on $1/z$ both at tree *and* one loop level demonstrates that these observables are excellent candidates for the determination of $Z_{\mathrm{V}}^{\mathrm{HQET}}$ and $Z_{\mathbf{A}}^{\mathrm{HQET}}$. These two currently unknown parameters enter already in the static approximation of the flavor currents. Hence they are the most important parameters to be included in the matching process.

We obtained loop results with reasonable numerical effort, demonstrating the fitness of `pastor` to produce production code. Further development and more applications of the `pastor` package are planned. The implementation of smeared links Blum et al. [1997] is planned in the near future, and the feasibility of parallelizing the programs generated by `pastor` and extending the output to two loop diagrams is investigated currently.

A. An Example Calculation with `pastor`.

In this chapter, we will give an overview over the most important features of the `pastor` package by guiding the reader through a simple calculation of the observable Φ^{V_0} as defined in (5.22).

We will frequently paste code examples and give instructions for shell commands to be issued by the user. We will delimit all such examples in the following way.

```
example computer code or shell commands
```

A.1. Prerequisites

- The `pastor` package relies on C++ and Python, and therefore a recent version of Python Python Software Foundation [2012] (the author recommends version 2.7) and a modern C++ compiler, e.g. the one contained in the GNU compiler collection (gcc) [Free Software Foundation] in version 4.5.
- If one desires a graphical output of the diagrams generated by `pastor`, the LaTeX package `feynmf` Ohl [2006] should be installed. The graphs will be generated automatically if LaTeX and `feynmf` are found on the host machine.
- The `pastor` package uses the boost C++ libraries Boost Project [2012]. These may be downloaded automatically when configuring `pastor`.
- A set of self tests is included in the distribution. These rely on the googletest framework Google Inc. [2012], which may be downloaded automatically as well.
- The build system of `pastor` uses the GNU autotools [Free Software Foundation,F,F] and GNU make [Free Software Foundation]. The author recommends `autoconf` version 2.68, `automake` version 1.11.2, `libtool` version 2.4.2 and `make` version `3.82`.

A.2. Obtaining and Compiling Pastor.

The `pastor` package may be obtained upon request from the author. We will assume that the user wants to keep the source directory and the build directory separate. We will use the shorthands `pastor-source` and `pastor-build` for those two directories. After extracting the `pastor` distribution archive in `pastor-source`, the software has to be configured. Calling the configure script with the --help flag,

```
pastor-build> pastor-source/configure --help
```

will give an overview over all options. The most important ones are as follows.

--with-boost=BOOST_DIR The boost libraries are expected to be found in the directory BOOST_DIR. If the option --enable-boost-download is given as well, BOOST_DIR will be used as the location to download boost if it is not found there.

--enable-boost-download Allows the configure script to download the boost libraries if they are not found in the system path or in BOOST_DIR.

--with-gtest=GTEST_DIR Location for googletest, in complete analogy to the option --with-boost.

--enable-gtest-download In complete analogy to the boost counter-part. Note that the configure script will abort if boost is not found. Googletest is considered optional and if it is neither found nor the download option is given, the self checks will simply not be compiled.

--enable-high-prec Instructs pastor to use the data type long double instead of double to increase the numerical precision, at the cost of slower code.

--enable-debug Turns on some debug features. These include higher compiler warning levels and extra checks within the code. This affects the performance of the software and is not recommended for generating production code.

--with-afs-sleep=T When using a PC farm to start multiple jobs (which pastor will do automatically), the access of multiple jobs to a network file system like AFS may cause trouble. Hence pastor will wait by default one second before it starts a new job. If this interval is undesirable, e.g. if one works only on a local machine, it can be changed to T seconds, where T may be fractional (e.g. 0.1).

After the options are selected, one may start the configuration and build the package,

```
pastor-build> pastor-source/configure --with-boost=boost \
                  --enable-boost-download
pastor-build> make
```

This will complete the compilation of the pastor package.

A.3. A First Calculation

The pastor distribution contains an example project that will be installed in the directory pastor-build/codegen/example_project. As mentioned above, the observable Φ^{V_0} will be calculated with the scripts provided. All the input files mentioned are present in the example's directory. The steps that have to be taken are as follows.

1. Parse the XML input file to generate programs for the diagrams associated with the process under investigation.

2. Prepare an input file to be used with a `pastor` script to run all programs and write the output in an easy to parse format.

3. Prepare an analysis script to calculate secondary quantities.

A.3.1. The XML Input File

The XML input file containing $f_1^{V_0}$, f_1 and their static counterparts can be found in the subdirectory named `codegen/example_project/xml`. Documentation for the XML format to be used is included in the pastor package, in the subdirectory `doc`. The document `tags.pdf` is generated automatically by parsing the python script that is used for evaluating the XML input and extracting its documentation. Thus also user-defined additions to `pastor` will be included here if they are implemented properly.

We will only paste a part of the XML input provided in the `pastor` package here to give the reader an impression of what the input looks like. To illustrate the use of two different actions, we present the input for $f_1^{V_0,\mathrm{stat}}$, copying verbatim from the file `phi_v0.xml`.

```
<process>
  <name>f1v0stat</name>
  <tex_comment><!-- Descriptive LaTeX comment -->
  [Left out for brevity.]
  </tex_comment>
  <background_field>trivial</background_field>
  <gauge_action>wilson</gauge_action>
  <!-- We have a product of four projectors, P_+ and P_- in the
  diagram, two of which can be dropped. They are represented as
  a  sum of Dirac matrices at the boundaries, and each of
  them comes with a factor of 0.5. Then, we take the factor
  1/2 from the definition into account and end up with
  a prefactor of (0.5)^3 = 0.125.  -->
  <factor>0.125</factor>
  <trace>
  <boundary>
    <where>0</where> <!--x_0 = 0-->
    <spin>dirac</spin>
    <spins>15 -14</spins>
    <!-- 2 * P_+ * gamma_5 * P_- = -->
    <!-- 2 * gamma_5 * P_- = gamma_5 - gamma_5 * gamma_0 -->
  </boundary>
  <propagator>
    <thetax>theta</thetax> <!-- user parameter: theta-->
    <thetay>theta</thetay>
    <thetaz>theta</thetaz>
    <spin>dirac</spin>
```

```
    <action>HQET_stat</action>
    <!--from and to are optional tags, helping pastor to
        generate more efficient code -->
    <from>1</from>
    <to>x0</to>
  </propagator>
    <insertion>
      <position>x0</position> <!-- user parameter: x_0-->
      <spin>dirac</spin>
      <spins>4</spins> <!-- gamma_0  -->
    </insertion>
    <propagator>
      <z_mass>0.0</z_mass> <!-- user parameter: z-->
      <thetax>theta</thetax> <!-- user parameter: theta-->
      <thetay>theta</thetay>
      <thetaz>theta</thetaz>
      <spin>dirac</spin>
      <action>clover</action>
    </propagator>
  <boundary>
    <where>1</where><!--x_0 = T-->
    <spin>dirac</spin>
    <spins>15 14</spins>
    <!-- 2 * P_- * gamma_5 * P_+ = -->
    <!-- 2 * gamma_5 * P_+ = gamma_5 + gamma_5 * gamma_0 -->
  </boundary>
  <boundary>
    <conjugate/> <!-- U_0^\dagger needed here -->
    <where>1</where><!--x_0 = T-->
    <spin>dirac</spin>
    <spins>0</spins>
  </boundary>
  <propagator>
    <z_mass>0.</z_mass>
    <thetax>theta</thetax> <!-- user parameter: theta-->
    <thetay>theta</thetay>
    <thetaz>theta</thetaz>
    <spin>dirac</spin>
    <action>clover</action>
  </propagator>
  <boundary>
    <conjugate/> <!-- U_0^\dagger needed here -->
    <where>0</where><!--x_0 = 0-->
    <spin>dirac</spin>
    <spins>0</spins>
  </boundary>
  </trace>
</process>
```

The elements occurring in the XML input are exactly the objects that were explained in chapter 3. A number of pre-defined actions are implemented in `pastor`, further ones can be added without much effort. At the time of writing, the list of pre-defined actions reads

Wilson Plain wilson quarks (2.6).

Clover Improved Wilson quarks, including the clover term (3.45).

HQET_stat Static quark action (2.29).

HQET_kin Static propagator with insertion of $\mathcal{O}_{\text{kin}}$ (2.36).

HQET_spin Static propagator with insertion of $\mathcal{O}_{\text{spin}}$ (2.37).

The next step is to parse the input file to produce programs to calculate the diagrams of all observables included in the input file. These in turn have to be compiled, all this is done by calling

```
pastor-build/codegen/example_project> ../parse.py xml/phi_v0.xml
pastor-build/codegen/example_project> cd source
pastor-build/codegen/example_project> ./configure
pastor-build/codegen/example_project> make
```

For each observable, `pastor` will generate a sub-directory in the `source` directory, named as the observable (c.f. the `name` tag). Inside this directory, a file named `diags.pdf` will be generated which contains the text contained in the `tex_comment` tag and the Feynman diagrams associated with all the generated programs.

For each diagram, a C++ program is generated, named `diagramXX.cc` where `XX` is a two digit integer. A descriptive text file named `diagramXX.info` is generated as well. The automatically generated configure script will output makefiles that can be used to compile and link all the programs.

Three further sub-directories will be created for each observable, containing the tree level diagram and the mass and boundary counter-terms as explained in section 3.5.

A.3.2. The `.get` File.

The next step is to call the programs, generally for a whole range of parameters. It is beneficial to automate this process as well. To this end, pastor contains the script `codegen/run.py`. It reads a file of the following form (copying verbatim from `codegen/example-project/input/f1_v0_small_L.get`)

```
# Base path for the executables
BasePath @abs_top_builddir@/codegen/example_project/source/

# Path for output and log files
WorkDir @abs_top_builddir@/codegen/example_project/run/
```

```
# Bool (yes|no) if the propagators should be written
# to hard disk and their location
Propagators no -

# subdirectories and names for the observables

SubDir f1v0/.    f1v0_loop
SubDir f1v0/tree f1v0_tree
SubDir f1v0/db   f1v0_db
SubDir f1v0/dm   f1v0_dm

# Parameters can be given in various ways ...

# 4 to 8 in steps of 2
Parameter L 4:8:2

# formulae
Parameter T = L
Parameter x0 = T/2

# fixed values
Parameter z = 1

# arrays
Parameter theta [0.0, 0.5, 1.0]
```

The format of this file is rather self-explanatory. All programs generated by `pastor` in all sub-directories that are specified in the input file will be executed, for every combination of the parameter values given. Calling the run script

```
pastor-build/codegen/example-project> ../run.py \
     input/f1_v0_small_L.get --help
```

will give an overview over all the possible command line options of `run.py`. To just start the calculations needed for Φ^{V_0}

```
pastor-build/codegen/example-project> ../run.py \
     input/f1_v0_small_L.get -a exe
pastor-build/codegen/example-project> ../run.py \
     input/f1_small_L.get -a exe
```

are the correct calls. If `pastor` finds the `qsub` command on the local machine, it will try to perform all calculations by submitting run scripts via `qsub`. The user can prevent this behavior by adding the `--no-grid` parameter. This will force all calculations to be performed locally. If the grid option is used, it is important that all paths that are given in the first few lines of the `.get` file are accessible from all computing nodes.

The output is written in a format that is easy to parse with a Python analysis script. `pastor` also contains a number of classes and methods to analyze perturbative data.

A.3.3. Data Analysis

An example analysis script can be found in the subdirectory `analysis` of the example project. It demonstrates the way the counter-terms as defined in section 3.5 should be taken into account and the usage of the `OneLoopObs` class. This class stores the tree level and one loop coefficients of an observable including the error on the loop coefficient and combines them in the correct way if one applies functions to calculate secondary quantities. All basic arithmetic operations for this type are implemented, plus some common functions like the square root and natural logarithm, all keeping track of the g_0 expansion and propagating the errors. Copying verbatim from the analysis script, some comments added:

```
# [...] read f1v0, f1z = f_1(theta, z), f10 = f_1(theta, 0)
# from disk
BV = 0.11492 * 4 / 3 # hep-lat/9704001
ZV = -0.129430 # hep-lat/9611015
# [...]
# the 'bare' quantity \phi^{V_0}
# note we use dt.sqrt, since it can handle the OneLoopObs type
# correctly
bare = f1v0 / dt.sqrt(f1z * f10)
# bV
b_V = dt.OneLoopObs(1, BV, 0.)
# m_{q,h} / 2
m_qh = dt.OneLoopObs(m0(p)/2, mq1(p)/2, 0.)
# (1 + b_V * m_{q,h} / 2)
opbm = b_V*m_qh
opbm.tree += 1
# Z_V
Z_V = dt.OneLoopObs(1, ZV, 0.)
# put everything together ...
bare = Z_V * opbm * bare
```

Furthermore the script shows how one can easily construct secondary quantities from the raw data generated by the run script. The user is encouraged to refer to the documentation found in the file `data_tools.py` that is located in the directory `codegen/tools` for further details. The method `uw_fit` can be found here as well, which may be used for the extraction of continuum limits, see appendix C.3.

B. Conventions

B.1. Generators of the Color Group $SU(3)$.

We choose to employ two different sets of generators of $SU(3)$. To stick with the standard notation, we will use the basis T_a if a trivial background field is involved. The T_a are defined as

$$T_a = \frac{1}{2}\lambda_a, \tag{B.1}$$

in terms of the Gell-Mann matrices Gell-Mann [1962]

$$\begin{aligned}
\lambda_1 &= \begin{pmatrix} 0 & 1 & 0 \\ 1 & 0 & 0 \\ 0 & 0 & 0 \end{pmatrix} \quad \lambda_2 = \begin{pmatrix} 0 & -i & 0 \\ i & 0 & 0 \\ 0 & 0 & 0 \end{pmatrix} \quad \lambda_3 = \begin{pmatrix} 1 & 0 & 0 \\ 0 & -1 & 0 \\ 0 & 0 & 0 \end{pmatrix} \\
\lambda_4 &= \begin{pmatrix} 0 & 0 & 1 \\ 0 & 0 & 0 \\ 1 & 0 & 0 \end{pmatrix} \quad \lambda_5 = \begin{pmatrix} 0 & 0 & -i \\ 0 & 0 & 0 \\ i & 0 & 0 \end{pmatrix} \quad \lambda_6 = \begin{pmatrix} 0 & 0 & 0 \\ 0 & 0 & 1 \\ 0 & 1 & 0 \end{pmatrix} \\
\lambda_7 &= \begin{pmatrix} 0 & 0 & 0 \\ 0 & 0 & -i \\ 0 & i & 0 \end{pmatrix} \quad \lambda_8 = \frac{1}{\sqrt{3}} \begin{pmatrix} 1 & 0 & 0 \\ 0 & 1 & 0 \\ 0 & 0 & -2 \end{pmatrix}.
\end{aligned} \tag{B.2}$$

The generators T_a obey the equations

$$\operatorname{tr} T_a = 0, \quad \operatorname{tr}[T_a T_b] = \frac{1}{2}\delta_{ab}, \quad [T_a, T_b] = i f_{abc} T_c, \tag{B.3}$$

where f_{ijk} are the totally antisymmetric structure constants of $SU(3)$. In case of an Abelian background field, as defined in Lüscher et al. [1992], it is more convenient to use another basis I_a for $su(3)$ Weisz [1996]. One defines a new set of matrices, $\tilde{\lambda}_a$, which conicide with λ_a except for the diagonal matrices with $a = 3, 8$, where one sets

$$\tilde{\lambda}_3 = -\frac{1}{2}\lambda_3 + \frac{\sqrt{3}}{2}\lambda_8, \quad \tilde{\lambda}_8 = \frac{\sqrt{3}}{2}\lambda_3 + \frac{1}{2}\lambda_8. \tag{B.4}$$

The matrices I_a are then given in terms of $\tilde{T}_a = \frac{1}{2i}\tilde{\lambda}_a$ by $I_3 = \tilde{T}_3, I_8 = \tilde{T}_8$, and

$$\begin{aligned}
I_1 &= \frac{1}{\sqrt{2}}(\tilde{T}_1 + i\tilde{T}_2), \quad I_4 = \frac{1}{\sqrt{2}}(\tilde{T}_4 + i\tilde{T}_5), \quad I_6 = \frac{1}{\sqrt{2}}(\tilde{T}_6 + i\tilde{T}_6), \\
I_2 &= \frac{1}{\sqrt{2}}(\tilde{T}_1 - i\tilde{T}_2), \quad I_5 = \frac{1}{\sqrt{2}}(\tilde{T}_4 - i\tilde{T}_5), \quad I_7 = \frac{1}{\sqrt{2}}(\tilde{T}_6 - i\tilde{T}_7).
\end{aligned} \tag{B.5}$$

B.2. Dirac Algebra

The Euclidean Dirac matrices γ_μ are given in terms of the Pauli matrices,

$$\sigma_1 = \begin{pmatrix} 0 & 1 \\ 1 & 0 \end{pmatrix}, \quad \sigma_2 = \begin{pmatrix} 0 & -i \\ i & 0 \end{pmatrix}, \quad \sigma_3 = \begin{pmatrix} 1 & 0 \\ 0 & -1 \end{pmatrix}. \tag{B.6}$$

Using 2×2 matrix notation, we get

$$\gamma_0 = \begin{pmatrix} 0 & 1 \\ 1 & 0 \end{pmatrix}, \quad \gamma_{1,2,3} = \begin{pmatrix} 0 & -i\sigma_{1,2,3} \\ i\sigma_{1,2,3} & 0 \end{pmatrix}. \tag{B.7}$$

The fifth Dirac matrix, γ_5, is defined as

$$\gamma_5 = \gamma_1\gamma_2\gamma_3\gamma_0 = \begin{pmatrix} 1 & 0 \\ 0 & -1 \end{pmatrix}. \tag{B.8}$$

It anti-commutes with all the other Dirac matrices and obeys $\gamma_5^2 = 1$. For the other ones, we have

$$\{\gamma_\mu, \gamma_\nu\} = 2\,\delta_{\mu\nu}. \tag{B.9}$$

Furthermore all the Dirac matrices including γ_5 obey

$$\gamma_\mu = \gamma_\mu^\dagger = \gamma_\mu^{-1}. \tag{B.10}$$

We furthermore define

$$\sigma_{\mu\nu} = \frac{i}{2}\left[\gamma_\mu, \gamma_\nu\right]. \tag{B.11}$$

C. Useful Formulae and Methods

C.1. Boundary Kernels For Improved Wilson Fermions

The boundary kernels for the improved Wilson action as defined in Lüscher et al. [1996] read

$$K(x,\mathbf{y})|_{x_0\neq 0} = \frac{1}{a}\tilde{c}_t\,\delta_{\mathbf{x},\mathbf{y}}\,\delta_{x_0,a}\,U_0(x-\hat{0})^{-1}, \tag{C.1}$$

$$K'(x,\mathbf{y})|_{x_0\neq T} = \frac{1}{a}\tilde{c}_t\,\delta_{\mathbf{x},\mathbf{y}}\,\delta_{x_0,T-a}\,U_0(x), \tag{C.2}$$

$$\tilde{K}(\mathbf{y},x)|_{x_0\neq 0} = \frac{1}{a}\tilde{c}_t\,\delta_{\mathbf{x},\mathbf{y}}\,\delta_{x_0,a}U_0(x-\hat{0}), \tag{C.3}$$

$$\tilde{K}'(\mathbf{y},x)_{x_0\neq T} = \frac{1}{a}\tilde{c}_t\,\delta_{\mathbf{x},\mathbf{y}}\,\delta_{x_0,T-a}\,U_0(x)^{-1}, \tag{C.4}$$

$$K(x,\mathbf{y})_{x_0=0} = \tilde{K}(\mathbf{x},y)_{y_0=0} = -\delta_{\mathbf{x},\mathbf{y}}\frac{\tilde{c}_s}{2}\,P_-\,\gamma_k(\nabla_k^*+\nabla_k)\,P_+ \tag{C.5}$$

$$K'(x,\mathbf{y})_{x_0=T} = \tilde{K}'(\mathbf{x},y)_{y_0=T} = -\delta_{\mathbf{x},\mathbf{y}}\frac{\tilde{c}_s}{2}\,P_+\,\gamma_k(\nabla_k^*+\nabla_k)\,P_- \tag{C.6}$$

Note that the appearance of the projectors in (C.5), (C.6) is due to the boundary conditions (3.14). With the operators above, one obtains the same list of all basic Wick contractions involving bulk and boundary fields as in section 2.3 of Lüscher and Weisz [1996].

C.2. Abelian Background Fields

We collect some basic facts about Abelian background fields in the Schrödinger functional as described in Lüscher et al. [1992], Weisz [1996]. The boundary fields $C_k = C, C'_k = C'$ are given by linear combination of the two diagonal generators $\tilde{\lambda}_3$ and $\tilde{\lambda}_8$ (B.4) and depend on the two parameters η and ν,

$$C = \frac{i}{L}\left\{\left(\eta\,\nu-\frac{\pi}{6}\right)\tilde{\lambda}_3 + \frac{\sqrt{3}}{2}\left(\eta-\frac{\pi}{3}\tilde{\lambda}_8\right)\right\} \tag{C.7}$$

$$C' = \frac{i}{L}\left\{\left(\eta\,\nu-\frac{\pi}{6}\right)\tilde{\lambda}_3 - \frac{\sqrt{3}}{2}\left(\eta+\frac{\pi}{3}\tilde{\lambda}_8\right)\right\}. \tag{C.8}$$

The background field obeys

$$V_0(x) = 1, \quad V_k(x) = V(x_0) = \exp\{i\,a\,b(x_0)\}, \tag{C.9}$$

where

$$b(x_0) = \mathcal{E}\, x_0 - iC, \quad \mathcal{E} = -i\{C' - C\}/T. \tag{C.10}$$

The choices of C, C' above give $\mathcal{E}$ a simple form,

$$\mathcal{E} = -\gamma\sqrt{3}\tilde{\lambda}_8, \quad \gamma = \frac{1}{LT}\left\{\eta + \frac{\pi}{3}\right\}. \tag{C.11}$$

The background field then has the properties

$$V(t)\; I_a = I_a\; V(t)\; e^{i\phi_a(t)}, \tag{C.12}$$

$$e^{ia^2\mathcal{E}}\; I_a = I_a e^{ia^2\mathcal{E}}\; e^{i\phi'_a}, \tag{C.13}$$

where the phases ϕ, ϕ' are listed in table C.1.

b	ϕ'_b	$\phi_b(t)$
1	$-3\,a^2\gamma$	$-3a\gamma t + \frac{a}{L}(\eta[\frac{3}{2} - \nu] - \frac{\pi}{3})$
3	0	0
4	$-3\,a^2\gamma$	$-3a\gamma t + \frac{a}{L}(\eta[\frac{3}{2} + \nu] - \frac{2\pi}{3})$
6	0	$\frac{a}{L}(2\eta\nu - \frac{\pi}{3})$
8	0	0

Table C.1.: Phases ϕ_a, ϕ'_a as in Takeda [2009]. Note that $\phi_2 = -\phi_1$, $\phi_5 = -\phi_4$, $\phi_7 = -\phi_6$, and analogous equations hold for ϕ'_a.

C.3. Extrapolation of Perturbative Data

If we evaluate an observable at one loop with `pastor`, we obtain numerical estimates $f(I)$, up to round-off errors, for a range of lattice resolutions $I = L/a$. We assume that f represents an observable that has at most a logarithmic divergence. The data is then expected to have the asymptotic expansion Lüscher and Weisz [1986]

$$f(I) = \sum_{n=0}^{\infty} \frac{a_n + b_n \log I}{I^n}. \tag{C.14}$$

In some cases, one may restrict some of the coefficients. If the observable is known to have a continuum limit, we may drop b_0. Furthermore, a_1 and b_1 may be set to zero if we deal with an $O(a)$-improved quantity. One is usually interested in obtaining estimates for the first few coefficients a_i, b_i. A method to extract these is described in Lüscher and Weisz [1986], where multiple data points are combined to improve the estimates successively, up to a point where round-off errors can no longer be neglected and become comparable to the systematic uncertainty.

We found it more convenient to work with another (in certain cases equivalent) method proposed in Bode et al. [2000]. Here, one performs a number of fits with a fit function

like (C.14), truncating the series at some N. Successive fits are then performed, omitting more and more data points at low resolutions I. As soon as the fit stabilizes, one repeats the procedure with e.g. three different fit functions, taking higher order terms in (C.14) into account one by one. The deviation of the results obtained with different fit functions is then used to estimate the systematic error. The stability of the fits may be controlled by checking the residuals,

$$\text{res.} = \sqrt{\sum_I \left(f(I) - \sum_{n=0}^{N} \frac{a_n + b_n \log I}{I^n} \right)^2}, \tag{C.15}$$

where a_n, b_n are the fit parameters.

To perform the fits, a singular value decomposition is used Press [2007]. This also allows us to propagate the round-off errors we estimated as described in section 4.2.1 to calculate their impact on the fit parameters.

C.3.1. An Explicit Example

The output of the code used to perform the extrapolations then looks like this:

phiv0stat - theta = 0.5

Imin	1.	log(I)/I**2	1./I**2	res.
4	-0.03569113614841(96)	-0.031067354666(90)	0.17474892548(11)	4.4255369108e-05
6	-0.0356717877918(15)	-0.03725609253(27)	0.18595325431(43)	3.12388158428e-05
8	-0.0356452529765(23)	-0.04912965668(63)	0.2103700687(12)	1.05153382459e-05
10	-0.0356317524285(35)	-0.0568665250(13)	0.2276115364(27)	2.79362362263e-06
12	-0.0356263117939(54)	-0.0606500103(26)	0.2365296178(58)	6.60706255605e-07
14	-0.0356243111215(83)	-0.0622788556(51)	0.240532955(12)	1.46102609095e-07
16	-0.035623598918(13)	-0.0629407109(98)	0.242213570(24)	3.37934379347e-08
18	-0.035623323315(22)	-0.063227621(20)	0.242961510(49)	1.03873977174e-08
20	-0.035623171510(41)	-0.063402121(42)	0.24342640(11)	4.20226849496e-09
22	-0.035623037309(87)	-0.06357053(10)	0.24388338(27)	1.52190381025e-09
24	-0.03562288997(25)	-0.06377054(32)	0.24443467(88)	4.27377285388e-15

phiv0stat - theta = 0.5

Imin	1.	log(I)/I**2	1./I**2	log(I)/I**3	res.
4	-0.03569178862734(94)	0.0159880734(11)	-0.0221164557(48)	0.3796099434(95)	3.22445791773e-05
6	-0.035570879484(16)	-0.314390402(41)	1.27138643(16)	-1.98414078(29)	2.87505115151e-05
8	-0.035565667297(16)	-0.269461356(39)	1.07396478(15)	-1.57991255(28)	4.07990445468e-06
10	-0.035600299557(23)	-0.154225374(62)	0.61375030(24)	-0.71736805(45)	8.9856897934e-07
12	-0.035613990023(37)	-0.10375818(12)	0.40981865(46)	-0.32823919(86)	1.9495276202e-07
14	-0.035619443925(65)	-0.08141196(23)	0.31844275(93)	-0.1505467(18)	3.60220893327e-08
16	-0.03562142236(12)	-0.07246757(50)	0.2814675(20)	-0.0773257(40)	4.29867187283e-09
18	-0.03562192695(26)	-0.0699717(12)	0.2710477(48)	-0.0563396(96)	5.03539340837e-10
20	-0.03562182137(62)	-0.0705385(32)	0.273435(13)	-0.061224(27)	3.52260593044e-10
22	-0.0356214788(20)	-0.072522(12)	0.281854(49)	-0.07870(10)	1.34073963402e-13

phiv0stat - theta = 0.5

Imin	1.	log(I)/I**2	1./I**2	1./I**3	res.
4	-0.0356475883637(23)	-0.05762774620(91)	0.2433981815(22)	-0.1304961275(40)	2.20620635921e-05
6	-0.0356068728795(42)	-0.0976741581(28)	0.3598927103(77)	-0.409678504(17)	1.35763362379e-06
8	-0.0356063147540(74)	-0.0984226770(72)	0.362222099(21)	-0.416192166(55)	1.34658738154e-06
10	-0.035613408700(13)	-0.086370497(17)	0.322929158(53)	-0.29298085(16)	5.1229090906e-07
12	-0.035618488782(23)	-0.075941646(39)	0.28773449(13)	-0.17234058(41)	1.36340132306e-07
14	-0.035621069508(43)	-0.069744492(88)	0.26625008(30)	-0.0932244(10)	2.71230645636e-08
16	-0.035622106747(85)	-0.06689868(20)	0.25616711(71)	-0.0538282(27)	2.95005719692e-09
18	-0.03562234512(18)	-0.06616456(51)	0.2535186(18)	-0.0429494(72)	7.86094460121e-10
20	-0.03562220565(45)	-0.0666401(14)	0.2552607(53)	-0.050419(22)	4.27740132864e-10
22	-0.0356219019(15)	-0.0677744(54)	0.259471(20)	-0.069159(88)	1.67936757532e-13

phiv0stat - theta = 0.5

Imin	1.	log(I)/I**2	1./I**2	log(I)/I**4	res.
4	-0.0356477458285(23)	-0.05384261423(80)	0.2274815194(17)	-0.2533667303(79)	2.15295569164e-05
6	-0.0356112550362(40)	-0.0829803798(21)	0.3028096074(52)	-0.750784170(31)	1.25600009156e-06
8	-0.0356099711118(68)	-0.0843318499(52)	0.306540445(14)	-0.78208228(10)	1.17580868523e-06
10	-0.035615427863(12)	-0.077190029(12)	0.285876166(33)	-0.57252331(30)	4.62643106448e-07
12	-0.035619439522(21)	-0.070920334(26)	0.267079186(76)	-0.35044087(81)	1.25086748588e-07
14	-0.035621492985(38)	-0.067196746(58)	0.25559826(18)	-0.1966484(21)	2.49116164174e-08
16	-0.035622313631(74)	-0.06550652(13)	0.25026636(41)	-0.1173045(57)	2.57563543405e-09
18	-0.03562248705(16)	-0.06510737(33)	0.2489829(10)	-0.096417(16)	8.89782590925e-10
20	-0.03562234958(39)	-0.06545647(93)	0.2501239(30)	-0.116477(51)	4.57322615121e-10
22	-0.0356220740(13)	-0.0662207(34)	0.252657(11)	-0.16411(21)	3.30887076406e-14

In the first column, we have the minimum lattice resolution I used for the fit. Then, the best fit values for the coefficients of the respective functions are listed, together with the round-off error from the data propagated to the fit parameters. Finally, we have the last column reserved for the residual of the fit such that we can check for its convergence. The data presented above belongs to the observable $\phi^{\mathrm{V}_0,\mathrm{stat}}$, c.f. (5.22). The a/L-dependence is weak and the extraction of the parameters rather simple. The QCD observable Φ^{V_0} at $z = 6$ exhibits stronger cut-off effects, as we will see below.

The results extracted from the examples presented in this section are $\Phi^{\mathrm{V}_0,(1)}(\theta = 0.5, z = 6) = -0.0472(1)$ and $X_{\mathrm{V}}^{\mathrm{bare},(1)}(\theta = 0.5) = -0.035622(1)$.

phiv0 - theta = 0.5 - z = 6			
Imin	1.	log(I)/I**2	1./I**2	res.
14	-0.048438162(43)	2.179628(30)	-6.298929(72)	0.000339372118958
16	-0.047763227(61)	1.385392(52)	-4.20643(13)	7.99470528815e-05
18	-0.047545860(88)	1.096119(89)	-3.42243(23)	2.56159518912e-05
20	-0.04744790(13)	0.95070(15)	-3.01884(40)	9.29668785388e-06
22	-0.04739600(19)	0.86571(25)	-2.77810(68)	3.52240706025e-06
24	-0.04736577(28)	0.81157(42)	-2.6221(12)	1.30835561605e-06
26	-0.04734706(43)	0.77526(71)	-2.5158(20)	4.41097130456e-07
28	-0.04733498(70)	0.7501(13)	-2.4411(38)	1.15618664131e-07
30	-0.0473269(14)	0.7322(29)	-2.3874(87)	3.58288898116e-15

phiv0 - theta = 0.5 - z = 6				
Imin	1.	log(I)/I**2	1./I**2	log(I)/I**3	res.
14	-0.04466156(25)	-15.6057(10)	67.1741(41)	-144.8141(80)	0.000123514742061
16	-0.04635837(38)	-6.0499(17)	26.9180(72)	-62.763(14)	2.16725413196e-05
18	-0.04682710(58)	-3.1372(30)	14.511(13)	-36.951(26)	5.31050843848e-06
20	-0.04701752(90)	-1.8441(52)	8.949(22)	-25.160(46)	1.46733881624e-06
22	-0.0471115(14)	-1.1534(94)	5.952(40)	-18.698(85)	4.11586918214e-07
24	-0.0471640(25)	-0.740(18)	4.143(77)	-14.74(17)	1.06646196469e-07
26	-0.0471960(50)	-0.472(39)	2.96(17)	-12.12(38)	2.16971202975e-08
28	-0.047217(14)	-0.29(12)	2.15(54)	-10.3(12)	7.23860984373e-13

phiv0 - theta = 0.5 - z = 6				
Imin	1.	log(I)/I**2	1./I**2	1./I**3	res.
14	-0.04575075(18)	-5.49057(41)	20.7913(14)	-103.5696(52)	9.80826705733e-05
16	-0.04674438(28)	-1.98914(77)	8.0058(27)	-49.986(11)	1.68959871133e-05
18	-0.04701674(43)	-0.9024(14)	3.9602(51)	-32.051(21)	4.11273971827e-06
20	-0.04712748(68)	-0.4098(25)	2.0962(94)	-23.379(41)	1.13470994249e-06
22	-0.0471824(11)	-0.1413(47)	1.066(18)	-18.383(82)	3.18509710743e-07
24	-0.0472132(19)	0.0224(92)	0.431(35)	-15.19(17)	8.26475170888e-08
26	-0.0472321(39)	0.130(21)	0.008(80)	-13.00(40)	1.68398574908e-08
28	-0.047245(11)	0.206(64)	-0.29(25)	-11.4(13)	6.96404645878e-14

phiv0 - theta = 0.5 - z = 6					
Imin	1.	log(I)/I**2	1./I**2	log(I)/I**4	res.
14	-0.04609446(15)	-2.88177(28)	9.63642(85)	-227.321(11)	9.03929592246e-05
16	-0.04688362(24)	-0.80344(51)	2.8629(16)	-113.861(24)	1.51661613236e-05
18	-0.04709284(38)	-0.18230(92)	0.7968(30)	-75.540(49)	3.61524483499e-06
20	-0.04717558(59)	0.0906(16)	-0.1269(54)	-56.829(99)	9.80859989445e-07
22	-0.04721564(96)	0.2355(30)	-0.625(10)	-45.94(20)	2.71570655259e-07
24	-0.0472377(17)	0.3220(58)	-0.925(20)	-38.92(43)	6.96571060688e-08
26	-0.0472510(33)	0.378(13)	-1.122(45)	-34.1(11)	1.40511939816e-08
28	-0.0472596(92)	0.416(40)	-1.26(14)	-30.5(36)	2.110741953e-14

C.4. Renormalization Group Functions

The RG functions for the running coupling, mass and matrix elements of multiplicatively renormalizable composite local fields Φ are defined as

$$\mu\frac{\partial g_R}{\partial \mu} = \beta(g_R), \tag{C.16}$$

$$\frac{\mu}{m_{\mathrm{R}}}\frac{\partial m_{\mathrm{R}}}{\partial \mu} = \tau(g_R), \tag{C.17}$$

$$\frac{\mu}{\Phi}\frac{\partial \Phi}{\partial} = \gamma(g_R). \tag{C.18}$$

$$\tag{C.19}$$

The asymptotic expansions read

$$\beta(g_R) \overset{g_R\to 0}{\sim} -g_R^3\left\{b_0 + g_R^2 b_1 + \ldots\right\}, \tag{C.20}$$

$$\tau(g_R) \overset{g_R\to 0}{\sim} -g_R^2\left\{d_0 + g_R^2 d_1 + \ldots\right\}, \tag{C.21}$$

$$\gamma(g_R) \overset{g_R\to 0}{\sim} -g_R^2\left\{\gamma_0 + g_R^2 \gamma_1 + \ldots\right\}. \tag{C.22}$$

D. Plots of the Cross Check

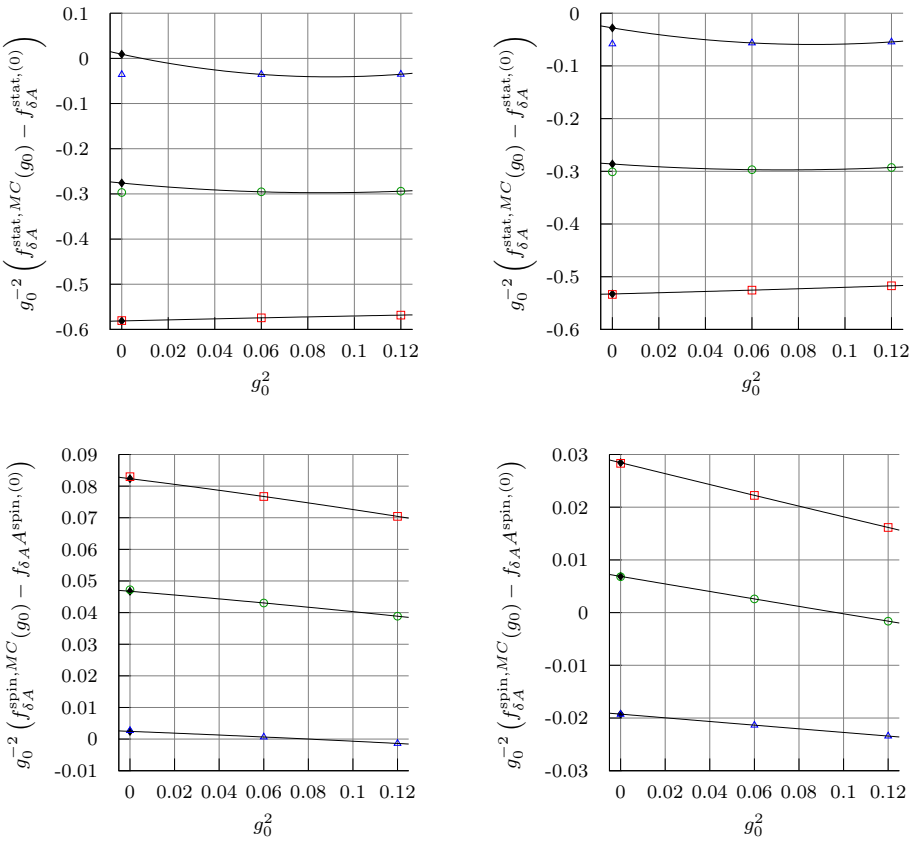

Figure D.1.: Various HQET correlation functions at $L = 4, 6$ for $\theta = 0.0$ (open boxes), $\theta = 0.5$ (open circles) and $\theta = 1.0$ (open triangles). The one loop data is depicted as filled diamonds. The statistical error is smaller than the symbol size. The small discrepancy between the linearly extrapolated Monte Carlo results and perturbative data in $f_{\delta A}^{\mathrm{stat}}$ hints at large higher order corrections.

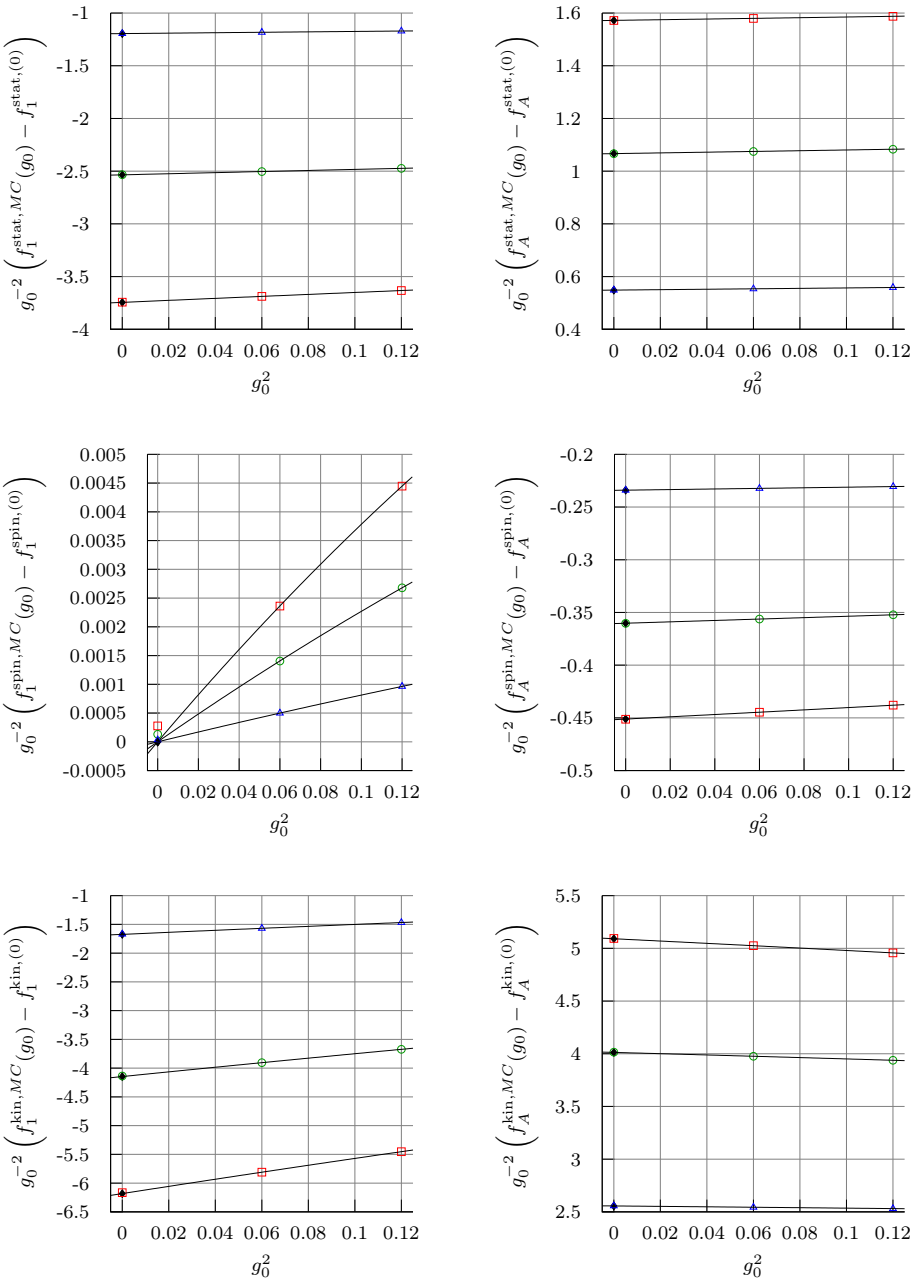

Figure D.2.: Various HQET correlation functions at $L = 6$ for $\theta = 0.0$ (open boxes), $\theta = 0.5$ (open circles) and $\theta = 1.0$ (open triangles). The one loop data is depicted as filled diamonds . The statistical error is smaller than the symbol size.

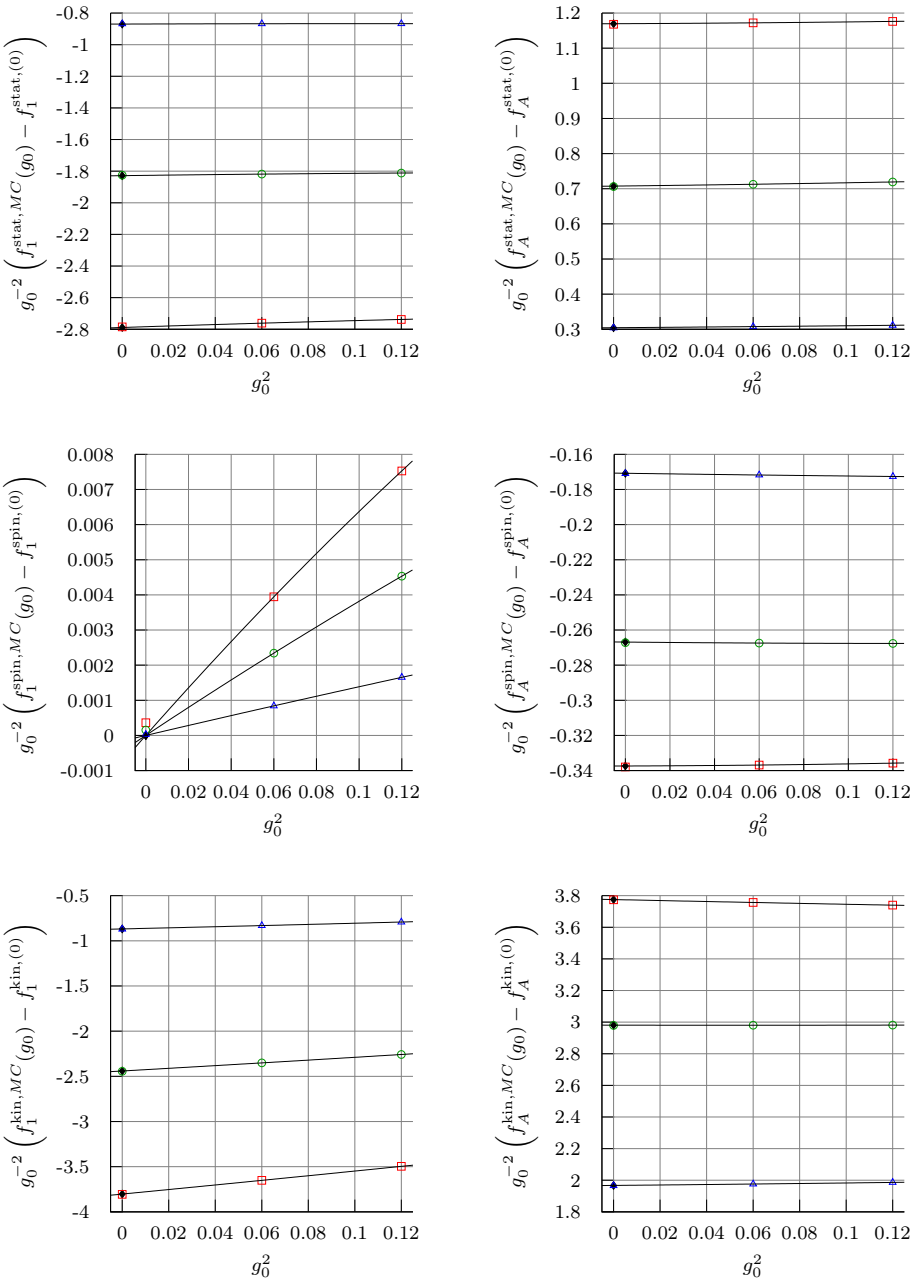

Figure D.3.: Various HQET correlation functions at $L = 4$ for $\theta = 0.0$ (open boxes), $\theta = 0.5$ (open circles) and $\theta = 1.0$ (open triangles). The one loop data is depicted as filled diamonds. The statistical error is smaller than the symbol size.

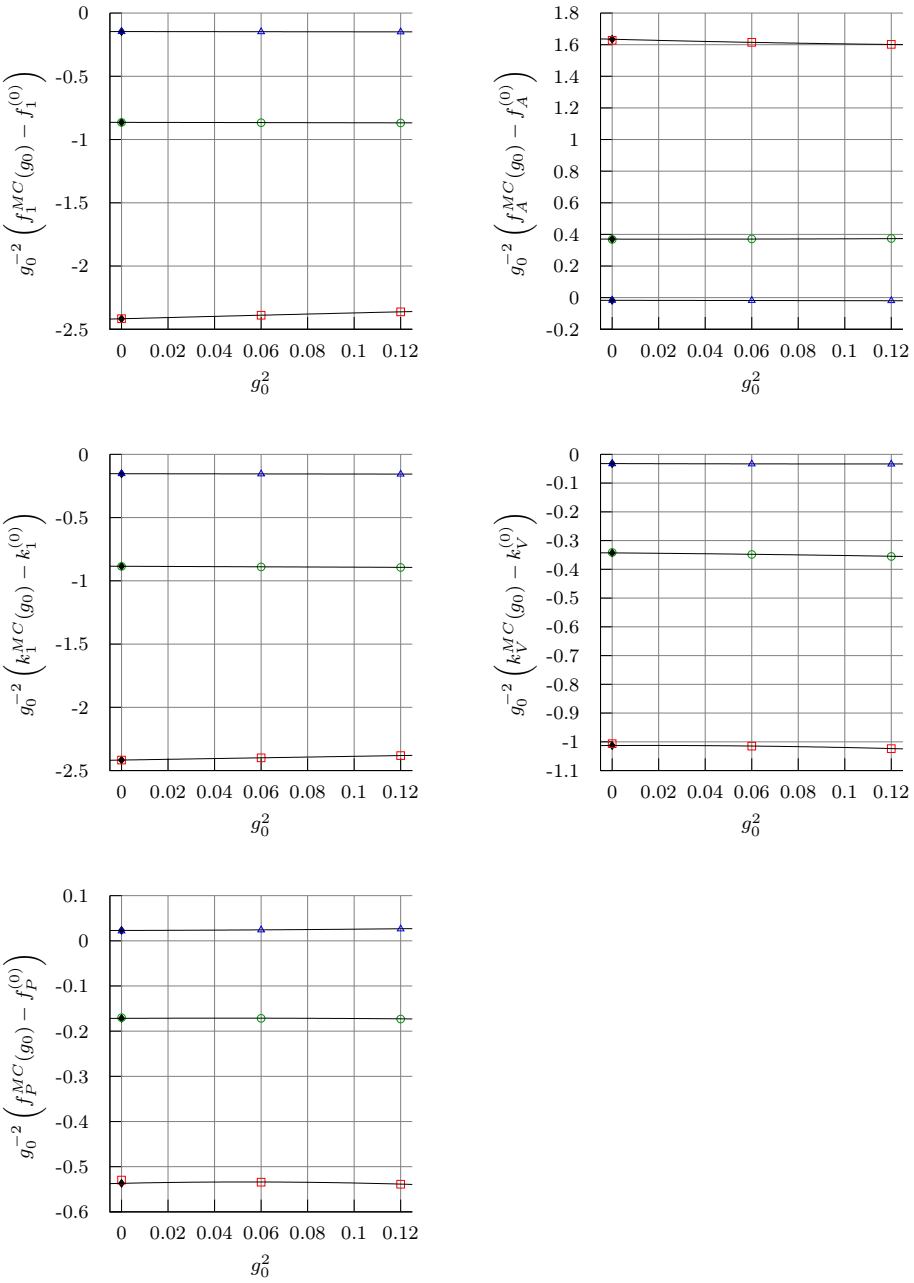

Figure D.4.: Various QCD correlation functions at $L = 4, z = 0$ for $\theta = 0.0$ (open boxes), $\theta = 0.5$ (open circles) and $\theta = 1.0$ (open triangles). The one loop data is depicted as filled diamonds. The statistical error is smaller than the symbol size.

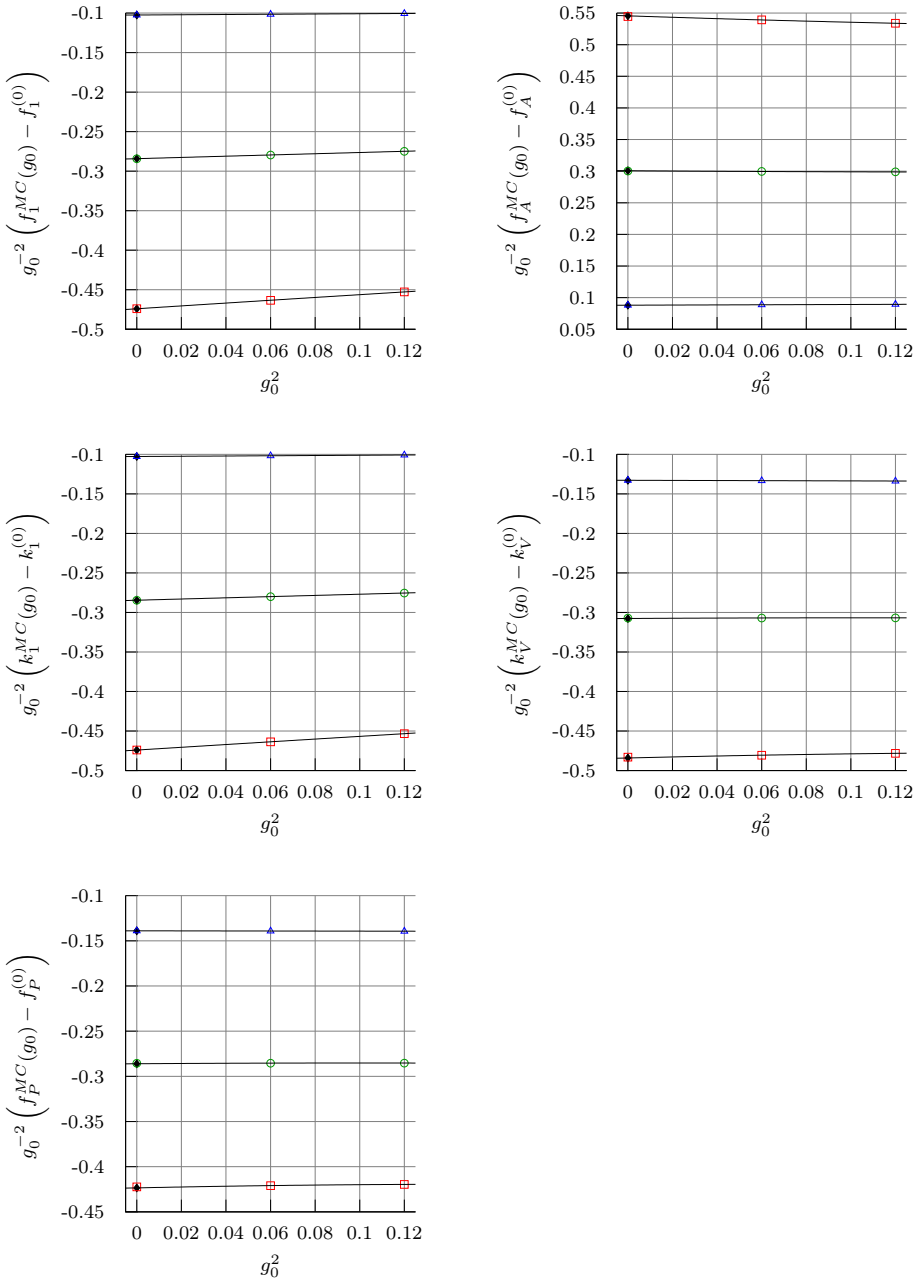

Figure D.5.: Various QCD correlation functions at $L = 4, z = 2$ for $\theta = 0.0$ (open boxes), $\theta = 0.5$ (open circles) and $\theta = 1.0$ (open triangles). The one loop data is depicted as filled diamonds. The statistical error is smaller than the symbol size.

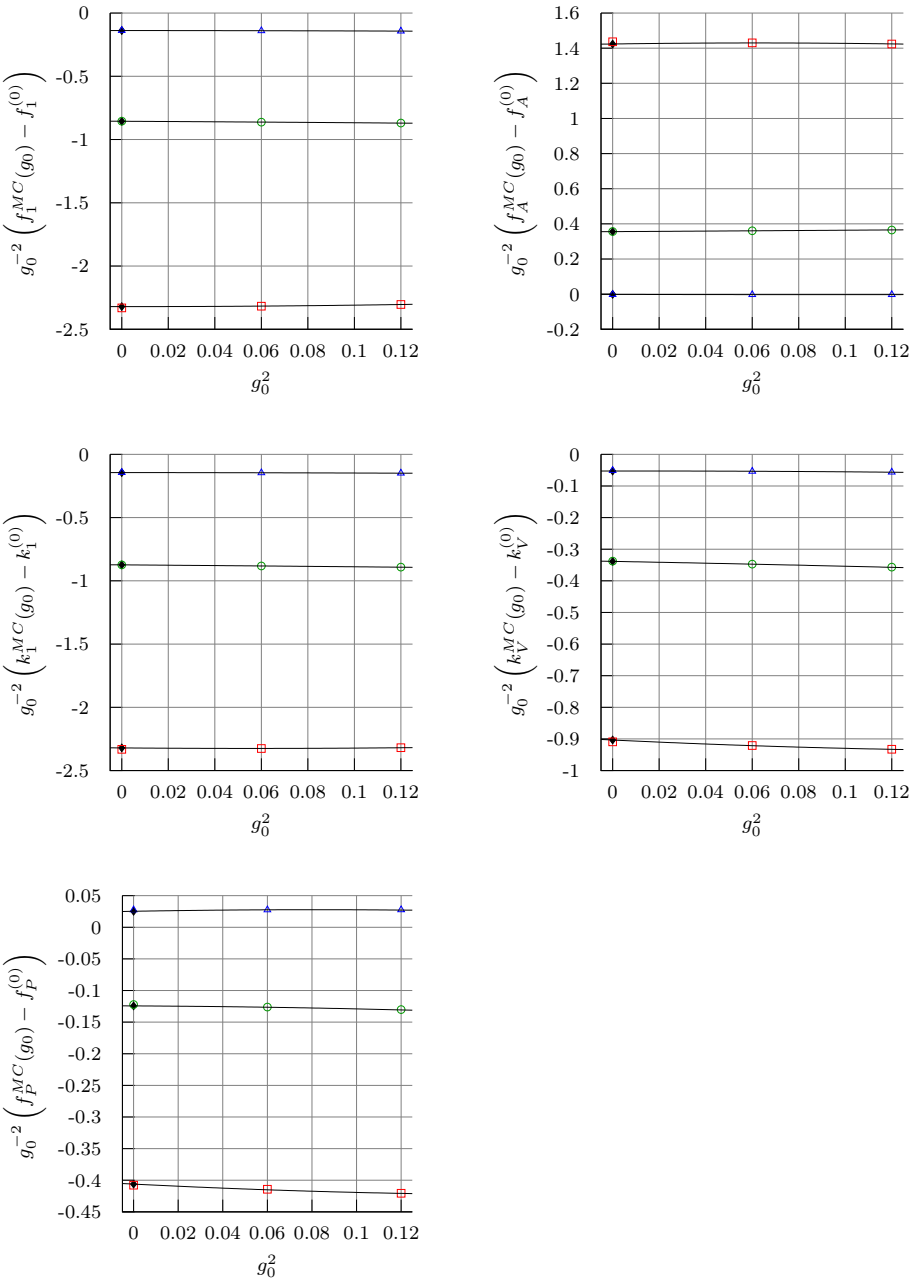

Figure D.6.: Various QCD correlation functions at $L = 6, z = 0$ for $\theta = 0.0$ (open boxes), $\theta = 0.5$ (open circles) and $\theta = 1.0$ (open triangles). The one loop data is depicted as filled diamonds. The statistical error is smaller than the symbol size.

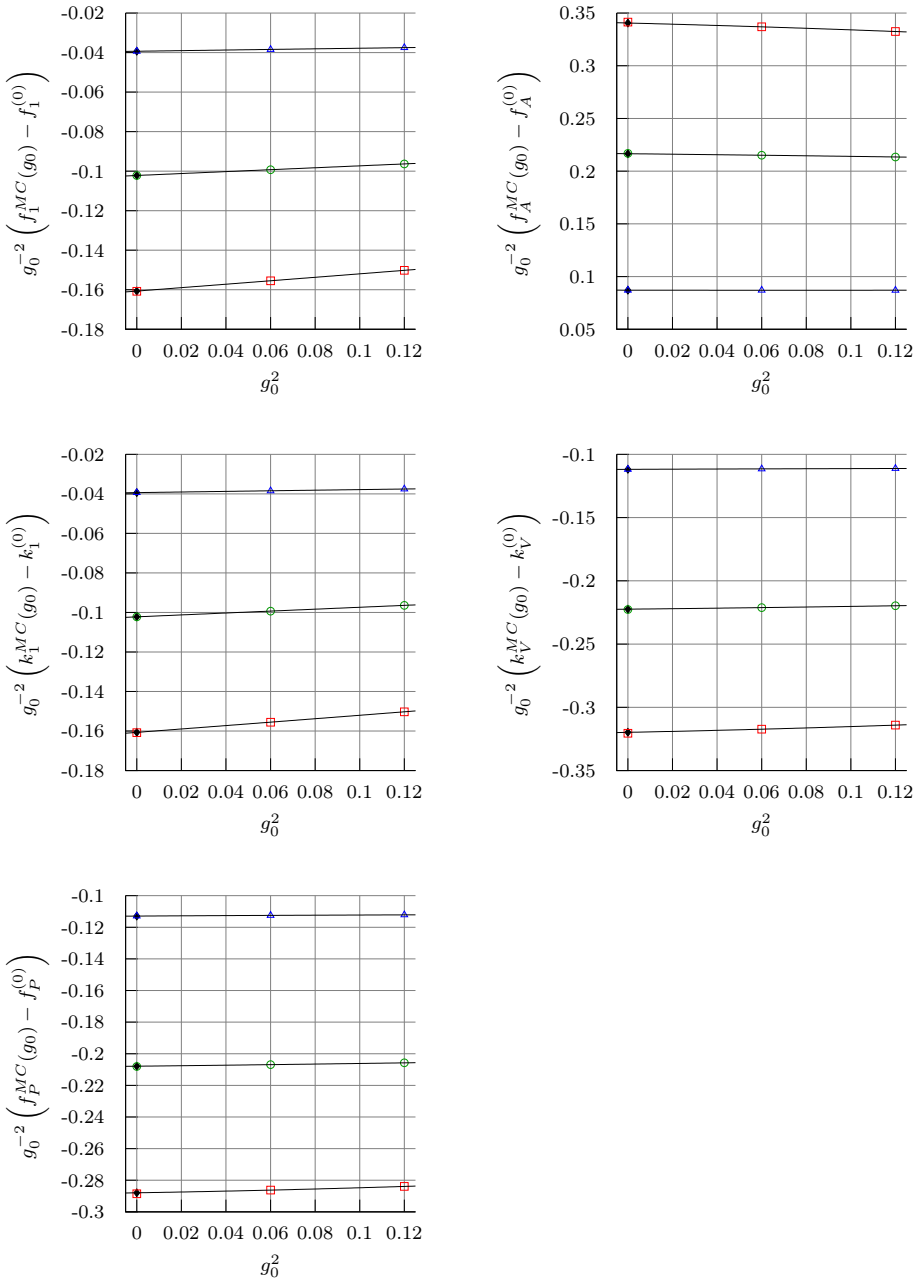

Figure D.7.: Various QCD correlation functions at $L = 6, z = 3$ for $\theta = 0.0$ (open boxes), $\theta = 0.5$ (open circles) and $\theta = 1.0$ (open triangles). The one loop data is depicted as filled diamonds. The statistical error is smaller than the symbol size.

Bibliography

S. L. Adler. An Overrelaxation Method for the Monte Carlo Evaluation of the Partition Function for Multiquadratic Actions. *Phys.Rev.*, D23:2901, 1981. doi: 10.1103/PhysRevD.23.2901.

S. Aoki, R. Frezzotti, and P. Weisz. Computation of the improvement coefficient c(SW) to one loop with improved gluon actions. *Nucl.Phys.*, B540:501–519, 1999. doi: 10.1016/S0550-3213(98)00742-1.

S. Aoki et al. Light hadron spectrum and quark masses from quenched lattice QCD. *Phys.Rev.*, D67:034503, 2003. doi: 10.1103/PhysRevD.67.034503.

B. Blossier, M. della Morte, N. Garron, and R. Sommer. HQET at order $1/m$: I. Non-perturbative parameters in the quenched approximation. *JHEP*, 1006:002, 2010a. doi: 10.1007/JHEP06(2010)002.

B. Blossier et al. B meson spectrum and decay constant from Nf=2 simulations. *PoS*, LATTICE2010:308, 2010b.

T. Blum, C. E. Detar, S. A. Gottlieb, K. Rummukainen, U. M. Heller, et al. Improving flavor symmetry in the Kogut-Susskind hadron spectrum. *Phys.Rev.*, D55:1133–1137, 1997. doi: 10.1103/PhysRevD.55.1133.

A. Bode, P. Weisz, and U. Wolff. Two loop computation of the Schrodinger functional in lattice QCD. *Nucl.Phys.*, B576:517–539, 2000. doi: 10.1016/S0550-3213(00)00187-5, 10.1016/S0550-3213(00)00187-5.

Boost Project. The Boost C++ Libraries. `http://boost.org`, 2012.

K. Bowler et al. Quenched QCD with O(a) improvement. 1. The Spectrum of light hadrons. *Phys.Rev.*, D62:054506, 2000. doi: 10.1103/PhysRevD.62.054506.

G. Buchalla, A. J. Buras, and M. E. Lautenbacher. Weak decays beyond leading logarithms. *Rev.Mod.Phys.*, 68:1125–1144, 1996. doi: 10.1103/RevModPhys.68.1125.

G. de Divitiis et al. Universality and the approach to the continuum limit in lattice gauge theory. *Nucl.Phys.*, B437:447–470, 1995. doi: 10.1016/0550-3213(94)00019-B.

L. Del Debbio. The conformal window on the lattice. *PoS*, LATTICE2010:004, 2010.

M. Della Morte and S. Dooling. Matching of the axial/vector currents at $1/m$. Technical report, Mainz Univ., Münster Univ., 2011.

M. Della Morte, N. Garron, M. Papinutto, and R. Sommer. Heavy quark effective theory computation of the mass of the bottom quark. *JHEP*, 0701:007, 2007. doi: 10.1088/1126-6708/2007/01/007.

P. A. M. Dirac. The Quantum Theory of the Electron. *Royal Society of London Proceedings Series A*, 117:610–624, Feb. 1928.

S. Duane and J. Kogut. The Theory of Hybrid Stochastic Algorithms. *Nucl.Phys.*, B275: 398, 1986. doi: 10.1016/0550-3213(86)90606-1.

S. Duane and J. B. Kogut. Hybrid Stochastic Differential Equations Applied to Quantum Chromodynamics. *Phys.Rev.Lett.*, 55:2774, 1985. doi: 10.1103/PhysRevLett.55.2774.

E. Eichten and B. R. Hill. An Effective Field Theory for the Calculation of Matrix Elements Involving Heavy Quarks. *Phys.Lett.*, B234:511, 1990a. doi: 10.1016/0370-2693(90)92049-O.

E. Eichten and B. R. Hill. Static Effective Field Theory: 1/m Corrections. *Phys.Lett.*, B243:427–431, 1990b. doi: 10.1016/0370-2693(90)91408-4.

L. D. Faddeev and V. N. Popov. Feynman diagrams for the Yang-Mills field. *Phys. Lett.*, B25:29–30, 1967. doi: 10.1016/0370-2693(67)90067-6.

R. Feynman. Space - time approach to quantum electrodynamics. *Phys.Rev.*, 76:769–789, 1949. doi: 10.1103/PhysRev.76.769.

F. (Free Software Foundation). GNU Autoconf. `http://www.gnu.org/software/autoconf/`, 2012a.

F. (Free Software Foundation). GNU Automake. `http://www.gnu.org/software/automake/`, 2012b.

F. (Free Software Foundation). GCC, the GNU Compiler Collection. `http://gcc.gnu.org`, 2012c.

F. (Free Software Foundation). GNU Libtool. `http://www.gnu.org/software/libtool/`, 2012d.

F. (Free Software Foundation). GNU Make. `http://www.gnu.org/software/make/`, 2012e.

E. Gabrielli, G. Martinelli, C. Pittori, G. Heatlie, and C. T. Sachrajda. Renormalization of lattice two fermion operators with improved nearest neighbor action. *Nucl.Phys.*, B362:475–486, 1991. doi: 10.1016/0550-3213(91)90569-J.

C. Gattringer and C. Lang. *Quantum chromodynamics on the lattice: an introductory presentation*. Lecture notes in physics. Springer, 2010. ISBN 9783642018497. URL `http://books.google.com/books?id=l2hZKnlYDxoC`.

M. Gell-Mann. Symmetries of baryons and mesons. *Phys.Rev.*, 125:1067–1084, 1962. doi: 10.1103/PhysRev.125.1067.

Google Inc. The Google C++ Testing Framework. `http://code.google.com/p/googletest/`, 2012.

D. Gross and F. Wilczek. Ultraviolet Behavior of Nonabelian Gauge Theories. *Phys.Rev.Lett.*, 30:1343–1346, 1973. doi: 10.1103/PhysRevLett.30.1343.

F. Halzen and A. Martin. *Quarks and leptons: an introductory course in modern particle physics*. Wiley, 1984. URL `http://books.google.de/books?id=zwDvAAAAMAAJ`.

A. Hart, G. von Hippel, R. Horgan, and E. Müller. Automated generation of lattice QCD Feynman rules. *Comput.Phys.Commun.*, 180:2698–2716, 2009. doi: 10.1016/j.cpc.2009.04.021.

S. Hashimoto, T. Ishikawa, and T. Onogi. Nonperturbative calculation of Z(A) / Z(V) for heavy light currents using Ward-Takahashi identity. *Nucl.Phys.Proc.Suppl.*, 106: 352–354, 2002. doi: 10.1016/S0920-5632(01)01711-X.

M. Hayakawa, K.-I. Ishikawa, Y. Osaki, S. Takeda, S. Uno, et al. Running coupling constant of ten-flavor QCD with the Schródinger functional method. *Phys.Rev.*, D83: 074509, 2011. doi: 10.1103/PhysRevD.83.074509.

G. Heatlie, G. Martinelli, C. Pittori, G. Rossi, and C. T. Sachrajda. The improvement of hadronic matrix elements in lattice QCD. *Nucl.Phys.*, B352:266–288, 1991. doi: 10.1016/0550-3213(91)90137-M.

J. Heitger. Towards precision heavy flavour physics from lattice QCD. *Nucl.Phys.Proc.Suppl.*, 209:117–122, 2010. doi: 10.1016/j.nuclphysbps.2010.12.020.

J. Heitger and R. Sommer. Nonperturbative heavy quark effective theory. *JHEP*, 0402: 022, 2004. doi: 10.1088/1126-6708/2004/02/022.

J. Heitger, H. Simma, R. Sommer, and U. Wolff. The Schrö-din-ger functional coupling in quenched QCD at low- energies. *Nucl.Phys.Proc.Suppl.*, 106:859–861, 2002. doi: 10.1016/S0920-5632(01)01867-9.

D. Hesse and R. Sommer. Schrödinger functional observables for the determination of matching coeffcients in heavy-light currents. Internal Notes, 2011.

I. Horvath and A. Kennedy. The Local hybrid Monte Carlo algorithm for free field theory: Reexamining overrelaxation. *Nucl.Phys.*, B510:367–400, 1998.

K. Jansen, C. Liu, M. Lüscher, H. Simma, S. Sint, et al. Nonperturbative renormalization of lattice QCD at all scales. *Phys.Lett.*, B372:275–282, 1996. doi: 10.1016/0370-2693(96)00075-5.

A. Kennedy. Algorithms for dynamical fermions. *Proceedings of the ILFTN workshop 'Perspectives in Lattice QCD*, 2006. 62 pages, 16 figures. Published by World Scientific in proceedings of the ILFTN workshop 'Perspectives in Lattice QCD'. Revised version corrects (or at least changes) some sign errors, and makes a few other improvements.

W. Kilian and T. Ohl. Renormalization of heavy quark effective field theory: Quantum action principles and equations of motion. *Phys.Rev.*, D50:4649–4656, 1994. doi: 10.1103/PhysRevD.50.4649.

J. Korner and G. Thompson. The Heavy mass limit in field theory and the heavy quark effective theory. *Phys.Lett.*, B264:185–192, 1991. doi: 10.1016/0370-2693(91)90725-6.

M. Kurth and R. Sommer. Renormalization and O(a) improvement of the static axial current. *Nucl.Phys.*, B597:488–518, 2001. doi: 10.1016/S0550-3213(00)00750-1.

M. Kurth and R. Sommer. Heavy quark effective theory at one loop order: An Explicit example. *Nucl.Phys.*, B623:271–286, 2002. doi: 10.1016/S0550-3213(01)00634-4.

L. Lellouch. Flavor physics and lattice quantum chromodynamics. In L. Lellouch, R. Sommer, B. Svetitsky, A. Vladikas, and L. F. Cugliandolo, editors, *Modern Perspectives in Lattice QCD: Quantum Field Theory and High Performance Computing: Lecture Notes of the Les Houches Summer School: Volume 93, August 2009*, Lecture Notes of the les Houches Summer School Series. Oxford University Press, 2011. ISBN 9780199691609. URL `http://books.google.com/books?id=lTnLFQAfZ5QC`.

M. E. Luke and A. V. Manohar. Reparametrization invariance constraints on heavy particle effective field theories. *Phys.Lett.*, B286:348–354, 1992. doi: 10.1016/0370-2693(92)91786-9.

M. Lüscher. Selected topics in lattice field theory. In E. Brezin and J. Zinn-Justin, editors, *Fields, Strings and Critical Phenomena*, Les Houches 1988, Session 49, 1990.

M. Lüscher. Computational Strategies in Lattice QCD. In L. Lellouch, R. Sommer, B. Svetitsky, A. Vladikas, and L. F. Cugliandolo, editors, *Modern Perspectives in Lattice QCD: Quantum Field Theory and High Performance Computing: Lecture Notes of the Les Houches Summer School: Volume 93, August 2009*, Lecture Notes of the les Houches Summer School Series. Oxford University Press, 2011. ISBN 9780199691609. URL `http://books.google.com/books?id=lTnLFQAfZ5QC`.

M. Lüscher and P. Weisz. On-Shell Improved Lattice Gauge Theories. *Commun.Math.Phys.*, 97:59, 1985. doi: 10.1007/BF01206178,10.1007/BF01206178.

M. Lüscher and P. Weisz. Efficient Numerical Techniques for Perturbative Lattice Gauge Theory Computations. *Nucl.Phys.*, B266:309, 1986. doi: 10.1016/0550-3213(86)90094-5.

M. Lüscher and P. Weisz. O(a) improvement of the axial current in lattice QCD to one loop order of perturbation theory. *Nucl.Phys.*, B479:429–458, 1996. doi: 10.1016/0550-3213(96)00448-8.

M. Lüscher, P. Weisz, and U. Wolff. A Numerical method to compute the running coupling in asymptotically free theories. *Nucl.Phys.*, B359:221–243, 1991. doi: 10.1016/0550-3213(91)90298-C.

M. Lüscher, R. Narayanan, P. Weisz, and U. Wolff. The Schrodinger functional: A Renormalizable probe for nonAbelian gauge theories. *Nucl.Phys.*, B384:168–228, 1992. doi: 10.1016/0550-3213(92)90466-O.

M. Lüscher, S. Sint, R. Sommer, and P. Weisz. Chiral symmetry and O(a) improvement in lattice QCD. *Nucl.Phys.*, B478:365–400, 1996. doi: 10.1016/0550-3213(96)00378-1.

M. Lüscher, S. Sint, R. Sommer, P. Weisz, and U. Wolff. Nonperturbative O(a) improvement of lattice QCD. *Nucl.Phys.*, B491:323–343, 1997. doi: 10.1016/S0550-3213(97)00080-1.

G. Martinelli, C. T. Sachrajda, and A. Vladikas. A Study of 'improvement' in lattice QCD. *Nucl.Phys.*, B358:212–230, 1991. doi: 10.1016/0550-3213(91)90538-9.

N. Metropolis, A. Rosenbluth, M. Rosenbluth, A. Teller, and E. Teller. Equation of state calculations by fast computing machines. *J.Chem.Phys.*, 21:1087–1092, 1953. doi: 10.1063/1.1699114.

K. Nakamura et al. Review of particle physics. *J.Phys.G*, G37:075021, 2010. doi: 10.1088/0954-3899/37/7A/075021.

T. Ohl. The feynmf Package. `http://ctan.org/tex-archive/macros/latex/contrib/feynmf/`, 2006.

E. Pallante. Strongly and slightly flavored gauge theories. *PoS*, LAT2009:015, 2009.

F. Palombi. Non-perturbative renormalization of the static vector current and its O(a)-improvement in quenched QCD. *JHEP*, 0801:021, 2008. doi: 10.1088/1126-6708/2008/01/021.

F. Palombi, M. Papinutto, C. Pena, and H. Wittig. Non-perturbative renormalization of static-light four-fermion operators in quenched lattice QCD. *JHEP*, 0709:062, 2007. doi: 10.1088/1126-6708/2007/09/062.

M. Peskin and D. Schroeder. *An introduction to quantum field theory*. Advanced Book Program. Addison-Wesley Pub. Co., 1995. ISBN 9780201503975. URL `http://books.google.com/books?id=_H-oPv1raioC`.

H. Politzer and M. B. Wise. Leading Logarithms of Heavy Quark Masses in Processes with Light and Heavy Quarks. *Phys.Lett.*, B206:681, 1988. doi: 10.1016/0370-2693(88)90718-6.

W. Press. *Numerical recipes: the art of scientific computing*. Cambridge University Press, 2007. ISBN 9780521880688. URL `http://books.google.it/books?id=DyykEZo4fwUC`.

Python Software Foundation. The Python Programming Language. `http://python.org`, 2012.

H. J. Rothe and N. Sadooghi. A New look at the axial anomaly in lattice QED with Wilson fermions. *Phys.Rev.*, D58:074502, 1998. doi: 10.1103/PhysRevD.58.074502.

S. Schaefer, R. Sommer, and F. Virotta. Critical slowing down and error analysis in lattice QCD simulations. *Nucl.Phys.*, B845:93–119, 2011. doi: 10.1016/j.nuclphysb.2010.11.020.

B. Sheikholeslami and R. Wohlert. Improved Continuum Limit Lattice Action for QCD with Wilson Fermions. *Nucl.Phys.*, B259:572, 1985. doi: 10.1016/0550-3213(85)90002-1.

M. A. Shifman and M. Voloshin. On Annihilation of Mesons Built from Heavy and Light Quark and anti-B0 <–> B0 Oscillations. *Sov.J.Nucl.Phys.*, 45:292, 1987.

S. Sint. On the Schrodinger functional in QCD. *Nucl.Phys.*, B421:135–158, 1994. doi: 10.1016/0550-3213(94)90228-3.

S. Sint and R. Sommer. The Running coupling from the QCD Schrodinger functional: A One loop analysis. *Nucl.Phys.*, B465:71–98, 1996. doi: 10.1016/0550-3213(96)00020-X.

S. Sint and P. Weisz. Further results on O(a) improved lattice QCD to one loop order of perturbation theory. *Nucl.Phys.*, B502:251–268, 1997. doi: 10.1016/S0550-3213(97)00372-6.

R. Sommer. Introduction to non-perturbative heavy quark effective theory. In L. Lellouch, R. Sommer, B. Svetitsky, A. Vladikas, and L. F. Cugliandolo, editors, *Modern Perspectives in Lattice QCD: Quantum Field Theory and High Performance Computing: Lecture Notes of the Les Houches Summer School: Volume 93, August 2009*, Lecture Notes of the les Houches Summer School Series. Oxford University Press, 2011. ISBN 9780199691609. URL `http://books.google.com/books?id=lTnLFQAfZ5QC`.

R. Sundrum. Reparameterization invariance to all orders in heavy quark effective theory. *Phys.Rev.*, D57:331–336, 1998. doi: 10.1103/PhysRevD.57.331.

K. Symanzik. Schrodinger Representation and Casimir Effect in Renormalizable Quantum Field Theory. *Nucl.Phys.*, B190:1, 1981. doi: 10.1016/0550-3213(81)90482-X.

K. Symanzik. Continuum Limit and Improved Action in Lattice Theories. 1. Principles and phi**4 Theory. *Nucl.Phys.*, B226:187, 1983a. doi: 10.1016/0550-3213(83)90468-6.

K. Symanzik. Continuum Limit and Improved Action in Lattice Theories. 2. O(N) Nonlinear Sigma Model in Perturbation Theory. *Nucl.Phys.*, B226:205, 1983b. doi: 10.1016/0550-3213(83)90469-8.

S. Takeda. Automatic generation of Feynman rules in the Schrodinger functional. *Nucl.Phys.*, B811:36–65, 2009. doi: 10.1016/j.nuclphysb.2008.11.022.

B. Thacker and G. Lepage. Heavy quark bound states in lattice QCD. *Phys.Rev.*, D43: 196–208, 1991. doi: 10.1103/PhysRevD.43.196.

P. Weisz. Computation of the improvement coefficient $c_s w$ to 1-loop. ALPHA Collaboration Internal Notes, 1996.

K. G. Wilson. Confinement of Quarks. *Phys.Rev.*, D10:2445–2459, 1974. doi: 10.1103/PhysRevD.10.2445.

U. Wolff. Dynamics of hybrid overrelaxation in the Gaussian model. *Phys.Lett.*, B288: 166–170, 1992. doi: 10.1016/0370-2693(92)91972-C.

U. Wolff. Monte Carlo errors with less errors. *Comput.Phys.Commun.*, 156:143–153, 2004. doi: 10.1016/S0010-4655(03)00467-3,10.1016/j.cpc.2006.12.001.

C. N. Yang and R. L. Mills. Conservation of Isotopic Spin and Isotopic Gauge Invariance. *Physical Review*, 96:191–195, Oct. 1954. doi: 10.1103/PhysRev.96.191.

List of Figures

List of Tables

Selbständigkeitserklärung

Ich erkläre, dass ich die vorliegende Arbeit selbständig und nur unter Verwendung der angegebenen Literatur und Hilfsmittel angefertigt habe.

Parma, den 1. April 2012 Dirk Hesse